

# System Identification and Modal Tracking on Ship Structures

by

Keith Soal



*Dissertation presented for the degree of Doctor of Philosophy  
in Mechanical Engineering in the Faculty of Engineering at  
Stellenbosch University*

UNIVERSITEIT  
STELLENBOSCH  
UNIVERSITY

100  
1918 · 2018

Supervisors:

Dr A. Bekker  
Mechanical Engineering  
University of Stellenbosch  
South Africa

Prof J. Bienert  
Fakultät Maschinenbau  
Technische Hochschule Ingolstadt  
Germany

March 2018

# Declaration

By submitting this dissertation electronically, I declare that the entirety of the work contained therein is my own, original work, that I am the sole author thereof (save to the extent explicitly otherwise stated), that reproduction and publication thereof by Stellenbosch University will not infringe any third party rights and that I have not previously in its entirety or in part submitted it for obtaining any qualification.

Date: March 2018

Copyright © 2018 Stellenbosch University  
All rights reserved.



UNIVERSITEIT•STELLENBOSCH•UNIVERSITY  
jou kennisvennoot • your knowledge partner

## Plagiaatverklaring / Plagiarism Declaration

- 1 Plagiaat is die oorneem en gebruik van die idees, materiaal en ander intellektuele eiendom van ander persone asof dit jou eie werk is.  
*Plagiarism is the use of ideas, material and other intellectual property of another's work and to present it as my own.*
- 2 Ek erken dat die pleeg van plagiaat 'n strafbare oortreding is aangesien dit 'n vorm van diefstal is.  
*I agree that plagiarism is a punishable offence because it constitutes theft.*
- 3 Ek verstaan ook dat direkte vertalings plagiaat is.  
*I also understand that direct translations are plagiarism.*
- 4 Dienooreenkomstig is alle aanhalings en bydraes vanuit enige bron (ingesluit die internet) volledig verwys (erken). Ek erken dat die woordelike aanhaal van teks sonder aanhalingstekens (selfs al word die bron volledig erken) plagiaat is.  
*Accordingly all quotations and contributions from any source whatsoever (including the internet) have been cited fully. I understand that the reproduction of text without quotation marks (even when the source is cited) is plagiarism.*
- 5 Ek verklaar dat die werk in hierdie skryfstuk vervat, behalwe waar anders aangedui, my eie oorspronklike werk is en dat ek dit nie vantevore in die geheel of gedeeltelik ingehandig het vir bepunting in hierdie module/werkstuk of 'n ander module/werkstuk nie.  
*I declare that the work contained in this assignment, except where otherwise stated, is my original work and that I have not previously (in its entirety or in part) submitted it for grading in this module/assignment or another module/assignment.*

15632555	
<b>Studentenommer / Student number</b>	<b>Handtekening / Signature</b>
KI Soal	23-11-2017
<b>Voorletters en van / Initials and surname</b>	<b>Datum / Date</b>

# Abstract

## System Identification and Modal Tracking on Ship Structures

K. Soal

*Department of Mechanical and Mechatronic Engineering,  
University of Stellenbosch,  
Private Bag X1, Matieland 7602, South Africa.*

Dissertation: PhD (Mechanical)

March 2018

Critical decisions regarding the safe and efficient operation of vessels in ice are currently based mainly on dynamic response feedback. Navigators decide on how to operate the vessel based on how they feel it pitching, heaving, rolling and vibrating. The aim of this thesis is to investigate the idea of using system identification and modal tracking on polar vessels towards the development of a decision aiding system. System identification provides a powerful tool for building mathematical models of dynamic systems. An open source toolbox (openSID) for system identification using Stochastic Subspace Identification (SSI) was developed as a research and learning tool. Full scale measurements were performed on the research vessel Polarstern during an expedition to the Arctic. This is the first comprehensive data set including vibration responses and environmental parameters to span the entire operational profile of a research voyage to the Arctic. System identification successfully identified seven global modes in the bandwidth 2 - 10 Hz. Comparisons between different methods were used to cross validate results. A modal tracking algorithm was developed and relationships between identified modes and system inputs were observed. A novel method is developed to improve the uncertainty and sensitivity of system identification and tracking, based on a data driven statistical model and a Kalman filter. A key objective is to make experimental data maximally informative by using additional system inputs. The model was found to accurately re-create the training data set and was used to make predictions based on future system inputs. The Kalman filter estimates were observed to produce balanced and consistent results. These results demonstrate the potential of an ice force estimation and structural health monitoring system.

# Uittreksel

## Stelselidentifikasie en Modale Naspeuring op Skip Strukture

*(“System Identification and Modal Tracking on Ship Structures”)*

K. Soal

*Departement Meganiese en Megatroniese Ingenieurswese,  
Universiteit van Stellenbosch,  
Privaatsak X1, Matieland 7602, Suid Afrika.*

Proefskrif: PhD (Meganies)

Maart 2018

Kritieke besluite in terme van die veilige en doelgerigte bedryf van skepe in ys is tans hoofsaaklik gebaseer op dinamiese hanterings terugvoer. Besluite oor hoe om die vaartuig te navigeer word toegelig deur hoe seevaarders die skip voel duik, heg, rol en vibreer. Die doel van hierdie tesis is om die idee van stelselidentifikasie en modale naspeuring op poolskepe te ondersoek ten einde die ontwikkeling van ’n besluitnemingstelsel. Stelselidentifikasie bied ’n kragtige metode vir die bou van wiskundige modelle van dinamiese stelsels. Oopbron gereedskap algoritme (openSID) vir stelselidentifikasie, met die gebruik van Stochastiese Subspasie Identifikasie (SSI) is ontwikkel as ’n navorsings en leer instrument. Volskaal metings is uitgevoer op die navorsing skip Polarstern tydens ’n ekspedisie na die Arktiese gebied. Dit is die eerste omvattende datastel wat vibrasierespons en omgewingsparameters insluit om die hele operasionele profiel van ’n navorsingsreis na die Arktiese omgewing te dek. Stelselidentifikasie het sewe globale modes in die bandwydte 2 - 10 Hz geïdentifiseer. Vergelykings tussen twee metodes is gebruik om resultate te bekragtig. Modale naspeuringsalgoritme is ontwikkel en verhoudings tussen geïdentifiseerde modusse en stelselinsette is waargeneem. Nuwe metode is ontwikkel om die onsekerheid en sensitiwiteit van stelselidentifikasie en naspeuring te verbeter, gebaseer op ’n data gedrewe statistiese model en ’n Kalman filter. ’n Hoof doelwit is om eksperimentele data maksimaal insiggewend te maak deur addisionele stelsel insette te gebruik. Dit is gevind dat die model die opleidingsdatastel akkuraat naboots. Hierna is dit gebruik om voorspellings te maak gebaseer op toekomstige stelselinsette. Beraming met die Kalman filter is waargeneem om gebalanseerde en konsekwente resultate te lewer. Hierdie

*UITTREKSEL*

v

resultate demonstreer die potensiaal van 'n besluitnemingsstelsel om ys kragte af te skat en strukturele integriteit te monitor.

# Acknowledgements

It has been a privilege to pursue my passion for research in Europe, Scandinavia and Africa as well as on the research vessels SA Agulhas II and Polarstern. These experiences have radically shaped my perspective and character. I would thank the National Research Foundation (NRF), Council of Managers of National Antarctic Programs (COMNAP) and German Academic Exchange Service (DAAD) for funding which made this possible. My supervisors deserve a special thank you. To Annie for encouraging me to dream my eccentric dreams. And one of the things I am most grateful for, the freedom and trust she showed me, and my decisions, in instrumenting polar vessels on a different continent and long research expeditions. And to Jörg for bringing me back to reality, and teaching me one of the most important lessons I have learnt - how to de-construct a problem into its foundation. I would like to thank my friends and colleagues in Germany, Finland, Portugal, South Africa and those from the research voyages to Antarctica and the Arctic. The close friendships I have made have had the most profound influence on me and I am very grateful to have been inspired by these incredible people. I would like to thank the Deutsches Zentrum für Luft und Raumfahrt (DLR), Alfred Wegener Institute (AWI) and Technische Hochschule Ingolstadt in Germany, Aalto University in Helsinki Finland, and Instituto Superior Técnico in Lisbon Portugal for hosting me during productive and inspiring research exchanges. I would also like to thank my family for supporting and encouraging me despite the very little time we have spent together since leaving home to the south of South Africa to pursue a bachelors degree nine years ago. Finally with probability, uncertainty and randomness of the universe in my mind, I would like to thank everyone and no-one for everything and nothing in particular.

“Inferring models from observations and studying their properties  
is really what science is about.”

— Lennart Ljung

# Contents

<b>Declaration</b>	<b>i</b>
<b>Abstract</b>	<b>iii</b>
<b>Uittreksel</b>	<b>iv</b>
<b>Acknowledgements</b>	<b>vi</b>
<b>Contents</b>	<b>viii</b>
<b>List of Figures</b>	<b>xi</b>
<b>List of Tables</b>	<b>xiv</b>
<b>1 Introduction</b>	<b>1</b>
1.1 Polar Research Vessels . . . . .	1
1.2 System Identification and Modal Tracking . . . . .	3
1.3 Project Aim and Novel Contribution . . . . .	4
1.4 Readers Guide . . . . .	6
<b>2 Literature Study</b>	<b>8</b>
2.1 Introduction . . . . .	8
2.2 Direct Ice Force Estimation . . . . .	8
2.2.1 Full Scale Measurements . . . . .	8
2.2.2 Model Scale Measurements . . . . .	10
2.2.3 Ice Mechanics . . . . .	10
2.3 Indirect Ice Force Estimation . . . . .	11
2.4 System Identification on Ship Structures . . . . .	14
2.5 System Identification Principles from other Structures . . . . .	17
2.6 Conclusion . . . . .	18
<b>3 openSID Open Source Stochastic Subspace Identification</b>	
<b>Toolbox</b>	<b>20</b>
3.1 Introduction . . . . .	20
3.2 Theory of Output Only System Identification . . . . .	22
3.3 State Space Model . . . . .	22

<i>CONTENTS</i>	<b>ix</b>
3.4 Data Driven Stochastic Subspace Identification (SSI) . . . . .	23
3.4.1 Projection . . . . .	25
3.4.2 Main Theorem . . . . .	27
3.4.3 Weightings . . . . .	28
3.4.4 Subspace Selection . . . . .	28
3.4.5 Determining the System Matrices . . . . .	29
3.5 Covariance Driven SSI . . . . .	31
3.6 Data vs. Covariance Driven SSI . . . . .	33
3.7 Modal Analysis . . . . .	33
3.8 openSID Toolbox and GUI . . . . .	34
3.9 Conclusion . . . . .	36
<b>4 Parametric Simulation Study</b>	<b>39</b>
4.1 Introduction . . . . .	39
4.2 Model Order . . . . .	39
4.3 Block Size . . . . .	42
4.4 3D Visualisation . . . . .	42
4.5 Noise . . . . .	45
4.6 Reference Channels . . . . .	46
4.7 Damping . . . . .	48
4.8 Harmonics . . . . .	50
4.9 Linear Time Invariance . . . . .	51
4.10 Total Prediction Error (TPE) . . . . .	52
4.11 Conclusion . . . . .	52
<b>5 Polar Research Vessel, Arctic Expedition and Open Data</b>	<b>55</b>
5.1 Description of the Vessel . . . . .	55
5.2 Measurement Setup and Equipment . . . . .	56
5.3 Field Measurements in the Arctic . . . . .	58
5.4 Open Data . . . . .	59
<b>6 Modal Tracking</b>	<b>60</b>
6.1 Introduction . . . . .	60
6.2 Least-Square Complex Frequency (LSCF) . . . . .	61
6.3 Mode Tracking . . . . .	61
6.4 Results . . . . .	63
6.4.1 Signal Processing . . . . .	63
6.4.2 Frequency Spectra . . . . .	65
6.4.3 System Identification . . . . .	68
6.4.4 Mode Tracking . . . . .	69
6.4.5 Modal Correlation . . . . .	72
6.5 Conclusion . . . . .	75
<b>7 Models for Modal Prediction using System Inputs</b>	<b>76</b>
7.1 Introduction . . . . .	76

<i>CONTENTS</i>	<b>x</b>
7.2 Background . . . . .	77
7.3 Automated Modal Parameter Selection . . . . .	78
7.4 Kalman Filter . . . . .	81
7.5 Idea . . . . .	82
7.6 Numerical Simulation . . . . .	83
7.7 Results . . . . .	84
7.7.1 Signal Processing . . . . .	84
7.7.2 Model Training . . . . .	85
7.7.3 Predictive Sliding Model . . . . .	88
7.8 Conclusions . . . . .	93
<b>8 Conclusions and Future Research</b>	<b>95</b>
8.1 Conclusions . . . . .	95
8.2 Future Research . . . . .	96
<b>List of References</b>	<b>99</b>

# List of Figures

1.1	SA Agulhas II in Antarctica. . . . .	1
1.2	Polar research vessel Polarstern. . . . .	2
1.3	Antarctic pack ice. . . . .	3
1.4	Southern ocean storm. . . . .	3
1.5	Decision aiding network metaphor. . . . .	5
2.1	Icebreakers used for full-scale measurements. . . . .	9
2.2	Ice failure modes (a)quasi-static (b) steady-state and (c) random. (Yue <i>et al.</i> , 2009). . . . .	11
2.3	The hand drawn first vertical bending mode of icebreaker SISU excited by ice impacts (Matusiak, 1982). . . . .	12
2.4	Mode shapes of a RoRo vessel. (Rosenow, 2007). . . . .	15
2.5	OMA modes (left) and FE modes (right) of the SA Agulhas II. (Soal, 2014) . . . . .	17
2.6	Simplified illustration of indirect force estimation method. . . . .	19
3.1	A system with interacting input variables $u$ , observable output sig- nals $y$ , process noise $w$ , and measurement noise $v$ . (Adapted from Pintelon and Schoukens (2001)) . . . . .	22
3.2	Work flow for SSI-Data. . . . .	24
3.3	Future output $Y_f$ projection onto past output $Y_p^{ref}$ . . . . .	25
3.4	Time data. . . . .	35
3.5	Power spectral density. . . . .	35
3.6	Statistical moments. . . . .	36
3.7	Stabilisation diagram. . . . .	37
3.8	MAC matrix. . . . .	37
3.9	Complexity plot. . . . .	38
3.10	Mode shapes. . . . .	38
4.1	Stabilization diagram for SSI-Data with block size $i = 30$ . ● MIF, + Stable pole, × Unstable pole. . . . .	40
4.2	Frequency, damping and Modal Assurance Criterion (MAC) errors for SSI-Data '+' and SSI-Covariance '□' with block size $[i = 30]$ . Minimum errors are indicated in green '+, □' . . . . .	41

4.3	Frequency, damping and MAC errors for SSI-Data $+$ and SSI-Covariance $\square$ for increasing block sizes to ( $i = 30$ ) with a fixed model order ( $n = 6$ ). . . . .	43
4.4	Frequency, damping and MAC errors for SSI-Data $+$ and SSI-Covariance $\square$ for increasing block sizes to ( $i = 300$ ) with a fixed model order ( $n = 6$ ). . . . .	44
4.5	3D plot of block size ( $i$ ), model order ( $n$ ) and % error in frequency. . . . .	45
4.6	(a-c) Box and whisker plots of errors as a result of different noise levels. (d) FFT of signal with (d1) 0 % noise (d2) 10 % noise and (d3) 80 % noise . . . . .	46
4.7	Reference channel investigation. . . . .	47
4.8	Frequency, errors for SSI-Data with all channels as references $+$ and [1 2 3] as reference $\square$ with block size [ $i = 10$ ]. . . . .	48
4.9	Frequency, damping and MAC errors for SSI-Data with $\sim 0.1$ % damping $+$ , 1 % damping $\square$ and 5 % damping $\triangle$ with block size [ $i = 30$ ]. . . . .	49
4.10	Frequency, damping and MAC errors for SSI-Data with no harmonic $+$ , harmonic $1.001 f_n$ $\square$ and harmonic $1.01 f_n$ $\triangle$ for increasing model order with a fixed block size ( $i = 10$ ). . . . .	50
4.11	SSI identification of a time varying system. . . . .	51
4.12	Power spectral density (PSD) of the 5 DOF system with different input force levels. Channel 1 $\bullet$ , Channel 2 $\bullet$ , Channel 3 $\bullet$ , Channel 4 $\bullet$ , Channel 5 $\bullet$ . . . . .	53
4.13	Total prediction error (%) versus model order ( $n$ ) and block size( $i$ ). Channel 1 $\square$ , Channel 2 $\square$ , Channel 3 $\square$ , Channel 4 $\square$ , Channel 5 $\square$ . . . . .	53
5.1	Polar research vessel Polarstern. (AWI/W von Appen) . . . . .	55
5.2	Polarstern in an Arctic ice field. . . . .	56
5.3	Polarstern during a storm in open water. (AWI/F Mehrrens) . . . . .	56
5.4	Measurement setup on the Polarstern: $\bullet$ Accelerometer locations, $\bullet$ Vertical (+Z) measurements, $\bullet$ Transverse (+Y) measurements, $\bullet$ Triaxial (+X, +Y, +Z) measurements . . . . .	57
5.5	Measurement equipment. . . . .	58
5.6	Cruise track of the PS100 expedition. (AWI/J Schaffer) . . . . .	59
6.1	Modal assurance criterion. . . . .	63
6.2	Time data of all accelerometers for five selected cases. . . . .	64
6.3	Statistical moments. . . . .	65
6.4	Auto power spectral densities (APSD) $\bullet$ Case 1 $\bullet$ Case 2 $\bullet$ Case 3 $\bullet$ Case 4 $\bullet$ Case 5. . . . .	65
6.5	Auto and cross power spectral densities of all accelerometers with the vertical accelerometer on the starboard side of the bow $\bullet$ Case 1 $\bullet$ Case 2. . . . .	66
6.6	Spectrograms of case 1 and 2. . . . .	67

## LIST OF FIGURES

xiii

6.7	SSI stabilisation diagram. . . . .	68
6.8	LSCF stabilisation diagram. . . . .	69
6.9	Polarstern mode shapes. . . . .	70
6.10	SSI mode tracking during the five selected cases. . . . .	71
6.11	SSI modal clusters. . . . .	71
6.12	LSCF mode tracking during the five cases. . . . .	72
6.13	Modal clusters frequency and damping. . . . .	72
6.14	Case 3 correlation. . . . .	73
6.15	Case 4 correlation. . . . .	74
6.16	Case 5 correlation. . . . .	74
6.17	Total correlation. . . . .	75
7.1	Ship system. . . . .	77
7.2	Kalman filter. . . . .	81
7.3	Kalman filter options. . . . .	83
7.4	Numerical simulation. * True value $\dashrightarrow$ True value + noise + temperature variation $\rightarrow$ Kalman filter estimate. . . . .	83
7.5	Signal processing of response and predictor variables. . . . .	84
7.6	Correlation of measured predictor variables. . . . .	85
7.7	Vibration channels containing NaN's during the voyage (a) before (b) after channel removal. . . . .	86
7.8	Constant speed model training. . . . .	86
7.9	Constant speed modal parameter tracking. . . . .	87
7.10	Polarstern mode shapes. . . . .	87
7.11	Acceleration time histories and ship speed for case 1 and 2. . . . .	88
7.12	Predictive model work flow for case 1. . . . .	89
7.13	Kalman prediction for case 1. $\circ$ SSI training set $\times$ Training set pre- diction $\square$ Statistical model prediction $\circ$ SSI estimates $\diamond$ Kalman estimates . . . . .	90
7.14	Predictive model work flow for case 2. . . . .	91
7.15	Kalman prediction for case 2. . . . .	92
7.16	Kalman filter estimates for method 1 $\square$ and method 2 $\diamond$ . . . . .	94

# List of Tables

6.1	Operational profile case study. . . . .	64
7.1	Automatic modal parameter selection methods. (Stab = Stabilisation) . . . . .	80
7.2	Predictive model parameters for case 1. . . . .	89
7.3	Predictive model parameters for case 2. . . . .	93

# Chapter 1

## Introduction

### 1.1 Polar Research Vessels

Polar research vessels such as the SA Agulhas II and Polarstern, shown in Figure 1.1 and 1.2, are relied upon by research institutes and their scientists to re-supply bases as well as to serve as floating laboratories. These vessels operate in the oceans surrounding Antarctica and the Arctic which provide valuable scientific insights into the system of our planet (AWI, 2017). These insights help decipher inter connectivities which are not only interesting, but also useful in understanding our impact on the Earth as well as the effects of changing climate.



Figure 1.1: SA Agulhas II in Antarctica.

Polar vessels operating in these environments are exposed to complex dynamic forces due to ice, waves, wind, engines and propellers as shown in Figure 1.3 and 1.4. The dynamic response of the structure to these forces is directly related to its performance in terms of stability, ice breaking capacity, power consumption and safety. The response to these forces over time also determine the vessel's fatigue life. These forces cause the propagation of energy through the structure resulting in vibration.



Figure 1.2: Polar research vessel Polarstern.

Vibration can damage the vessel's structure as well as navigational or sensitive scientific equipment. It can also cause fatigue of crew or scientists on board. The importance of the human factor should not be underestimated since humans are responsible for making decisions regarding the operation and safety of vessels at sea.

Critical decisions regarding the safe and efficient operation of vessels in ice are currently based mainly on dynamic response feedback. This means that navigators decide on headings and speeds in challenging ice conditions based on how they feel the ship responding i.e. how much it is pitching, heaving, rolling and vibrating. In certain operating conditions this subjective experience may not accurately reflect the magnitude of the associated forces.

A vision to develop a decision support system for polar vessels is therefore proposed. The aim of such a system would be to display semi-real time information about ice forces and structural health to the navigating officers on the bridge. The use of system identification and modal tracking as tools to achieve this goal will be further developed in the following section. Finally, this system

would not replace the experience of captains and navigating officers but rather provide a tool which integrated with ice radar, ice and weather forecasts and satellite images could result in safer and more efficient navigational decisions.



Figure 1.3: Antarctic pack ice.



Figure 1.4: Southern ocean storm.

## 1.2 System Identification and Modal Tracking

System identification provides a powerful tool for building mathematical models of dynamic systems. A system is an object on which different variables interact to produce observable signals. Models are aimed at linking these observations together into a pattern from which useful information can be extracted (Ljung, 1987). In mechanical and civil engineering the system identification framework has been successfully applied to structures, where vibration responses are used to extract modal parameters (Ewins, 2000).

This is not a trivial task when dealing with real structures with complex inputs, low excitation forces and noise. A further challenge involves dealing with unmeasurable input forces such as wind or wave loads on large structures in actual operating conditions. Output only system identification or Operational Modal Analysis (OMA), see (Brincker and Ventura, 2015), was developed to identify modal parameters without knowledge of the input forces. This is achieved by making assumptions about the unmeasured forces which are modelled as stochastic white noise quantities. The advantages of OMA are that modal parameters can be estimated from real data in actual operating conditions. The drawback is that long time records are often needed to fulfil assumptions.

For the purposes of this work we consider a polar vessel as our ‘system’. This framework allows the identification of modal parameters consisting of natural frequencies, damping and mode shapes from measured acceleration signals. These parameters can be used to build modal models which have applications in Inverse Force Estimation (IFE) and Structural Health Monitoring (SHM) (Peeters, 2000).

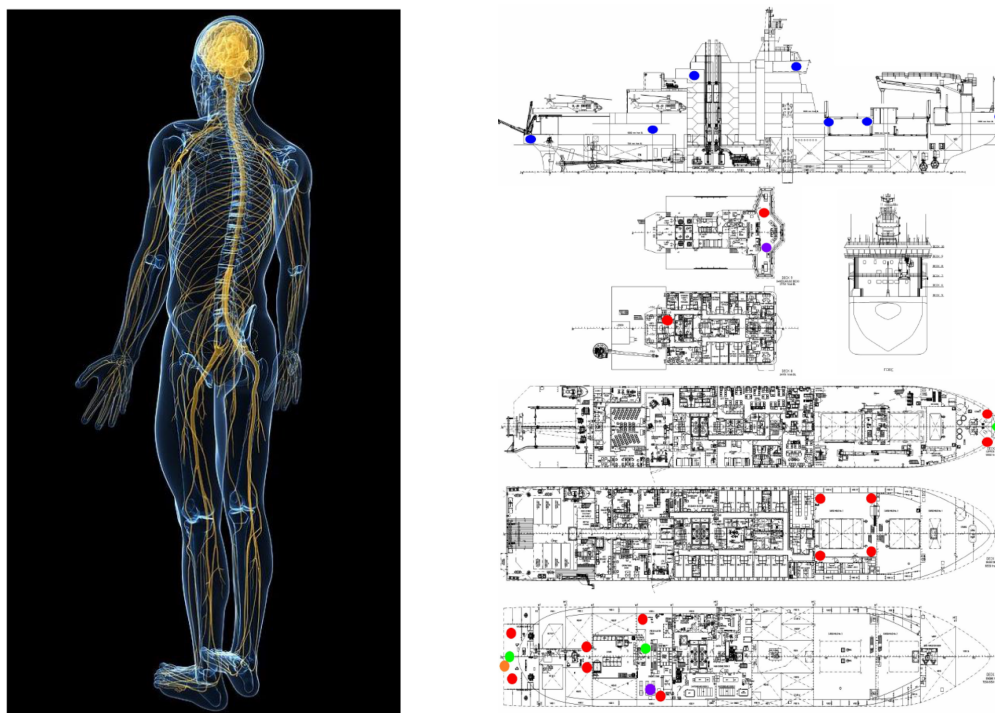
A key observation is that changes in physical parameters such as temperature, draft or speed, cause detectable changes in the vibration properties (Liu and DeWolf, 2007). Modal parameter tracking deals with identifying and following the trail of system modes. The sensitivity of system identification and modal tracking to changing environmental and operational parameters is important for SHM and IFE. This is because damage to a structure can be misidentified or masked by modal shifts as a result of environmental parameters.

### 1.3 Project Aim and Novel Contribution

The aim of this thesis is to investigate the idea of using system identification and modal tracking on polar vessels towards the development of a decision aiding system. This is proposed through the use of a sensor network to transmit signals for decision making in a similar way to the functioning of the nervous system in the human body as shown in Figure 1.5. Signals from accelerometers, gyroscopes and ship based weather stations can be used to build mathematical models. These models can then be used to quantify ice forces and monitor the health of the structure.

Investigations were first conducted into different system identification algorithms such as Enhanced Frequency Domain Decomposition (EFDD), Least Square Complex Frequency (LSCF), Ibrahim Time Domain (ITD) and Stochastic Subspace Identification (SSI). Initial investigations on full scale data of polar vessels by Soal (2014) as well as literature by Peeters (2000); Magalhães *et al.* (2008); Reynders (2009) found improved estimates from SSI methods.

Current SSI methods were found to be available only as commercial closed software. Open source software and development has proven to drive innova-



(a) Human nervous system. (Sciepro, 2013)

(b) Polar vessel sensor network. (Soal, 2014)

Figure 1.5: Decision aiding network metaphor.

tion, result in more robust code and be a force multiplier (Balter, 2015). The need for an open source toolbox which can be used both as a learning and research tool was identified. The first aim of this thesis is the development of an open source toolbox for system identification using SSI. It is envisioned to use this platform to demystify SSI and help students and researchers gain insights into the practical application of these techniques.

The second aim is to investigate the performance of SSI through a parametric study. Where the effect of key user defined parameters such as model order and block size are investigated. The response of the algorithms to physical phenomena such as noise, damping, harmonics and linear time invariance will subsequently be performed. The objective is to use analogies from simple systems to aid in understanding more complex results from real structures.

The third aim of this thesis is to conduct full scale measurements on the polar research vessel *Polarstern* during a voyage to the Arctic. There is currently no comprehensive data set including vibration responses and environmental parameters to span the entire operational profile of a vessel in the Arctic. It is planned to instrument the *Polarstern* with over 2 km of cable in Germany. Accelerometers and the Data Acquisition System (DAQ) will be installed before the vessel departs the harbour in Tromsø, Norway. Continuous vibration measurements will be recorded throughout the voyage. Environmental and

operational parameters such as weather, sea state, ice conditions, vessel speed, ballast, trim and fuel will also be recorded during the expedition.

An associated aim is to make this data set openly available. The main goals for making the data open access are (1) so that results in this thesis can be tested, recreated and validated (2) opening the data to other researchers has the potential to bring a diversity of ideas and optimal solutions and provide additional human capital to drive innovation (3) a variety of open source data sets will allow open and transparent benchmarking of state of the art algorithms.

The fourth aim is to investigate the potential of using system identification and modal tracking to identify and follow the trail of system modes. Different system identification techniques will be used to cross validate results. Investigations into the performance of the identification algorithms during different operating conditions will also be performed. The relationships between environmental and operational inputs and system identification outputs will also be investigated.

The fifth and final aim of this thesis is to investigate an idea to improve the uncertainty and sensitivity of system identification estimates using a statistical model and a Kalman filter. A key objective is to make experimental data maximally informative by using additional system inputs.

A summary of the original contributions of this work are therefore as follows:

1. Development of an open source toolbox for system identification in structural dynamics using SSI (openSID), as an innovative platform for open development and learning.
2. Provide fundamental insights into the mathematical algorithms of SSI through a parametric study as a guide for users.
3. Conducting the first comprehensive full scale measurements including vibration responses and environmental parameters on a polar vessel to span the entire operational profile of a research voyage to the Arctic.
4. Investigate system identification and modal tracking using state of the art algorithms on full scale data from a polar vessel.
5. Development of a novel method to improve system identification estimates using a statistical model and a Kalman filter.

## 1.4 Readers Guide

The organisation of the thesis is presented in this section as an overview and guide to the reader.

## Chapter 2

Provides a review of relevant literature into the ice force estimation and dynamic response of polar vessels. The chapter begins with key developments in ice force estimation using direct methods followed by indirect methods. Examples of system identification applied to ship structures are then discussed followed by relevant insights from other structures.

## Chapter 3

The system identification framework and Stochastic Subspace Identification (SSI) method are presented. Theory is presented together with implemented code to provide hands on understanding and insight to students and researchers. The openSID toolbox and GUI are then presented and demonstrated.

## Chapter 4

A parametric simulation study is conducted to investigate the effects of model order, block size, noise, reference channels, damping, harmonics, linear time invariance and total prediction errors. This is intended as a guide to the user interested in understanding the algorithms and their application.

## Chapter 5

Presents a description of the polar research vessel Polarstern, the full scale measurement setup and research voyage. The open data vision is further explained together with details of how to access the data.

## Chapter 6

Presents the system identification and modal tracking results from full scale data. The modal tracking algorithm is explained together with the signal processing and statistical investigation.

## Chapter 7

Proposes a novel approach to improve the uncertainty and sensitivity of system identification and tracking based on a data driven statistical model and a Kalman filter.

# Chapter 2

## Literature Study

### 2.1 Introduction

This thesis aims at investigating the use of system identification and modal tracking to model a ship's dynamic behaviour. The objective is to develop a decision support system capable of inverse force estimation and structural health monitoring. This chapter provides a review of relevant work on the dynamic response and ice force estimation of polar vessels. The chapter begins with key developments in ice force estimation using direct methods. Limitations and complexities in these methods lead to the idea of using the system response to estimate the forces, known as indirect methods. The strengths and weaknesses of indirect methods are discussed and the potential of system identification in making a novel contribution is proposed. Examples of system identification as applied to ship structures are then reviewed followed by relevant insights from other structures. This review forms the basis for the idea development in the current research.

### 2.2 Direct Ice Force Estimation

#### 2.2.1 Full Scale Measurements

Edwards *et al.* (1972) conducted the first scientific investigations into ice load estimation. They hypothesized that ice loads could be expressed as statistical functions of environmental parameters such as ice thickness, strength, elastic modulus and snow cover. The complexity of ship ice interaction however defied the development of purely analytical ice load solutions. Edwards *et al.* (1972) then conducted full scale measurements of local ice loads using strain gages on the USCGC Mackinaw, shown in Figure 2.1a. Force estimates were plotted against observations of ice thickness, ship speed and flexural ice strength. A linear relationship was proposed between the product of ice thickness and ship speed versus ice load. The results showed considerable scatter and were limited by unobserved variables, and most significantly the variability in location of the

ice impacts. Suominen *et al.* (2015) found that depending on the location of the force applied to an instrumented panel, that the actual measured value could vary from between 0 and 1.4 times the magnitude of the actual applied load. The random nature of ice impacts on a dynamic structure pose a significant limitation on direct force measurement.



(a) The USCGC Mackinaw on the Great Lakes. (Wikimedia Public Domain)



(b) USCG Polar Sea and Polar Star assisting a tanker in Antarctica. (Morris, 2002)



(c) The Oden in the Bay of Bothnia. (Kerkmann, 2007)



(d) The Nathaniel B. Palmer in Antarctica's Ross Sea. (Eastman, 2013)

Figure 2.1: Icebreakers used for full-scale measurements.

The first investigations into global ice forces during ramming of heavily ridged ice features were conducted by Chen *et al.* (1990) on the USCG Polar Sea, shown in Figure 2.1b. The vessel was instrumented with strain gages and accelerometers to measure longitudinal bending moments as well as compressive strain of the hull. Chen *et al.* (1990) found the 2 node bending mode of the hull at 3,1 Hz to be dominant during ramming. The exact location of the impact force was found to be one of the most important factors. Variations in the measured and predicted impact forces were largely attributed to not knowing the location of the impact. Minnick and John (1990) conducted full scale measurements on the USCG Polar Star, shown in Figure 2.1b. Minnick and John (1990) placed greater emphasis on accurately determining the location of the ice impact from a centreline bulkhead compression gage. The method was limited when the vessel moved deeper into the broken ice field and the impact locations increased and distributed randomly around the hull.

John and Minnick (1995) performed full scale measurements on the research vessel Nathaniel B. Palmer, see Figure 2.1d. The main objectives were to compare ice loads measured at the bow on the Nathaniel B. Palmer to those measured on the USCG Polar Sea as well as the Swedish icebreaker Oden, shown in Figure 2.1c. The Nathaniel B. Palmer has a similar bow shape to the Polar Sea but is approximately half the displacement. While the Oden has a similar displacement to the Polar Sea but a wide flat bow with a low stem angle. The Nathaniel B. Palmer was instrumented in three different locations which was the first time that ice loads were measured at multiple locations on a ship hull. John and Minnick (1995) found that ice loads and pressures did not show a clear trend with ice thickness, ice concentration or ship speed. Peak loads or pressures occurred at the most common ice thickness, ice concentration and speed, indicating the random nature of the loading. In other words more impacts result in higher extremes. These results were consistent with those from the Polar Sea and the Oden.

### 2.2.2 Model Scale Measurements

Mueller and Ettema (1984) conducted model scale tests in a tow tank and measured the dynamic response. They proposed a characteristic equation,  $V_0/f_0L_c$  relating the hull's natural frequencies  $f_0$  of pitching and heaving to the hull velocity  $V_0$  and characteristic ice sheet length  $L_c$ . This was related to the distance between consecutive cracks formed around the bow and was used to estimate the forcing function of ice loads. Model scale tests conducted by Ettema *et al.* (1987) focused on the relationships between ice resistance and patterns of ice breaking. Ettema *et al.* (1987) showed how these factors are influenced by, and in turn influence hull motions. Key findings included larger ship hull resistances during significant pitch, heave and roll motions as well as strong correlations between ice breaking pattern, hull motions and the dominant cycles of hull resistance.

### 2.2.3 Ice Mechanics

Varsta (1983) conducted investigations into the mechanics of ice loads. The aim of this work was to analyse ice loads in detail and develop a mathematical model to determine loads based on ice characteristics and ship parameters. Comparisons of full scale ice loads to numerical predictions did not show strong correlations due to the stochastic nature of the measured ice loading. Varsta (1983) concluded that the level of knowledge of ice mechanics was not yet sufficient for the accurate prediction of ice loading. This study sparked new interest in ice mechanics.

Further investigations into ice loads from an ice mechanics perspective were conducted by Yue *et al.* (2009). They observed that dynamic ice forces could be separated by the ice encounter speed into three modes. Each mode had

an associated force pattern which depended on the natural frequency of the structure, the form of the impact area and the energy delivered by the ice into the structure. The modes were classified as quasi-static, steady-state and random. From the quasi-static ice force pattern in Figure 2.2a it can be seen that the ice force increases slowly until a critical limit and then fails suddenly. This process is dominated by plastic deformation and ductile behaviour. Figure 2.2b shows the steady-state mode which occurs in the ductile-brittle transition zone and Figure 2.2c the random mode where the ice behaves in a brittle manner. Yue *et al.* (2009) noted that the failure mode depended significantly on the available energy of the ice which is related to the ice velocity (kinetic energy) as well as the mass of the ice (potential energy) which can be related to the thickness (Timco and Weeks, 2010). Timco and Weeks (2010) and Kärnä and Jochmann (2003) observed that the ice thickness is one of the most important engineering properties and is directly related to the way that ice fails. Bjerikås *et al.* (2007) observed that the ductile to brittle transition zone is related to rate dependency of the ice strength, which was found to be lower in the brittle failure mode than the ductile failure mode. This means that large forces could still occur on the ship hull when the vessel is stationary in a moving ice field. During actual ice navigation the ice is expected to act mostly in a brittle manner with a random force spectrum. However in very thick ice conditions where the ice may completely stop the vessel, the low navigation speeds can result in ice failing in the ductile-brittle or ductile regime.

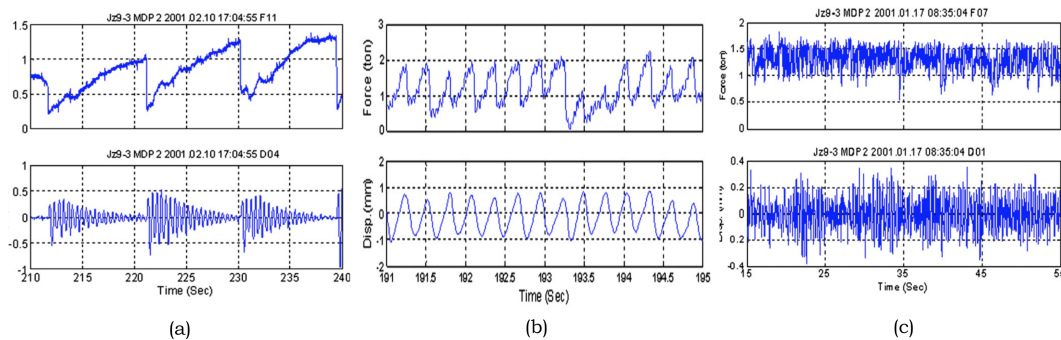


Figure 2.2: Ice failure modes (a) quasi-static (b) steady-state and (c) random. (Yue *et al.*, 2009).

### 2.3 Indirect Ice Force Estimation

Matusiak (1982) conducted the first full scale vibration measurements on ice-breaker SISU using two transducers. The main objectives of the study were to identify the vibration modes and evaluate the vibration level during ice breaking. Matusiak (1982) observed that forces due to ice hull interaction were complex, and that ice loads could be regarded as a random broadband

process. The analysis of the full scale measurements showed that the four lowest natural modes were excited, the first bending mode excited by ice impacts is shown in Figure 2.3. It was also found that the presence of the broken ice field significantly increased the damping ratio and mass of the structure. These findings provided novel insight into the effects of ship ice interaction on structural dynamic response.

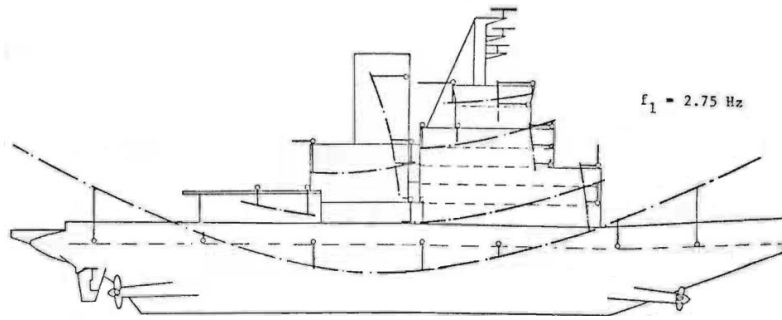


Figure 2.3: The hand drawn first vertical bending mode of icebreaker SISU excited by ice impacts (Matusiak, 1982).

Since the complete characterization of ice loading is highly complex Johnston *et al.* (2001) proposed a new method whereby ship motion was measured using an inertial measurement system called MOTAN (MOTION ANALYSIS). Measurements from the MOTAN system were then used to calculate global ice forces. The MOTAN system provided time data of ship motion in six degrees of freedom. Full scale measurements were conducted on the USCGC Healy during ice trials. A variety of loading conditions were sampled ranging from light ice conditions to backing and ramming in first year and multi year ice. It was found that pitch angles ranged from  $0.2^\circ$  to  $0.8^\circ$  and roll angles ranged from  $0.6^\circ$  to  $4.9^\circ$ . The method was however limited due to neglecting roll motions which were significant during ice breaking.

The method for calculating the global vertical force was as follows. The equations of motion for coupled heave and pitch motions, derived in Matusiak (2013), are presented in Equations 2.3.1 and 2.3.2.

$$(m + a) \frac{d^2 z}{dt^2} + b \frac{dz}{dt} + cz + d \frac{d^2 \theta}{dt^2} + e \frac{d\theta}{dt} + h\theta = F(t) \quad (2.3.1)$$

$$(I_y + A) \frac{d^2 \theta}{dt^2} + B \frac{d\theta}{dt} + C\theta + D \frac{d^2 z}{dt^2} + E \frac{dz}{dt} + Hz = M(t) \quad (2.3.2)$$

where  $\theta$  is pitch,  $z$  is heave,  $m$  is mass,  $a$  is added mass,  $I_y$  is mass moment of inertia of the ship about the midship  $y$ -axis,  $F(t)$  is total external force,  $M(t)$  is total external moment. Since MOTAN measures the rate of change

of the pitch angle ( $\frac{d\theta}{dt}$ ), Equation 2.3.2 was chosen as it is less sensitive to integration error (since gyros measure velocity).

The cross-coupling coefficients D and E were neglected in Equation 2.3.2, which then simplified the pitching moment equation to

$$(I_y + A)\frac{d^2\theta}{dt^2} + B\frac{d\theta}{dt} + C\theta + Hz = M(t) \quad (2.3.3)$$

where the first term is the moment due to the mass moment of inertia of the ship ( $I_y$ ) and the hydrodynamic added mass effects ( $A$ ). The second term, ( $B\frac{d\theta}{dt}$ ) is the moment due to the hydrodynamic damping effects. The third term ( $C\theta$ ) is the hydrostatic restoring moment in pitch. The last term  $H_z$  is the hydrostatic heave cross-coupling moment due to the difference between the longitudinal centre of flotation and the longitudinal centre of buoyancy of the vessel. The pitching moment equation is then used to obtain the ice impact force based on

$$F_l(t) = \frac{M(t)}{R} \quad (2.3.4)$$

where  $F_l(t)$  is the ice impact force at specified location along the hull,  $M(t)$  is the pitching moment and  $R$  is the external ice impact force radius.

Johnston *et al.* (2008) furthered this idea by including the effects of sway, roll and yaw in MOTAN7A. Six linear coupled differential equations were solved to calculate three global excitation forces and three global excitation moments. Additionally, two methods were used to calculate the global forces. The centre of gravity (COG) approach determined the resultant global impact force at the ship's COG, and therefore did not require information about the location of the ice impact. The second approach called the point of impact (POI) approach assumed that the force acted at a single known point.

Johnston *et al.* (2008) then conducted full scale measurements on the CCGS Terry Fox. The CCGS Terry Fox was also instrumented with an optical impact panel and an array of strain gages to compare direct and indirect ice force estimates. More than 150 controlled collisions with glacial ice at speeds up to 12.8 knots were performed. The motions were filtered using a low-pass filter with cut off frequency of 5 Hz in order to remove elastic dynamics. The translational velocities and displacements were calculated using numerical integration from accelerometer signals, while the angular accelerations and displacements were calculated using numerical differentiation and integration respectively. Resultant global forces for 51 bergy bit impacts ranged from 0.5 MN to 6.7 MN for the POI approach and 0.9 MN to 10.6 MN for the COG approach. These results did not compare well with the measured strain gage ice loads with the POI approach varying between 17 % lower and 33 % higher, while the COG approach forces were up to 120 % different from those measured by the strain gages.

While direct force estimates were again limited by the variability of the location of the ice impact, indirect force estimates faced their own unique lim-

itation of static system coefficients. The vessel properties represented by the generalized mass matrix  $M$ , added mass  $A$ , damping coefficients  $B$  and restoring force coefficients  $C$  were developed from analytical methods for vessels in open water and were static. The effect of ice impacts on changing the vessel mass, damping and stiffness were found to be significant by Matusiak (1982). Neglecting these effects will therefore result in inaccurate ice load predictions.

Broman and Nordqvist (2013) developed a similar system using a Motion Reference Unit (MRU) on the KV Svalbard. Their rigid body model was limited to perpendicular ice impacts from open water. This was due to previous impacts resulting in a superposition of motions which would be difficult to separate. This limited the usefulness of the method as a tool in real navigation. Broman and Nordqvist (2013) noted that the rigid body assumption was a limitation as it neglected the energy dissipated through elastic body response and therefore underestimated the true force. Broman and Nordqvist (2013) made an improvement to Johnston *et al.* (2008) work by including the use of a Kalman filter to remove noise on the measurements. Broman and Nordqvist (2013) also investigated the effects of the low pass filter cut off frequency. It was found that if the cut off frequency was chosen too high, that contributions of the elastic dynamics would propagate through the rigid body model equation, and if chosen too low would reduce the amplitude of the rigid body response. This would result in over or underestimates of the ice forces. It was suggested that this filter would need to be designed individually for different vessels and would need to update in different conditions or vessel configurations. Nyseth *et al.* (2013) further discussed the strengths and limitations of using ship motion to calculate global ice impacts with specific reference to the MRU system on the KV Svalbard. An improvement is made in their model whereby they account for the added mass, damping and restoring forces by determining the hydrodynamic coefficients using the hydrodynamic software WASIM. The software was further modified to account for the presence of ice. Matching software predictions to actual operating conditions requires further research and limits the ability to provide semi real time information for vessel navigation and decision making.

The use of indirect ice load estimation has shown much potential. Furthermore motion units are already available on most vessels (Heyn and Skjetne, 2015). The key challenges facing the current state of the art techniques are (1) static or non real time system parameters (mass, damping and stiffness) (2) inability to provide reliable estimates in a broken ice field with multiple input forces.

## 2.4 System Identification on Ship Structures

Rosenow *et al.* (2007) conducted the first Operational Modal Analysis (OMA) on ships during full scale sea trials. The aim of this work was the extraction of modal parameters in the presence of stochastic and harmonic excitation. Har-

monic excitation results from imbalances in rotating machinery which occur in the propulsion system of ships (main engine and propeller) as well as auxiliary machines on board. Harmonics provide a challenge to OMA since they violate the assumption of Gaussian white noise excitation and can therefore be identified as physical poles and can also bias closely spaced poles.

System identification was performed on measurements from a container vessel and a Roll-on/Roll-off (RoRo) vessel. The Enhanced Frequency Domain Decomposition (EFDD) and Stochastic Subspace Identification (SSI) methods were used. It was found that harmonics could be detected from sharp peaks in the Singular Value Decomposition (SVD) and could be removed using linear interpolation in the frequency domain. If the harmonic was very close or exactly coincident with the physical pole, a bias in the estimates was found to occur. SSI was found to be more robust to the presence of harmonics however biased estimates especially in damping were still observed. The first six global modes of the RoRo vessel are presented in Figure 2.4. Rosenow *et al.* (2007) observed that the dynamic properties depended on operational and boundary conditions. Notable changes in the natural frequencies of the first and second bending modes were observed as a result of increased propulsion power.

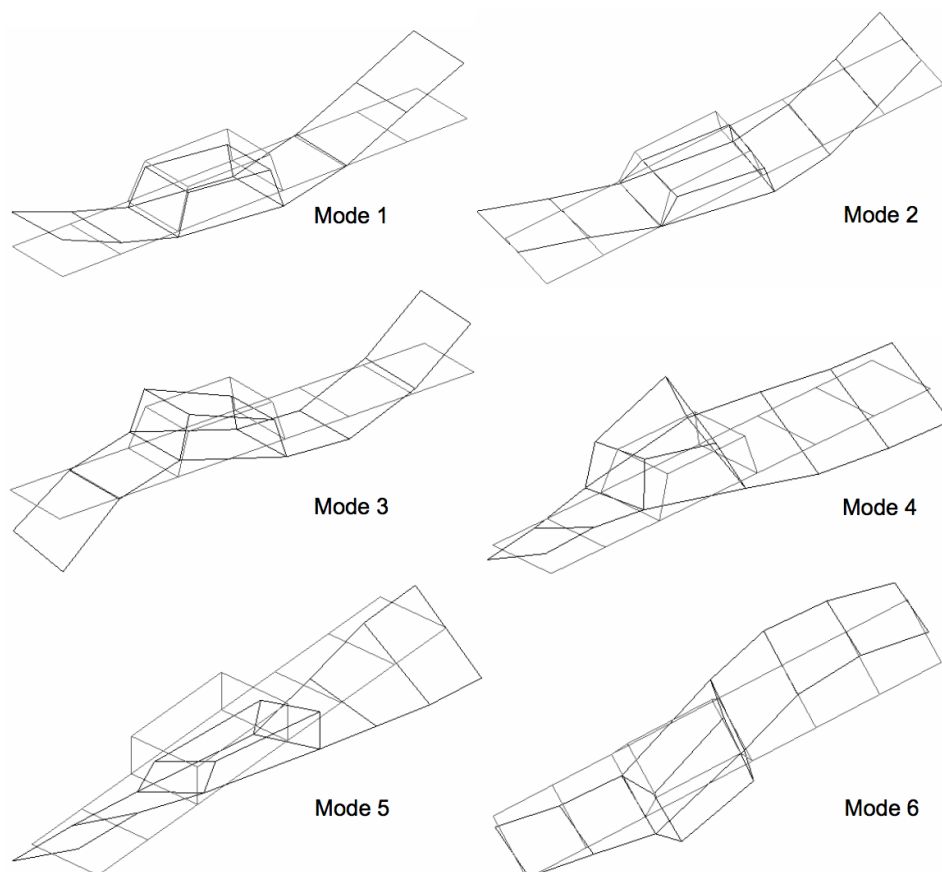


Figure 2.4: Mode shapes of a RoRo vessel. (Rosenow, 2007).

Rocca *et al.* (2009) conducted full scale measurements on the Japanese research vessel the BOSEI MARU. OMA was performed using the frequency domain technique Operational PolyMAX. Modes were identified during engine run up and run down tests, as well as during a wave induced vibration and anchor drop test. Due to short impact durations during the wave induced vibration and anchor drop test, the natural frequencies were only identified using peak picking, as it was found that the PolyMAX technique was not suited to the analysis of time histories with short durations. A pre-analysis of the data was also performed to identify the engine and propeller harmonics. Five modes were identified across the three cases and the modal parameters were found to be dependent on the excitation.

Orlowitz and Brandt (2014) conducted full scale vibration measurements on a Roll-on Lift-off (Ro-Lo) vessel to investigate the effects of different operational conditions on the modal parameters using OMA. Three operating conditions were defined consisting of cruising in calm open water at 10 knots and 18 knots as well as an anchor condition in deep water. The Multiple-reference Ibrahim Time Domain (MITD) method was used to estimate the modal parameters. Five stable modes were identified and included vertical bending, horizontal bending and torsional modes. A key finding was that natural frequencies decreased with increasing cruising speed, while damping ratios increased with increasing cruising speed. This was in agreement with results from Rosenow (2007), however model scale results by Coppotelli *et al.* (2008) found that both natural frequencies and damping ratios increased (non-linearly) with increasing speed. A significant variation in modal damping was found with approximately 400 %, 200 % and 400 % differences in the first three global vertical bending modes respectively.

Soal *et al.* (2015) conducted full scale vibration measurements on the SA Agulhas II while anchored in Cape Town harbour. The PolyMAX frequency domain and SSI time domain techniques were used to estimate the modal parameters. Both techniques identified three stable vertical bending modes, and a comparison of the frequencies between the two methods agreed to within 1.2 %. The damping estimates however showed less agreement especially for mode 3 which differed by 59 %. The results of OMA were also compared to those of the Finite Element (FE) model developed by STX Finland, shown in Figure 2.5. Soal *et al.* (2015) found that OMA frequencies were lower than FE frequencies. The FE calculations were based on a vessel draught of 7.7 m which was deeper than the 6.8 m draught during OMA testing. It was hypothesized that based on the equation relating natural frequency to stiffness and mass that increasing the draft would further lower the operational natural frequencies. Resulting in a larger discrepancy between the model used to design the vessel and the actual vessel behaviour.

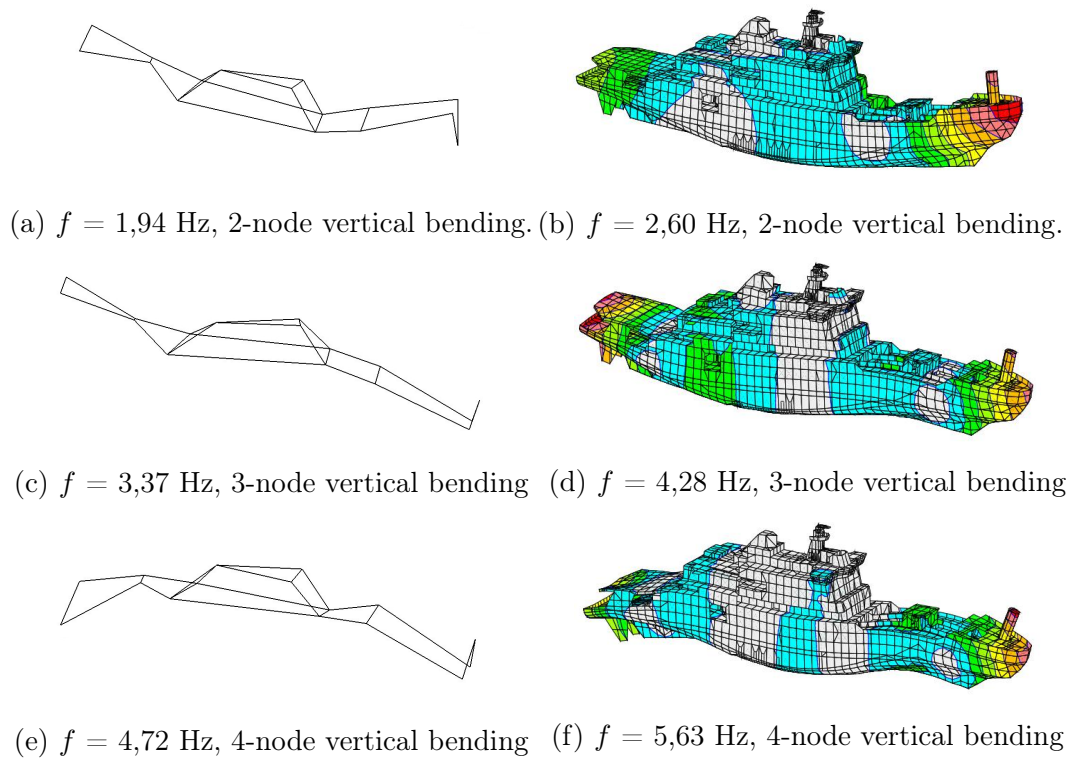


Figure 2.5: OMA modes (left) and FE modes (right) of the SA Agulhas II. (Soal, 2014)

## 2.5 System Identification Principles from other Structures

Although only four full scale open water OMA studies on ships have been reported in literature, several principles investigated on other structures provide insight into future possibilities for output only system identification.

Since ship structures are inherently subject to harmonic forces, methods to deal with these should be investigated. There are currently two classes of methods available for dealing with harmonics in system identification: Method (1) includes the harmonics in the system identification and subsequently removes them in post processing using pre-knowledge of rotational speeds, or unrealistically low damping estimates. Techniques aiming to detect and avoid harmonics have been proposed by Brincker *et al.* (2000); Jacobsen *et al.* (2007); Peeters *et al.* (2007). Investigations have also been conducted to include harmonic frequencies as a priori in the identification by Mohanty and Rixen (2004) as well as to make system identification robust in the presence of harmonics by Goursat *et al.* (2010). The drawbacks of these methods are that the harmonics may bias the modal parameter estimates of physical modes in a way which cannot be reversed in post processing. Method (2) removes the harmonic from the raw time or frequency data before performing the system identification. These methods

address the problem at the root and have been found capable of removing bias when harmonics are close to physical poles. The current state of the art techniques include the Gauss-Newton parametric time domain technique (Bienert *et al.*, 2015), the Periodogram smoothing non-parametric frequency domain technique (Brandt and Linderholt, 2012), the Vold-Kalman filter (Vold *et al.*, 2017) and the Resampling semi-non-parametric method (Brandt, 2015). The Gauss-Newton and Periodogram smoothing techniques require pre-knowledge of the harmonics while the Vold-Kalman and Resampling techniques require a measured tachometer channel to track harmonics. The Polarstern vessel operates with constant engine rpm and propeller rotational speed. The effects of stationary harmonics on modal estimates will therefore need to be weighed against improvements and computational costs to determine the necessity for harmonic removal in the current research focus.

Since the dynamic parameters of a structure are directly related to the boundary and loading conditions, accurate modal models need to be sensitive to these parametric changes. Peeters *et al.* (2005) conducted OMA on a stadium during a football game, where the modal parameters were observed to shift while the stadium was filling up, emptying as well as between when people were sitting or standing to cheer for a goal. The natural frequencies were reported to decrease when the stadium was filling up due to the added mass while the damping ratios increased. The durations over which modal parameters were estimated was crucial, and due to slow changes in the stadium structure, the PolyMAX technique was able to estimate and track the parameters. Goursat *et al.* (2010) conducted measurements on the space launcher Ariane 5, which is an example of a complex structure with rapidly changing system parameters. SSI was used with a sliding window to follow the time evolution of specific natural frequencies based on eigenvector tracking. The choice of sensor location was found to be critical for mode tracking and SSI was in general able to provide reliable estimates despite highly non-stationary data.

## 2.6 Conclusion

Direct ice force estimation provided valuable insight into the complex nature of ship ice interaction. The major limitation was the effect of variability of the impact location on the measured force. Indirect methods were proposed as a possible solution, allowing force estimates from global ship motions rather than local impact measurements. Indirect methods showed promising results and were expanded to include all six rigid body motions to estimate resultant forces. Current methods are limited by static system parameters mass  $M$ , damping  $D$  and stiffness  $K$ . The current research proposes a novel addition through the use of system identification to provide semi-real time system parameters. The concept is illustrated in Figure 2.6. Since OMA results in unscaled eigenvectors investigations into sensitivity based scaling methods will

also need to be performed. Techniques such as Parloo *et al.* (2002), Brincker and Andersen (2003) and Foltête (2008) can be used as sensitivity based scaling methods but are outside the scope of this thesis.

System identification also has the potential to monitor the health of a ship structure. This is done by building a model of the operational profile of a vessel in normal operation. Discrepancies in the measured behaviour and the predictive models can provide an indication of structural damage. This methodology could provide useful information in a broken ice field where current ice force estimation methods are limited by complex superposition of vessel motion.

Examples of system identification on ship structures provide a basis for the current idea development and insights into associated challenges. This was followed by insights regarding harmonics and modal tracking. In order to achieve inverse force estimation and structural health monitoring, system identification and modal tracking results need to be thoroughly investigated.

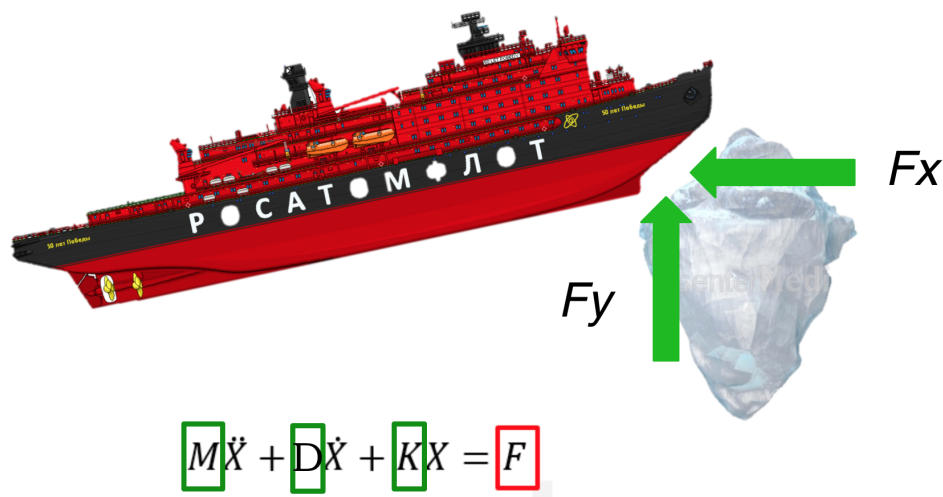


Figure 2.6: Simplified illustration of indirect force estimation method.

# Chapter 3

## openSID Open Source Stochastic Subspace Identification Toolbox

### 3.1 Introduction

System identification is a powerful tool for building mathematical models of dynamic systems based on observed data. In mechanical and civil engineering system identification is used to model the dynamic response of structures such as aircraft, ships or bridges in order to optimize their design, estimate input forces or perform structural health monitoring. Output only system identification, also known as Operational Modal Analysis (OMA) deals with identifying a mathematical model of a system without measured inputs. This is achieved by making assumptions about the unmeasured forces which are modelled as stochastic white noise quantities. This is particularly suited to large structures which cannot be tested in a laboratory, or excited sufficiently with shakers or modal hammers. It is also suited to structures where complex excitation forces and boundary conditions affect the system properties.

Advances in technology have reduced the cost of measurement sensors, data acquisition systems and computer hardware and software as well as improved measurement quality. The result is that system identification is finding new applications in various fields. It is therefore important that students and researchers are equipped with an understanding of the theoretical and experimental aspects of system identification in order to apply and innovate in different fields. Lennart Ljung (1987) the author of ‘System Identification: Theory for the User’ as well as the Mathworks System Identification toolbox advocates that the best way to master system identification is to combine theoretical knowledge with hands on data processing. At present the Mathworks System Identification toolbox remains proprietary over and above the standard Mathworks license, limiting it’s usefulness as a learning and development tool.

A number of modal analysis software packages currently exist. Most deal with the identification of systems from input/output data based on Frequency Response Functions (FRFs) or Impulse Response Function (IRFs). Output

only modal analysis software is also available, most notably from Siemens LMS and ARTEMIS which are commercial closed software. This has the drawback that it is impossible to access the implementation of the algorithm, and therefore not possible to add further developments, resolve bugs or innovate in ways not envisioned by the developers. Other options such as Modal Analysis on Civil Engineering Constructions (MACEC) from KU Leuven are Matlab based but require annual renewal of a license which limits its ability as a learning tool and innovative platform. Open source free toolboxes for signal processing and experimental modal analysis such as Abravibe by Brandt (2013) and the control engineering Subspace Identification for Linear Systems by van Overschee (2002) are examples of innovative learning and research platforms and inspired the development of the openSID toolbox presented in this work.

openSID is an open source system identification toolbox for structural dynamics, developed in the open on github. Open source software and development has proven to (1) drive innovation - by reducing developers time spent re-inventing advanced wheels and rather focusing on novel and unresolved challenges. (2) increasing security and reducing bugs - due to more eyes reading source code, as well as testing, applying and extending existing software. Since software written by humans will always contain bugs open source allows users to trouble shoot and implement bug fixes immediately rather than waiting for future software releases. (3) open source software is a force multiplier - Balter (2015) explains how this happens in three ways: firstly communities form around shared challenges (as opposed to individuals in one organisation) resulting in a diversity of ideas and optimal solutions. Secondly opening the problem to other interested developers provides additional human capital to solve the challenge. Thirdly more users mean more cases are explored resulting in more robust code. With software giants such as Microsoft, Apple and IBM increasing their active participation in open source community, the current software landscape is undergoing transformation, and open source is the innovative way of the future.

For these reasons the need for an open source toolbox which can be used both as a learning and research tool in output only system identification was identified. The current chapter presents the theory behind a powerful technique called Stochastic Subspace Identification (SSI). The theory is presented together with the relevant code as implemented in Matlab. Users can download the toolbox from <https://github.com/keithsoal/openSID>. In the following section the data driven and covariance driven SSI algorithms are presented, compared and extended to modal analysis. The openSID toolbox and GUI are then presented and discussed.

## 3.2 Theory of Output Only System Identification

The objective of system identification is to “identify” the unknowns in a mathematical model of a “system”. The concept of a system is illustrated in Figure 3.1 where  $u$  is the input,  $y$  is the output,  $w$  is the process noise and  $v$  is the measurement noise. Output only system identification, also known as Operational Modal Analysis (OMA) deals with identification of the system parameters from the system outputs  $y$  in the absence of measured system inputs  $u, w$  or  $v$ .

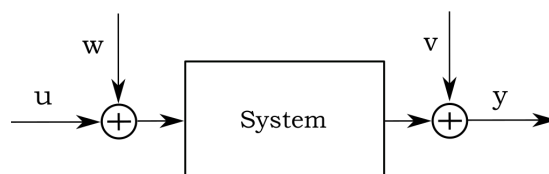


Figure 3.1: A system with interacting input variables  $u$ , observable output signals  $y$ , process noise  $w$ , and measurement noise  $v$ . (Adapted from Pintelon and Schoukens (2001))

In structural dynamics the “system” represents the physical structure. In this thesis this is the polar research vessel Polarstern. The input  $u$  are forces from waves, ice, engines and propellers. The output  $y$  is the structural response, which in this case is acceleration. The process noise  $w$  accounts for disturbances and modelling noise, and the measurement noise  $v$  accounts for noise from sensors and cables. The mathematical model of the system is described by Newton’s equation of motion

$$M\ddot{z}(t) + D\dot{z}(t) + Kz(t) = F(t) = bu(t) \quad (3.2.1)$$

where  $M, D, K \in \mathbb{R}^{n \times n}$  are the mass, damping and stiffness matrices of the  $n$  Degree Of Freedom (DOF) system.  $F(t) \in \mathbb{R}^{n \times 1}$  is the input force and  $z(t) \in \mathbb{R}^{n \times 1}$  is the displacement vector at time  $t$ . The input force is factorised into a matrix  $b \in \mathbb{R}^{n \times m}$  describing the spacial distribution of the inputs and a vector  $u(t) \in \mathbb{R}^{m \times 1}$  describing the  $m$  inputs in time.

## 3.3 State Space Model

The SSI algorithm is used to identify the system parameters by writing equation 3.2.1 in state space. State space is an expanded space guaranteed to contain the state description (Franklin *et al.*, 1990). Equation 3.2.1 is transformed into state space, through the introduction of a state vector  $x(t) \in \mathbb{R}^{N \times 1}$  ( $N = 2n$ )

$$x(t) = \begin{pmatrix} z(t) \\ \dot{z}(t) \end{pmatrix}. \quad (3.3.1)$$

The second order differential equation can then be written as a first order state equation

$$\dot{x}(t) = A_c x(t) + B_c u(t) \quad (3.3.2)$$

with

$$A_c = \begin{pmatrix} 0 & I_n \\ -M^{-1}K & -M^{-1}D \end{pmatrix}, \quad B_c = \begin{pmatrix} 0 \\ M^{-1}b \end{pmatrix} \quad (3.3.3)$$

where  $A_c \in \mathbb{R}^{N \times N}$  is the state matrix, and  $B_c \in \mathbb{R}^{N \times 1}$  is the input matrix. An observation equation is then defined, relating the  $l$  measured outputs  $y(t) \in \mathbb{R}^{l \times 1}$  to the state vector  $x(t)$

$$y(t) = Cx(t) + Eu(t) \quad (3.3.4)$$

through  $C \in \mathbb{R}^{l \times N}$  the output matrix and  $E \in \mathbb{R}^{l \times m}$  the direct transmission matrix. Equations 3.3.2 and 3.3.4 represent a continuous time deterministic state-space model. Since data is measured discretely ( $\Delta t$ ), the input-output data cannot be measured exactly (deterministically), and the input forces are unknown (assumed to be Gaussian white noise) the model is modified to a discrete-time deterministic-stochastic state-space model:

$$\begin{aligned} x_{k+1} &= Ax_k + w_k \\ y_k &= Cx_k + v_k \end{aligned} \quad (3.3.5)$$

with discrete time  $k\Delta t$ ,  $k \in \mathbb{N}$ , where  $x_k = x(k\Delta t)$  is the discrete time state vector,  $A = e^{(A_c \Delta t)}$  is the discrete state matrix. Stochastic noise components are included as  $w_k \in \mathbb{R}^{N \times 1}$  process noise due to disturbances and modelling inaccuracies and  $v_k \in \mathbb{R}^{l \times 1}$  measurement noise from the sensors, cables and data acquisition system. The reference based data driven SSI algorithm is a powerful time domain system identification technique, and will be explained in the following section. The interested reader is referred to Peeters and De Roeck (1999) and Van Overschee and De Moor (1996) for further details. The aim is to now identify the above parameters based on measured data. The main work flow of the SSI-Data method is illustrated in Figure 3.2 providing contextualisation of the sections which follow.

### 3.4 Data Driven Stochastic Subspace Identification (SSI)

The Stochastic Subspace Identification (SSI) algorithm is used to identify the state matrix  $A$  in the mathematical model of the system. The output mea-

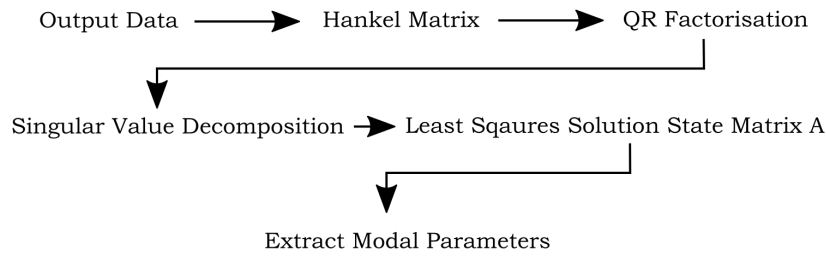


Figure 3.2: Work flow for SSI-Data.

measurements are built into a block Hankel matrix  $H$ , which is a square matrix with constant skew diagonals. The Hankel matrix has  $2 * i$  block rows and  $j = n_y - 2 * i + 1$  columns, where  $n_y$  is the number of samples. The first  $i$  blocks are known as the past reference  $Y_p^{ref}$  and have  $r$  rows. The last  $i$  blocks are known as the future output  $Y_f$  and have  $l$  rows.

$$H = \frac{1}{\sqrt{j}} \begin{pmatrix} y_0^{ref} & y_1^{ref} & \cdots & y_{j-1}^{ref} \\ y_1^{ref} & y_2^{ref} & \cdots & y_j^{ref} \\ \cdots & \cdots & \cdots & \cdots \\ y_{i-1}^{ref} & y_i^{ref} & \cdots & y_{i+j-2}^{ref} \\ \hline y_i & y_{i+1} & \cdots & y_{i+j-1} \\ y_{i+1} & y_{i+2} & \cdots & y_{i+j} \\ \cdots & \cdots & \cdots & \cdots \\ y_{2i-1} & y_{2i} & \cdots & y_{2i+j-2} \end{pmatrix} = \begin{pmatrix} Y_{0|i-1}^{ref} \\ Y_{i|2i-1}^{ref} \end{pmatrix} = \begin{pmatrix} Y_p^{ref} \\ Y_f \end{pmatrix} \begin{matrix} \updownarrow r * i \\ \updownarrow l * i \end{matrix} \in \mathbb{R}^{(r+l)i \times j} \quad (3.4.1)$$

Listing 3.1 shows the Matlab implementation of the Hankel matrix with no reference channels. It can be seen that the size of the matrix is  $2 * i * l \times j$ , is related to the maximum possible model order by  $maxorder = i/2$  since the poles occur in complex conjugate pairs. The structure of the Hankel matrix reveals that the time data is shifted by  $k = 2i$  consecutive columns in total. The Hankel matrix can therefore be thought of as a ‘data covariance’ matrix, functioning in a similar way to the convolution of the impulse response and shifted input vector resulting in the system response, which forms the basis of system modelling.

Listing 3.1: Hankel matrix - no reference channels ( $r = 1$ ).

```

1 ih = 2*i;
2 H = zeros(l*ih,j);
3 for k = 1:ih
4   H((k-1)*l+1:k*l,:) = y(:,k:k+j-1);
5 end
  
```

Listing 3.2 shows the reference based implementation. Here the Hankel matrix is built in two parts:  $H_p$  contains the first or ‘past’ measurements from time index  $k = 1 : i$  of the selected reference channels  $I_r$  only. While  $H_f$

contains the ‘future’ part of the measurements from time shift  $k = i + 1 : 2i$  for all the measurement channels.

Listing 3.2: Hankel matrix - reference channels ( $r < l$ ).

```

1 Hp = zeros(r*i,j); % past part
2 for k = 1:i
3   Hp((k-1)*r+1:k*r,:) = y(Ir,k:k+j-1);
4 end
5 Hf = zeros(l*i,j); % future part
6 for k = 1:i
7   Hf((k-1)*l+1:k*l,:) = y(:,k+i:k+i+j-1);
8 end
9 H = [Hp;Hf];

```

The number of block rows  $i$  is an important user defined parameter. Van Overschee and De Moor (1996) provide a suggestion where  $i = 2(\text{max order})/(\text{no. outputs})$ . Where the maximum order is the maximum number of modes expected to occur in the relevant bandwidth. Since the exact number of modes in a particular bandwidth is usually unknown, the maximum order is usually over specified. Also due to noise the maximum order should be chosen higher than the expected number of physical modes to account for the modelling of noise modes.

### 3.4.1 Projection

A key step of the SSI algorithm is the projection of the row space of the future outputs  $Y_f$  onto the row space of the past outputs  $Y_p^{ref}$  as shown in Figure 3.3. In the projection step the algorithm finds the orthogonal component of the future outputs in the direction of the past outputs. The idea of this projection is to retain the information in the past that is useful to predict the future.

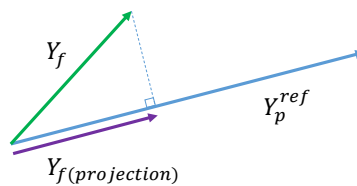


Figure 3.3: Future output  $Y_f$  projection onto past output  $Y_p^{ref}$ .

The projection is achieved by performing a QR-factorisation of the block Hankel matrix

$$H = \begin{pmatrix} Y_p^{ref} \\ Y_f \end{pmatrix} = RQ^T \quad (3.4.2)$$

where  $Q \in \mathbb{R}^{j \times j}$  is an orthonormal matrix  $Q^T Q = Q Q^T = I_j$  and  $R \in \mathbb{R}^{(r+l)i \times j}$  is a lower triangular matrix. Since  $(r+l)i < j$  we can omit the

zeros in  $R$  and the corresponding zeros of  $Q$ . Due to their orthonormality the  $Q$  factors cancel out, resulting in an important data reduction. The QR-factorisation of the Hankel matrix is then written in the following form

$$H = \begin{array}{c} ri \\ r \\ l-r \\ l(i-1) \end{array} \begin{array}{c} \updownarrow \\ \updownarrow \\ \updownarrow \\ \updownarrow \end{array} \begin{array}{cccc} ri & r & (l-r) & l(i-1) \\ \leftrightarrow & \leftrightarrow & \leftrightarrow & \leftrightarrow \\ \left( \begin{array}{cccc} R_{11} & 0 & 0 & 0 \\ R_{21} & R_{22} & 0 & 0 \\ R_{31} & R_{32} & R_{33} & 0 \\ R_{41} & R_{42} & R_{43} & R_{44} \end{array} \right) & \begin{array}{c} \leftrightarrow \\ \left( \begin{array}{c} Q_1^T \\ Q_2^T \\ Q_3^T \\ Q_4^T \end{array} \right) \end{array} \end{array} \quad (3.4.3)$$

Listing 3.3 presents the QR factorisation as well as the extraction of the R spaces, see Peeters and De Roeck (1999), for both the reference channel, and non-reference channel cases.

Listing 3.3: QR factorisation.

```

1 % QR Factorisation
2 R = triu(qr(H'))';
3 % {No reference channels}
4 Rf = R(l*i+1:2*l*i,:); % Future outputs
5 Rp = R(1:l*i,:); % Past outputs
6 % {Reference channels}
7 % Extract R spaces
8 R21 = R(r*i+1:r*i+r,1:r*i);
9 R31 = R(r*i+r+1:r*i+r+(l-r),1:r*i);
10 R41 = R(r*i+r+1+(l-r):r*i+r+(l-r)+l*(i-1),1:r*i);

```

In theory the projection  $\mathcal{P}_i^{ref}$  of the row space of the future outputs onto the row space of the past reference outputs is defined as

$$\mathcal{P}_i^{ref} = Y_f / Y_p^{ref} = Y_f Y_p^{refT} (Y_p^{ref} Y_p^{refT})^\dagger Y_p^{ref} \quad (3.4.4)$$

In practice this is achieved by substituting Equation 3.4.3 into 3.4.4. Resulting in the following simple expression for the projection based on the structure identified in Equation 3.4.3

$$\mathcal{P}_i^{ref} = \begin{pmatrix} R_{21} \\ R_{31} \\ R_{41} \end{pmatrix} Q_1^T \in \mathbb{R}^{li \times j} \quad (3.4.5)$$

Listing 3.4 presents the projection matrices  $P$  for the non-reference  $r == l$  and reference channel  $r < l$  cases. The variable AUXin is an auxiliary variable to increase the speed of the algorithm.

Listing 3.4: Oblique Projection.

```

1 if (isempty(AUXin)) && r == l
2   % no reference channels
3   P = [Rf(:,1:l*i), zeros(l*i,l*i)];
4 elseif (isempty(AUXin)) && r < l

```

```

5 | % reference channels
6 | P = [R21;R31;R41];
7 | else
8 | P = AUXin(bb+1:bb+l*i,1:2*(l)*i);
9 | bb = bb+l*i;
10| end

```

### 3.4.2 Main Theorem

The main theorem of SSI (Van Overschee and De Moor, 1996) states that the projection  $\mathcal{P}_i^{ref}$  can be factorised as the product of the observability matrix  $O_i$  and the Kalman filter state sequence  $\hat{X}_i$

$$\mathcal{P}_i^{ref} = O_i \hat{X}_i \quad (3.4.6)$$

where the observability matrix is defined as

$$O_i = \begin{pmatrix} C \\ CA \\ CA^2 \\ \dots \\ CA^{i-1} \end{pmatrix} \in \mathbb{R}^{li \times n} \quad (3.4.7)$$

The Kalman filter state estimates form the Kalman filter state sequence  $\hat{X}_i$

$$\hat{X}_i = (\hat{x}_i \hat{x}_{i+1} \dots \hat{x}_{i+j-1}) \in \mathbb{R}^{n \times j} \quad (3.4.8)$$

from the iterative predictor-corrector Kalman filter (Kalman, 1960)

$$\begin{aligned} \hat{x}_{k+1} &= A\hat{x}_k + K_k(y_k - C\hat{x}_k) \\ K_k &= (G - AP_k C^T)(\Lambda_0 - CP_k C^T)^{-1} \\ P_{k+1} &= AP_k A^T + (G - AP_k C^T)(\Lambda_0 - CP_k C^T)^{-1}(G - AP_k C^T)^T \end{aligned} \quad (3.4.9)$$

where  $\hat{x}_{k+1}$  is the optimal prediction for the future state,  $\hat{x}_k$  is the current state prediction,  $K_k$  is the Kalman filter gain,  $y_k$  is the output measurement,  $P_{k+1}$  is the state covariance matrix,  $G$  is the state output covariance matrix and  $\Lambda_0$  is the output covariance matrix.

The observability matrix  $O_i$  and the state sequence  $\hat{X}_i$  are obtained through a Singular Value Decomposition (SVD) of the projection matrix as follows

$$\mathcal{P}_i^{ref} = U_1 S_1 V_1^T \quad (3.4.10)$$

$$O_i = U_1 S_1^{\frac{1}{2}}, \quad \hat{X}_i = O_i^\dagger \mathcal{P}_i^{ref} \quad (3.4.11)$$

Before showing the implementation, a weighting technique is first introduced.

### 3.4.3 Weightings

There are three weighting methods for the projection matrix, the Principal Component (PC), Unweighted Principal Component (UPC) and the Canonical Variate Analysis (CVA). To the best of the authors knowledge there exists no conclusive study on real data regarding when the different techniques work best and why. The theory of the weighting methods can be found in Van Overschee and De Moor (1996). The implementation, which has been adapted by the current author to the reference based method, is presented in Listing 3.5.

Listing 3.5: Weighting methods (PC, UPC and CVA).

```

1  if W == 1 % PC algorithm
2      R11 = R(1:r*i,1:r*i);
3      Pw = P*R11';
4  elseif W == 2 % UPC algorithm
5      Pw = P;
6  else % CVA algorithm
7      R21 = R(r*i+1:2*i*r,1:r*i);
8      R22 = R(r*i+1:2*i*r,r*i+1:2*i*r);
9      wc = sqrtm(R21*R21'+R22*R22');
10     Pw = wc\P;
11 end

```

The weighted projection matrix  $P_w$  can then be decomposed using the SVD as shown in Listing 3.6

Listing 3.6: Singular Value Decomposition (SVD).

```

1  [U,S,V] = svd(Pw);

```

### 3.4.4 Subspace Selection

An important step in the determination of the system parameters is the selection of a subspace  $n$ . The size of the subspace determines the size of the state matrix  $A$  and therefore the number of modes contained in the model. The subspace must be chosen to include twice as many modes as occur in the analysis bandwidth since the eigenvalues occur in complex conjugate pairs. Since the number of modes occurring within a selected bandwidth is usually unknown at this point, the significant singular values  $S_1$  can be used as an indicator of the subspace dimension. Choosing the subspace dimension based on the significant singular values works well when the physical modes are well excited and when system, measurement and algorithm noise are negligible. This is usually not the case for real data. In this case a stabilization diagram should be used together with the singular values to determine the optimal subspace selection. This will be shown in the section which demonstrates the openSID toolbox. The subspace selection of the singular values  $S$  and vectors  $U$  is shown in Listing 3.7, which can be performed interactively in openSID toolbox. The

calculation of the observability matrix  $O_i$  and the state sequence  $X_h$  are also presented in Listing 3.7.

Listing 3.7: Subspace selection.

```

1 S1 = S(1:n);
2 U1 = U(:,1:n);
3 % observability matrix
4 Oi = U1*diag(sqrt(S1));
5 % state sequence
6 Xh = pinv(Oi)*P;

```

### 3.4.5 Determining the System Matrices

The aim is to now recover the desired system matrices  $A$  and  $C$  and covariances  $Q$ ,  $R$  and  $S$ , from the observability matrix  $O_i$  and the state sequence  $\hat{X}_i$ . This is achieved by introducing a shifted projection  $\mathcal{P}_{i-1}^{ref}$

$$\mathcal{P}_{i-1}^{ref} = Y_f^- / Y_p^{ref+} = \begin{pmatrix} R_{41} & R_{42} \end{pmatrix} \begin{pmatrix} Q_1^T \\ Q_2^T \end{pmatrix} \in \mathbb{R}^{l(i-1) \times j} \quad (3.4.12)$$

It should be noted that in order to implement equation 3.4.12, it must be zero padded to enable concatenation as shown in Listing 3.8.

Listing 3.8: Shifted projection matrix.

```

1 Ps = [R41,R42,zeros(size(R41,1),size(R33,2))];

```

The main theorem in equation 3.4.6 can be re-written in terms of the shifted parameters as follows

$$\mathcal{P}_{i-1}^{ref} = O_{i-1} \hat{X}_{i+1} \quad (3.4.13)$$

where  $O_{i-1}$  is built by deleting the last  $l$  rows of  $O_i$  computed in Equation 3.4.11. The shifted state sequence is then obtained as

$$\hat{X}_{i+1} = O_{i-1}^\dagger \mathcal{P}_{i-1}^{ref} \quad (3.4.14)$$

The Kalman state sequences  $\hat{X}_i$  and  $\hat{X}_{i+1}$  are now calculated using only the output data in Equations 3.4.11 and 3.4.14. The system matrices can then be recovered using the original and shifted Kalman state sequences and one block row of the Hankel matrix in the fundamental stochastic state space equation defined in Equation 3.3.5:

$$\begin{pmatrix} \hat{X}_{i+1} \\ Y_{i|i} \end{pmatrix} = \begin{pmatrix} A \\ C \end{pmatrix} \hat{X}_i + \begin{pmatrix} \rho_w \\ \rho_v \end{pmatrix} \quad (3.4.15)$$

where  $Y_{i|i}$  is a Hankel matrix with only one block row.  $Y_{i|i}$  is extracted using the structure identified in the QR-factorization

$$Y_{i|i} = \begin{pmatrix} R_{21} & R_{22} & 0 \\ R_{31} & R_{32} & R_{33} \end{pmatrix} \begin{pmatrix} Q_1^T \\ Q_2^T \\ Q_3^T \end{pmatrix} \in \mathbb{R}^{l \times j} \quad (3.4.16)$$

since the residuals  $(\rho_w^T \rho_v^T)^T$  are uncorrelated with  $\hat{X}_i$ , the set of equations can be solved for the system matrices  $A$  and  $C$  in a least-squares sense

$$\begin{pmatrix} A \\ C \end{pmatrix} = \begin{pmatrix} \hat{X}_{i+1} \\ Y_{i|i} \end{pmatrix} (\hat{X}_i^\dagger) \quad (3.4.17)$$

Listing 3.9 shows the implementation of the above theory in order to determine  $A$  and  $C$ .

Listing 3.9: Determination of  $A$  and  $C$ .

```

1 Ois = Oi(1:l*(i-1),:); % shifted observability matrix
2 Xhs = pinv(Ois)*Ps; % shifted state sequence
3 Yii = [R21 R22 zeros(size(R22,1),size(R33,2));R31 R32 R33];
4 Rhs = [Xh,zeros(n,l)];
5 Lhs = [Xhs;Yii];
6 sol = Lhs/Rhs; % Solve least squares
7 % Extract the system matrices A and C
8 A = sol(1:n,1:n); % state matrix
9 C = sol(n+1:n+l,1:n); % output matrix

```

The noise covariances  $Q$ ,  $R$  and  $S$ , are recovered as the covariances of the residuals in Equation 3.4.15, as implemented in Listing 3.10. This guarantees the positive realness of the identified covariance sequence.  $A$ ,  $C$ ,  $Q$ ,  $R$  and  $S$  can be transformed into  $A$ ,  $G$ ,  $C$ ,  $\Lambda_0$  by solving the Lyapunov equations. This is shown in Listing 3.10 which uses the Matlab control toolbox function *dlyap.m* which solve discrete Lyapunov equations to determine  $G$  and  $L0$  and the *gl2kr.m* function which solves for the Kalman gain  $K$  and the innovation covariance  $Ro$  using  $A$ ,  $G$ ,  $C$  and  $L0$  in the Riccati solution. Interested readers are referred to Penzl (1998) regarding the details of *dlyap.m*, and Van Overschee and De Moor (1996) for details of *gl2kr.m*.

Listing 3.10: Determination of  $Q$ ,  $S$ ,  $R$ ,  $G$ ,  $L0$ ,  $K$  and  $Ro$ .

```

1 % Determine the residuals
2 res = Lhs - sol*Rhs;
3 % Determine QSR from the residuals
4 cov = res*res'; % Covariance
5 Qs = cov(1:n,1:n);
6 Ss = cov(1:n,n+1:n+l);
7 Rs = cov(n+1:n+l,n+1:n+l);
8 % Determine system matrices G,L0
9 sig = dlyap(A,Qs);
10 G = A*sig*C' + Ss;
11 L0 = C*sig*C' + Rs;
12 % Determine Kalman gain K and system noise covariance Ro
13 % Riccati solution
14 [K,Ro] = gl2kr(A,G,C,L0);

```

While the parameters  $Q, S, R, G, L0, K$  and  $Ro$  are not required to determine the eigenvalues and eigenvectors of the system, they can be useful when the intention of modelling the system is to perform inverse force estimation or damage detection in state space. For this reason future versions of openSID will also include Lyapunov and Riccati solution functions which do not rely on the Matlab control toolbox.

### 3.5 Covariance Driven SSI

The covariance-driven algorithm is based on the covariance matrices between all the outputs and a set of reference outputs. The covariance matrices are defined as  $\Lambda_i^{ref} = E[y_{k+i} y_k^{refT}]$ . The covariances are built in a block Toeplitz matrix, where each diagonal from left to right is constant

$$T_{1|i}^{ref} = \begin{pmatrix} \Lambda_i^{ref} & \Lambda_{i-1}^{ref} & \cdots & \Lambda_1^{ref} \\ \Lambda_{i+1}^{ref} & \Lambda_i^{ref} & \cdots & \Lambda_2^{ref} \\ \cdots & \cdots & \cdots & \cdots \\ \Lambda_{2i-1}^{ref} & \Lambda_{2i-2}^{ref} & \cdots & \Lambda_i^{ref} \end{pmatrix} \in \mathbb{R}^{li \times ri} \quad (3.5.1)$$

The correlation matrix  $R$  is built using the `xcorr.m` function in Matlab as shown in Listing 3.11. The correlation function with time lags greater than zero is then selected and an additional user defined time lead is defined due to improved numerical results.

Listing 3.11: Correlation matrix.

```

1 % correlation matrix
2 for nn = 1:ir
3   for m = 1:l
4     [R(:,m,nn),t] = xcorr(y(:,m),Y(:,nn),'unbiased');
5   end
6 end
7 % correlation from 0 lag with time shift (lead)
8 [~,lag] = find(t==0);
9 for nn = 1:ir
10  for m = 1:l
11    Rs(:,m,nn) = R(lag+lead:end,m,nn);
12  end
13 end

```

The Toeplitz matrix is built from the correlation matrix  $R$  by first building a Hankel matrix and then flipping it as shown in Listing 3.12.

Listing 3.12: Toeplitz matrix.

```

1 % Build block Hankel matrix
2 Hank=zeros(l*i,r*i);
3 for c = 1:i
4   for w = 1:i
5     Hank(1+(w-1)*l:w*l,1+(c-1)*r:c*r)=squeeze(R(w+c-1,,:))';

```

```

6   end
7   end
8   % Flip Hankel matrix to Toeplitz matrix
9   Toep = flip(Hank,2);

```

An important user defined parameter is the block size of the Toeplitz matrix  $i$ . This determines the length of covariance function, or the amount by which the two random variables are shifted relative to one another. Since covariances at large time lags are expected to have weaker relationships, less information is included in the Toeplitz matrix as  $i$  increases.

Assuming ergodicity, where the time average is the same as the system state average, the block Toeplitz matrix can be decomposed into an observability matrix  $O_i$ , see equation 3.4.7, and a reference-reversed controllability matrix  $C_i^{ref}$

$$T_{1|i}^{ref} = O_i C_i^{ref} \quad (3.5.2)$$

where

$$C_i^{ref} = (A^{i-1}G^{ref} \ A^{i-2}G^{ref} \ \dots \ AG^{ref} \ G^{ref}) \in \mathbb{R}^{n \times ri} \quad (3.5.3)$$

The observability matrix  $O_i$  and the reference-reversed controllability matrix  $C_i^{ref}$  can be determined by finding the SVD of the block Toeplitz matrix

$$T_{1|i}^{ref} = USV^T = (U_1 U_2) \begin{pmatrix} S_1 & 0 \\ 0 & 0 \end{pmatrix} \begin{pmatrix} V_1^T \\ V_2^T \end{pmatrix} = U_1 S_1 V_1^T \quad (3.5.4)$$

Where  $U \in \mathbb{R}^{li \times li}$  and  $V \in \mathbb{R}^{ri \times ri}$  are orthonormal matrices  $U^T U = U U^T = I_{li}$  and  $V^T V = V V^T = I_{ri}$  and  $S \in \mathbb{R}^{li \times ri}$  is a diagonal matrix containing the singular values. The rank of the matrix product  $O_i C_i^{ref}$  is found as the number of non-zero singular values in  $S$ . Using equation 3.5.2 and 3.5.4 the observability matrix  $O_i$  and controllability matrix  $C_i^{ref}$  can be written as

$$\begin{aligned} O_i &= U_1 S_1^{1/2} \\ C_i^{ref} &= S_1^{1/2} V_1^T \end{aligned} \quad (3.5.5)$$

From equations 3.4.7 and 3.5.3,  $C$  can be seen to be the first  $l$  rows of  $O_i$  and  $G^{ref}$  the last  $r$  columns of  $C_i^{ref}$ . The state matrix  $A$  can then be solved by decomposing a shifted block Toeplitz matrix

$$T_{2|i+1}^{ref} = O_i A C_i^{ref} \quad (3.5.6)$$

Which can be written in terms of  $A$  using equation 3.5.5

$$A = O_i^\dagger T_{2|i+1}^{ref} C_i^{ref \dagger} \quad (3.5.7)$$

The main steps for determining the observability  $O_i$  and reference-reversed controllability  $C_i$  matrices, the shifted Toeplitz matrix  $Toeps$  and the state matrix  $A$  from the above theory are shown in Listing 3.13.

Listing 3.13: The observability, controllability, shifted Toeplitz and state matrices.

```

1 Oi = U1*diag(sqrt(ss(1:n))); % Observability
2 Ci = diag(sqrt(ss(1:n)))*transpose(V1); % Controllability
3 % Shifted Toeplitz
4 for c = 1:i
5     for w = 1:i
6         Hanks(1+(w-1)*l:w*l,1+(c-1)*r:c*r)=squeeze(R(w+c, :, :))';
7     end
8 end
9 Toeps = flip(Hanks,2);
10 A = pinv(Oi)*Toeps*pinv(Ci); % State matrix

```

### 3.6 Data vs. Covariance Driven SSI

The main similarities between SSI-Data and SSI-Covariance include a data reduction step: (SSI-Data) using QR factorisation and SVD and (SSI-Covariance) a covariance estimation and SVD. Followed by a subspace selection in order to determine the system matrices. The main differences include faster SSI-Covariance computational times. This is due to the numerical implementation of the covariance convolution performed by complex conjugate multiplication in the frequency domain, outperforming the slower QR factorisation. The drawback is that the covariance estimates may be less accurate due to leakage as a result of the Fourier transform. Advantages of SSI-Data are that it is a numerically robust square root algorithm unlike SSI-Covariance. SSI-Data also has guaranteed positive realness which enables the determination of the full  $G$  matrix which is necessary for the forward innovation form to estimate the Kalman gain  $K$ , the system noise covariance  $R_0$  and the one step ahead prediction  $\hat{x}_k$ .

### 3.7 Modal Analysis

The goal of modal analysis is to create a physically meaningful model which describes the dynamic behaviour of the structure. This is achieved by describing a structure in terms of its modes of vibration which can be characterised by a natural frequency, a damping ratio and a mode shape (eigenvalues and eigenvectors). These modal parameters can be determined from an eigenvalue decomposition of the state matrix ( $A$ )

$$A = \Psi \Lambda \Psi^{-1} \quad (3.7.1)$$

where  $\Lambda = \text{diag}(\lambda_q) \in \mathbb{C}^{n \times n}$ ,  $q = 1, \dots, n$ , is a diagonal matrix containing the discrete-time complex conjugate eigenvalues and  $\Psi \in \mathbb{C}^{n \times n}$  contains the eigenvectors. Since the state matrix is discrete it must be related to the continuous time equations in order to have physical meaning as follows

$$A = e^{(A_c \Delta t)} \quad (3.7.2)$$

$$\Psi_c = \Psi, \quad \lambda_{cq} = \frac{\ln(\lambda_q)}{\Delta t} \quad (3.7.3)$$

The eigenvalues occur in complex conjugate pairs and can be written as:

$$\lambda_{cq}, \lambda_{cq}^* = -\zeta_q \omega_q \pm j \omega_q \sqrt{1 - \zeta_q^2} \quad (3.7.4)$$

where  $\omega_q$  is the natural frequency of mode  $q$ , and  $\zeta_q$  is the damping ratio of mode  $q$ . The estimated states of the system  $x_k$  do not necessarily have a physical meaning, and the eigenvectors of the state matrix  $\Psi_c$  must be transformed using the observation matrix  $C$  to obtain physical eigenvectors  $\Phi$

$$\Phi = C\Psi_c \in \mathbb{C}^{l \times n} \quad (3.7.5)$$

This is achieved in Matlab as shown in Listing 3.14.

Listing 3.14: Modal analysis.

```

1 % eigenvalue problem
2 [Vs,Ds] = eig(A);
3 % Convert eigenvector to have physical meaning
4 Vs = C*Vs;
5 % extract modal parameters from state space identification
6 ws = abs(log(Ds)/(1/fs));
7 d = (-real(log(Ds)/(1/fs))./ws)*100;
8 fn = ws/(2*pi);

```

## 3.8 openSID Toolbox and GUI

This section describes the functionality of the openSID toolbox. openSID can be downloaded for free at <https://github.com/keithsoal/openSID>, and added to the Matlab path by running *opensid.m*. This provides access to the toolbox without needing to navigate to the file locations. All openSID functions begin with *os\_* standing for ‘open system’. openSID uses selected functions from the Abravibe toolbox of Brandt (2011), and the system identification toolbox by Van Overschee and De Moor (1996).

Since the aim of openSID is to provide a scripted toolbox for learning and research purposes the functions and layout are kept flexible. A demonstration is provided by *opensid\_demo.m*, and displays the toolbox functionality as follows: (1) a simulated data set is generated by *os\_generateData.m*. (2) a class is defined by ‘*os\_dataVisual.m*’ which builds a GUI allowing the user to view time data, see Figure 3.4, PSD’s see Figure 3.5 and statistical moments, see Figure 3.6.

System identification can then be performed using SSI-Data *os\_ssid.m* or SSI-Covariance *os\_ssic.m* algorithms. Both functions have the structure with

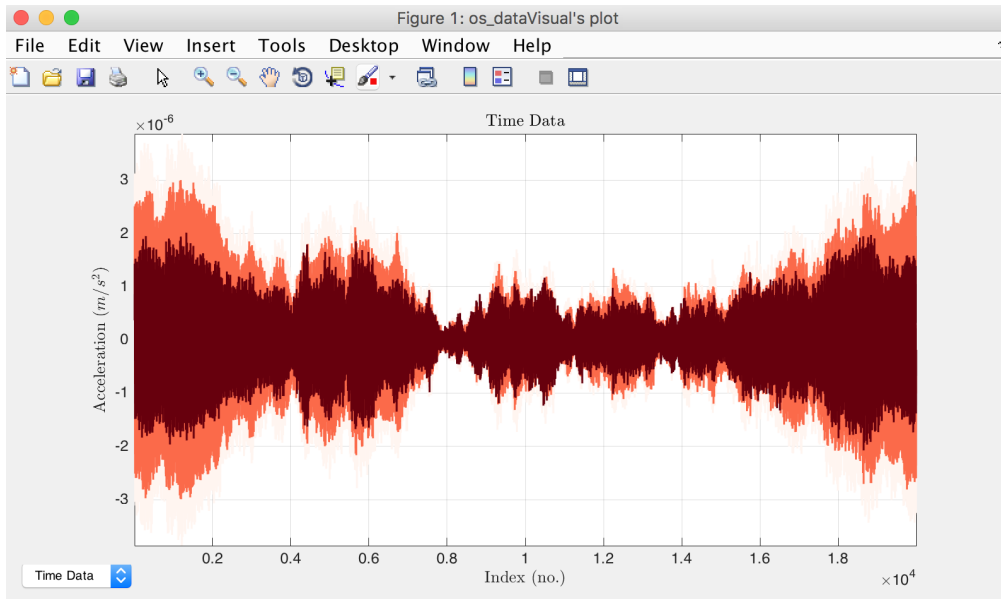


Figure 3.4: Time data.

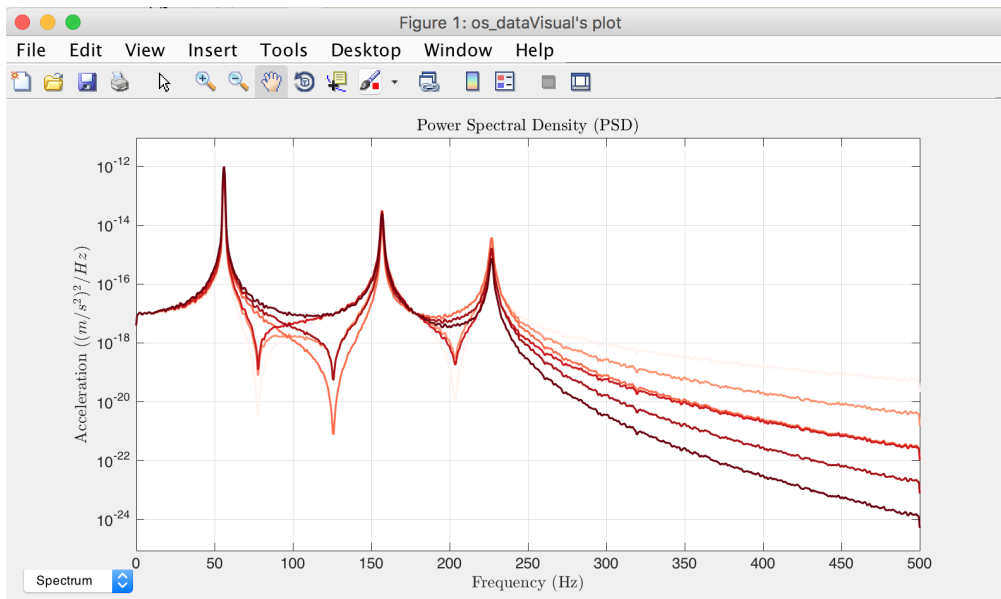


Figure 3.5: Power spectral density.

function inputs:  $y$  measured output data,  $i$  block size,  $fs$  sample frequency,  $Ir$  reference channels,  $W$  weighting,  $n$  model order,  $AUXin$  auxiliary variable to increase computational speed and  $sil$  display variable. The function outputs consist of  $sys = [A, C, K, Ro, AUX]$  and  $modal = [ss, EW, fn, d, EV]$  where  $A$  state matrix,  $C$  output matrix,  $K$  Kalman filter gain matrix,  $Ro$  system error covariance,  $AUX$  optional auxiliary variable to increase speed,  $ss$  singular values from the SVD of the projection matrix,  $EW$  complex conjugate eigenvalues (Eigenvalue),  $fn$  eigenfrequency (Hz),  $d$  damping ratio (%) and

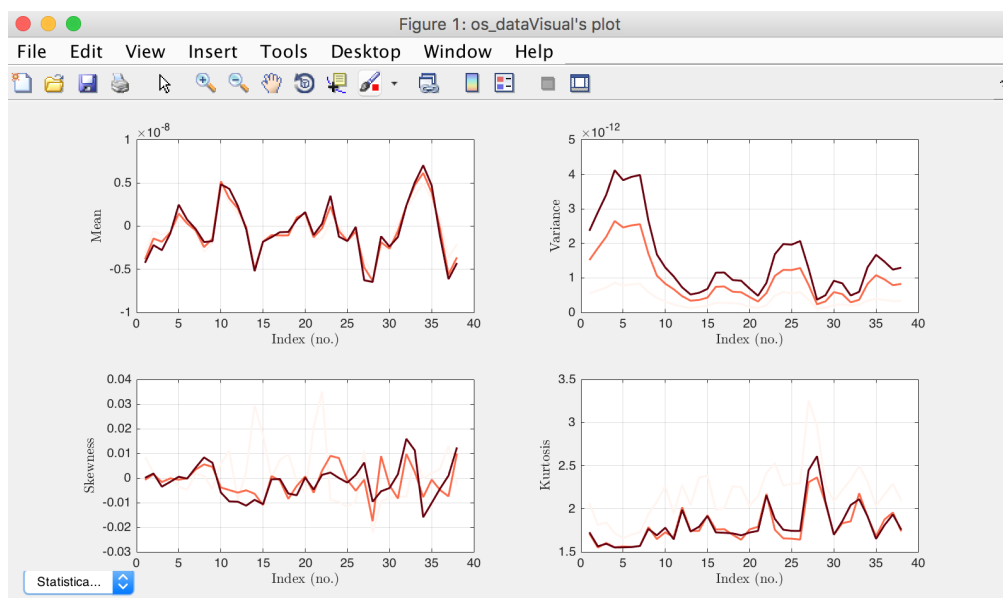


Figure 3.6: Statistical moments.

$EV$  mode shape (rotated but unscaled) (Eigenvector).

A stabilisation diagram is then built using *os\_stabilisation.m* as shown in Figure 3.7. A mode indicator function (MIF) is plotted in the background together with the singular values from the SVD of the projection matrix. The MIF is used as an indication of the agreement between the identified poles and the frequency spectrum of the measured data, and the singular values provide an indication of the number of physical poles and therefore the model order of the system. The identified poles are then plotted at consecutive model orders as  $\circ$  representing poles stable in frequency within 0.1 % and damping within 5 %. Unstable poles are plotted as  $\times$ . The user is then requested to select physical poles by clicking close to the desired pole at the respective model order.

The results of the system identification are then displayed in a plot of the modal assurance criterion (MAC) Figure 3.8, the modal complexity Figure 3.9, the mode shapes Figure 3.10 as a modal validation step.

### 3.9 Conclusion

In this chapter system identification was presented as a tool for building mathematical models of structural dynamic systems. The focus was to present the theory together with the implemented code to provide insight and understanding for students and researchers interested in applying system identification techniques. To this end SSI-Data and SSI-Covariance were described, compared and extended to output only modal analysis. openSID was then introduced as an open source toolbox for system identification in structural dynamics, and an innovative platform for learning and research purposes.

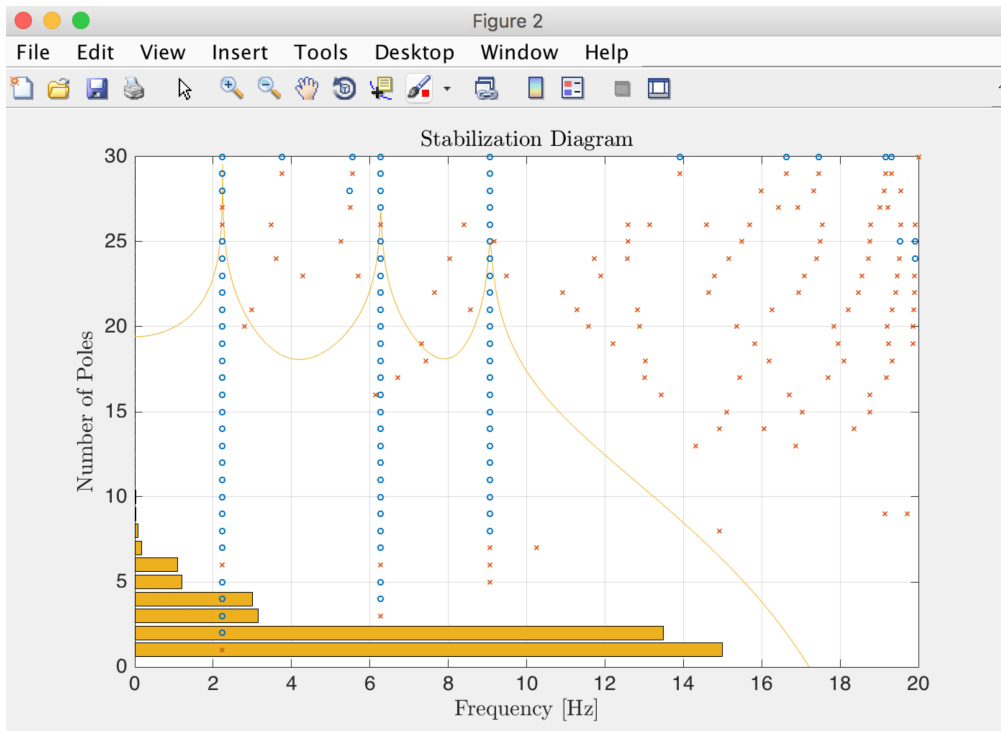


Figure 3.7: Stabilisation diagram.

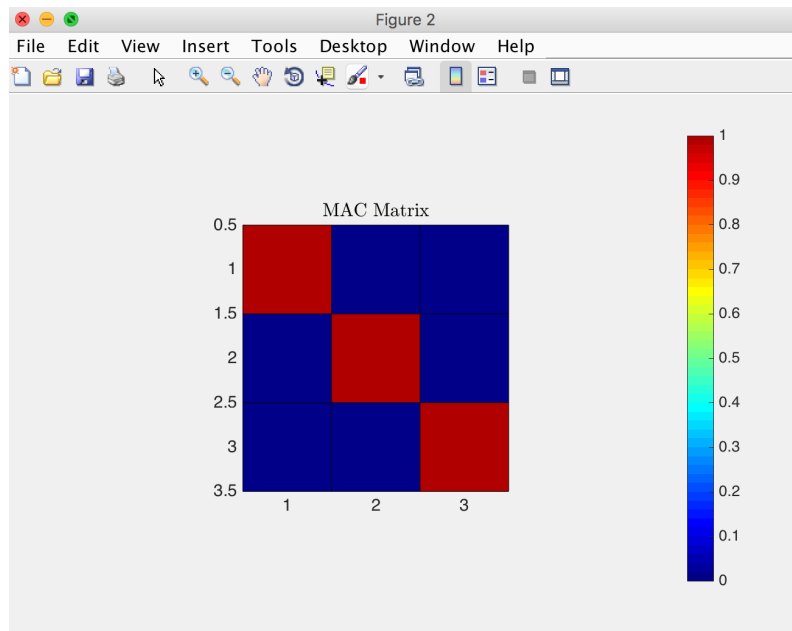


Figure 3.8: MAC matrix.

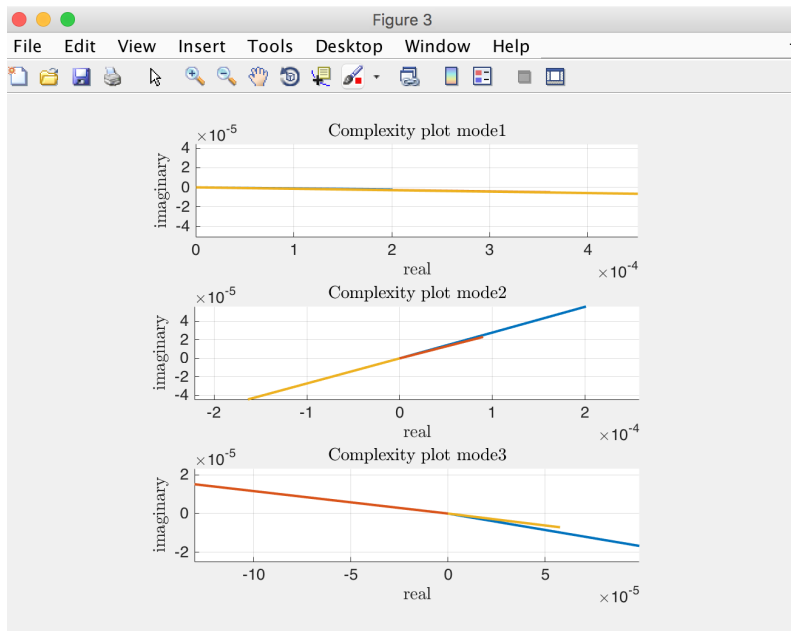


Figure 3.9: Complexity plot.

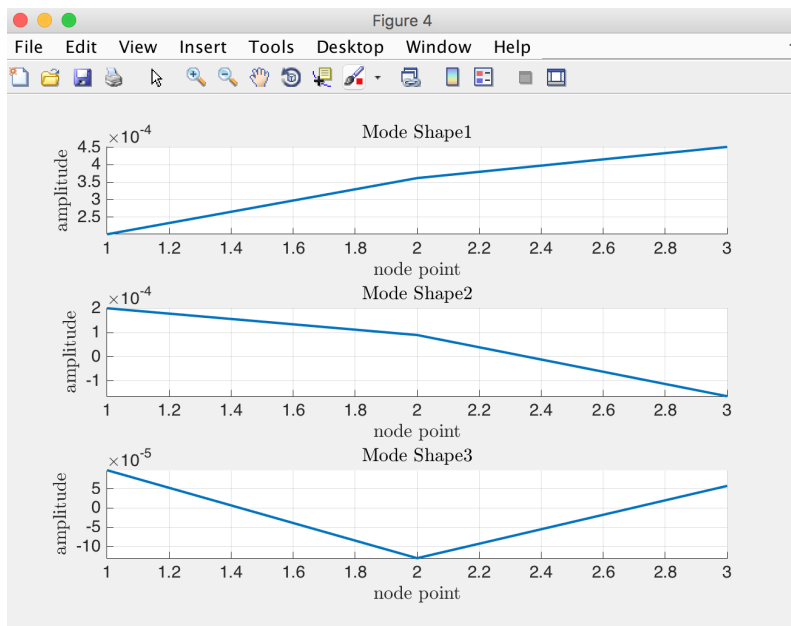


Figure 3.10: Mode shapes.

# Chapter 4

## Parametric Simulation Study

### 4.1 Introduction

In order to study the performance of SSI, a parametric study was conducted using simulated data to investigate the following phenomena (1) model order, (2) block size, (3) noise, (4) reference channels, (5) damping, (6) harmonics, (7) linear time invariance and (8) total prediction error. These parameters are investigated with regard to the following questions:

1. What is the relationship between block size  $i$  and model order  $n$ ? How should these parameters be chosen? And what is the effect of very large block sizes and model orders i.e. over-specifying the model?
2. What provides more accurate estimates SSI-Data or SSI-Covariance?
3. What is the effect of noise, reference channels, damping, harmonics and linear time invariance on the identification algorithms?
4. What is the relationship between the modal parameters,  $f_n, \zeta, \Phi$ , and the prediction error  $\epsilon$ ?

The simulated data for a 3 DOF system was generated in Matlab with white noise excitation, sample frequency  $f_s = 1000$  Hz and data length of 480 000 samples.

### 4.2 Model Order

The model order  $n$  determines the size of the subspace used for the estimation of the state matrix  $A$ . The size of the state matrix determines how many complex conjugate eigenvalues can be estimated and therefore the number of modes contained in the model. In practice  $n$  can be chosen by counting the number of peaks in a frequency spectrum, or the number of significant singular values. Practical experience with parametric models have shown that

it is better to over specify the model order and eliminate spurious numerical poles during post processing.

A popular approach for selecting the model order, see Ewins (2000) and Maia *et al.* (1997), involves plotting the identification results at increasing model orders in a stabilization diagram. By over specifying the model order physical poles remain stable and can be separated from spurious poles which are identified differently at different model orders. Stability limits are commonly set as  $\Delta f < 1\%$ ,  $\Delta\zeta < 5\%$  and  $\Delta MAC < 2\%$ . Using data from a 3 DOF simulated system excited with Gaussian white noise at all 3 DOFs results in the stabilisation diagram shown in Figure 4.1. All three poles are identified as stable from model order 8 to 30.

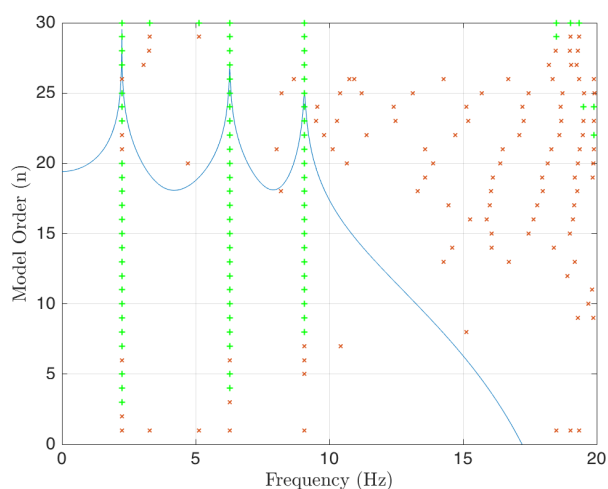


Figure 4.1: Stabilization diagram for SSI-Data with block size  $i = 30$ . ● MIF, + Stable pole, × Unstable pole.

Figure 4.2 presents the percentage error compared to the analytical solution of the frequency, damping and MAC for each mode using SSI-Data + and SSI-Covariance □. SSI-Covariance is seen to provide more accurate and stable estimates of the frequency of mode 1 and 3. The system damping and mode shapes are in general estimated more accurately by SSI-Data. Both methods show the possibility of an estimation bias such as in the damping estimate for mode 2. Furthermore SSI-Covariance shows a trend of underestimating the mode shape. It is suggested in literature, (Ewins, 2000; Heylen *et al.*, 1997; Maia *et al.*, 1997), that the model order be chosen at the lowest stable order, as higher model orders result in over fitting which can distort the parameters (especially the damping). In the current investigations the modal parameters are however seen to remain stable even at high model orders. Finally, the three DOF system is theoretically fully determined at a model order  $n = 6$ . The best estimates are indicated in green, and are seen to occur at model orders both higher and lower than 6, but never exactly at 6. There is also no clear trend regarding either method as to how to choose the best model order.

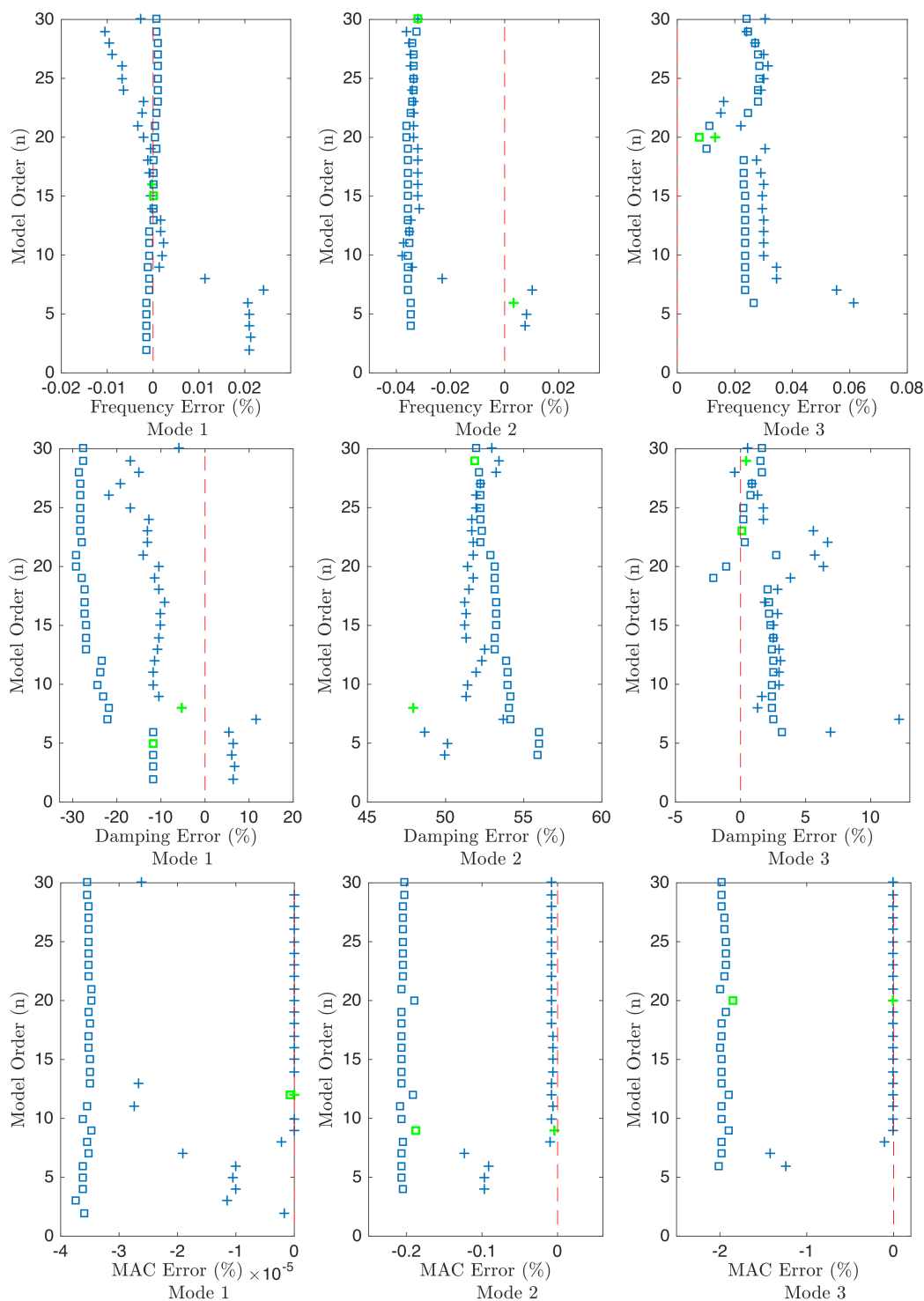


Figure 4.2: Frequency, damping and Modal Assurance Criterion (MAC) errors for SSI-Data '+' and SSI-Covariance '□' with block size  $[i = 30]$ . Minimum errors are indicated in green '+, □'

### 4.3 Block Size

The block size  $i$  determines how much data is included in the Hankel matrix  $[(r+l)i \times j]$  in SSI-Data, and the length of the covariance sequences included in the Toeplitz matrix  $[li \times ri]$  in SSI-Covariance. In both cases  $r$  is the number of reference sensors and  $l$  is the total number of sensors. The number of columns of the Hankel matrix is  $j = ly - 2i + 1$  where  $ly$  is the number of sample points in each channel. Increasing the block size therefore has the effect of increasing the row dimension by  $(r+l)i$  while decreasing the column dimension by  $2i$  of the Hankel matrix. The row size therefore increases faster than the column size decreases. Together with the fact that  $H_{columns} \gg H_{rows}$  this has the effect that large block sizes result in very large Hankel matrices which become slow or impossible (due to RAM availability) to solve. Increasing the block size of the Toeplitz matrix has the effect of including longer covariance sequences known as the tails of the covariance function which contain less information due to low correlation at large time lags. The size of the Toeplitz matrix is significantly smaller than the Hankel matrix due to the covariance data reduction step which is also performed very efficiently in the frequency domain.

The mathematical relationship between the block size and model order is that the maximum model order is determined by  $r \times i$  where  $r$  is the number of reference channels. Peeters (2000) states that the block size should be chosen such that it is significantly larger than the desired model order  $i \gg n$ . Especially if the model is required to identify poles which are buried in noise. The relationship between the block size, model order and identified parameters has not been thoroughly investigated in literature. The use of large block sizes has been recommended for future work by Zhang *et al.* (2015) due to findings on full scale bridge measurements. The current authors have also observed improved estimations using large block sizes on full scale ship data. An important question is whether there may be divergence at large block sizes.

The results of the frequency, damping and MAC errors for increasing block size  $i$  with model order  $n = 6$  are presented in Figure 4.3. Both SSI-Data and SSI-Covariance show convergence. SSI-Covariance shows improved frequency estimates, while SSI-Data shows improved mode shape estimates. Damping is equally well estimated by both methods. The result of increasing the maximum block size to 300 is shown in Figure 4.4. Both SSI-Data and SSI-Covariance remain stable and show convergence at high model orders. While the optimal block size, indicated in green, is generally under 100, this could be different when the estimations are performed on real data with higher modal densities and more noise.

### 4.4 3D Visualisation

The relationship between block size  $i$ , model order  $n$  and % error for the frequency estimates of SSI-Data are plotted in 3D in Figure 4.5. Large block

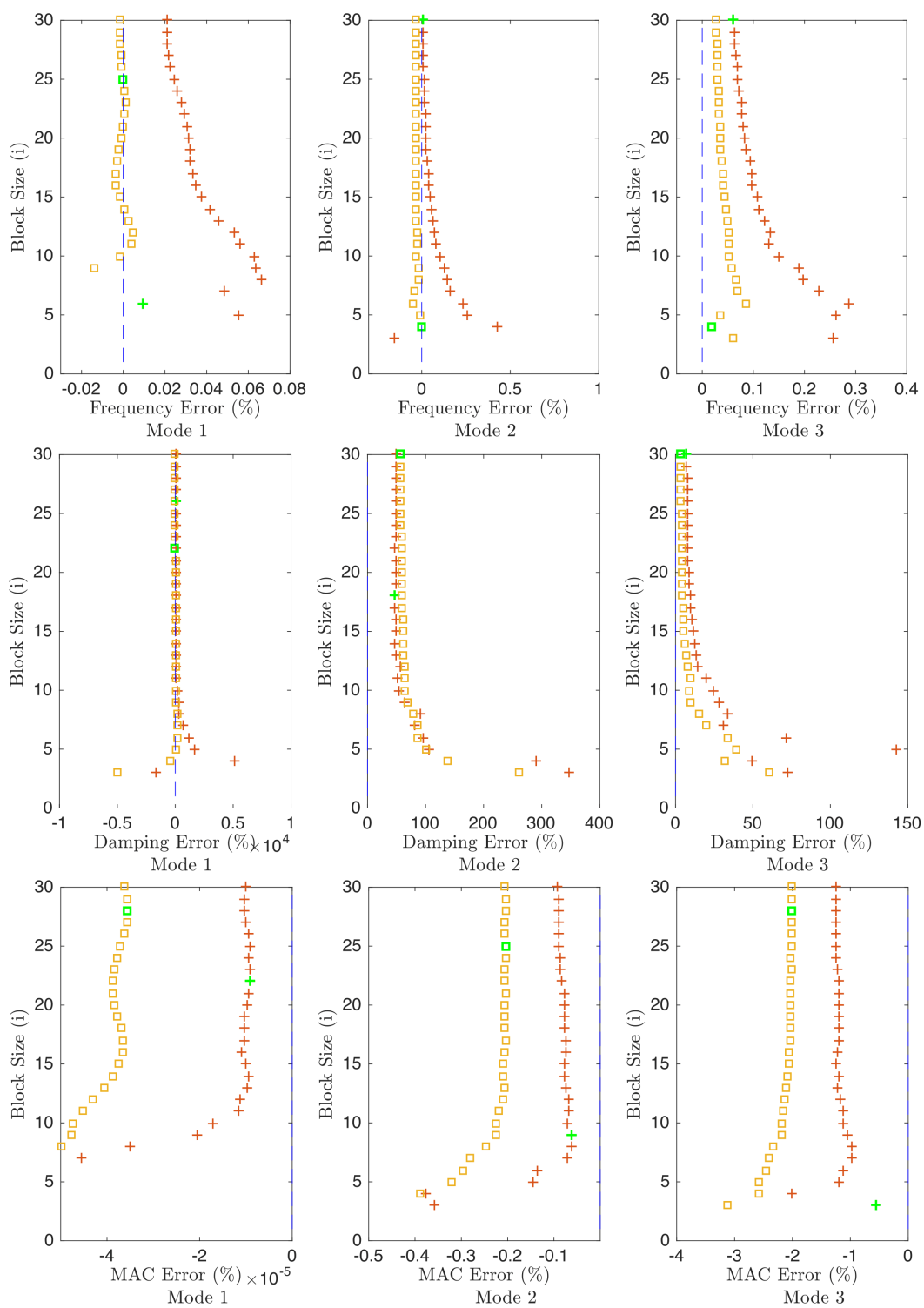


Figure 4.3: Frequency, damping and MAC errors for SSI-Data + and SSI-Covariance □ for increasing block sizes to (i = 30) with a fixed model order (n = 6).

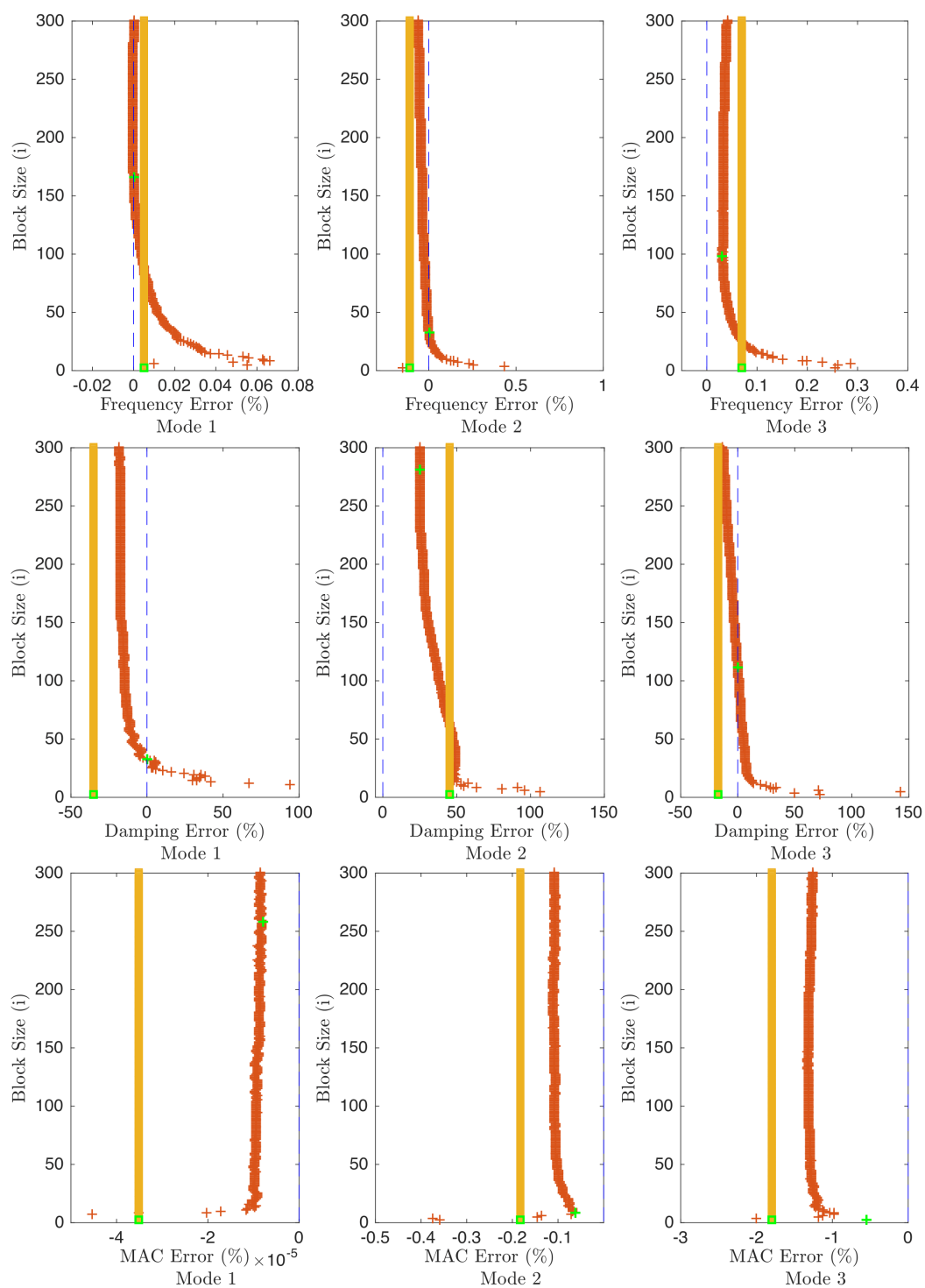


Figure 4.4: Frequency, damping and MAC errors for SSI-Data + and SSI-Covariance □ for increasing block sizes to ( $i = 300$ ) with a fixed model order ( $n = 6$ ).

sizes often result in the identification of several closely spaced modes. When

these estimates are close to a real pole it may be difficult to choose the best solution. The three Figures in Figure 4.5 row (a) show the worst estimate for the three modes respectively while row (b) shows the best estimate. It is therefore an important task to determine the best identification parameter from real data which does not have an analytical solution. It can be seen that the % error is smallest in the region of high block size with low model order.

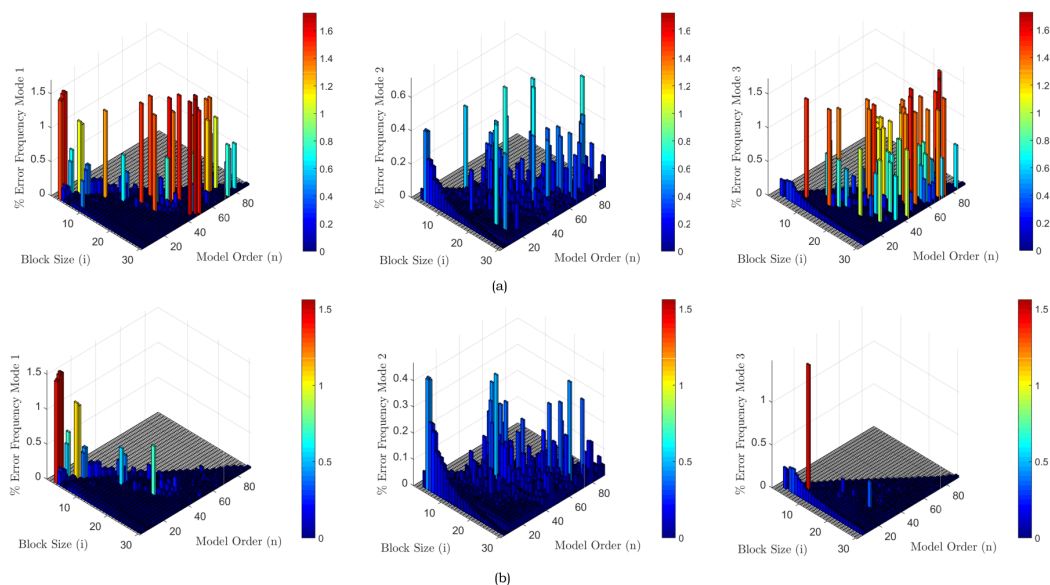


Figure 4.5: 3D plot of block size (i), model order (n) and % error in frequency.

## 4.5 Noise

Noise is a characteristic part of our physical universe. It is inherent in structural dynamic systems due to sensors, cables, modelling inaccuracies, finite data length, finite precision numbers and signal pre and post processing techniques. To investigate the effect of noise on the SSI algorithms, Gaussian white noise was added to each channel with an RMS equal to  $x\%$  of the RMS of the respective channel. Figure 4.6 shows the result of (a) frequency, (b) damping and (c) MAC errors as a result of 0 %, 10 %, 20 % and 50 % noise in a box and whisker plot. Firstly it can be seen that for mode 1 frequency error and mode 2-3 MAC error, adding noise to the signal has the effect of improving the mean error. This should be kept in mind when adding noise to simulated data in order to make it more realistic. It can also be seen that as the % noise is increased the variance of the estimates increases. The variance in the modal parameters is effected differently with frequency variance of  $\sim 0.07\%$ , damping variance  $\sim 34\%$  and MAC variance  $\sim 0.2\%$  at 20 % added noise. The reason for this result is thought to be due to the basis assumption of SSI which is that the system is excited by Gaussian white noise. Therefore as the

input signal is made more white, the identification results improve, up to a point where the signal is drowned out by the noise. Figure 4.6 (d) shows the frequency spectra of a signal with (d1) 0 %, (d2) 10 % and (d3) 80 % noise. Here it can be seen that the spectrum is more white at 10 % noise and that the third peak disappears at 80 % noise.

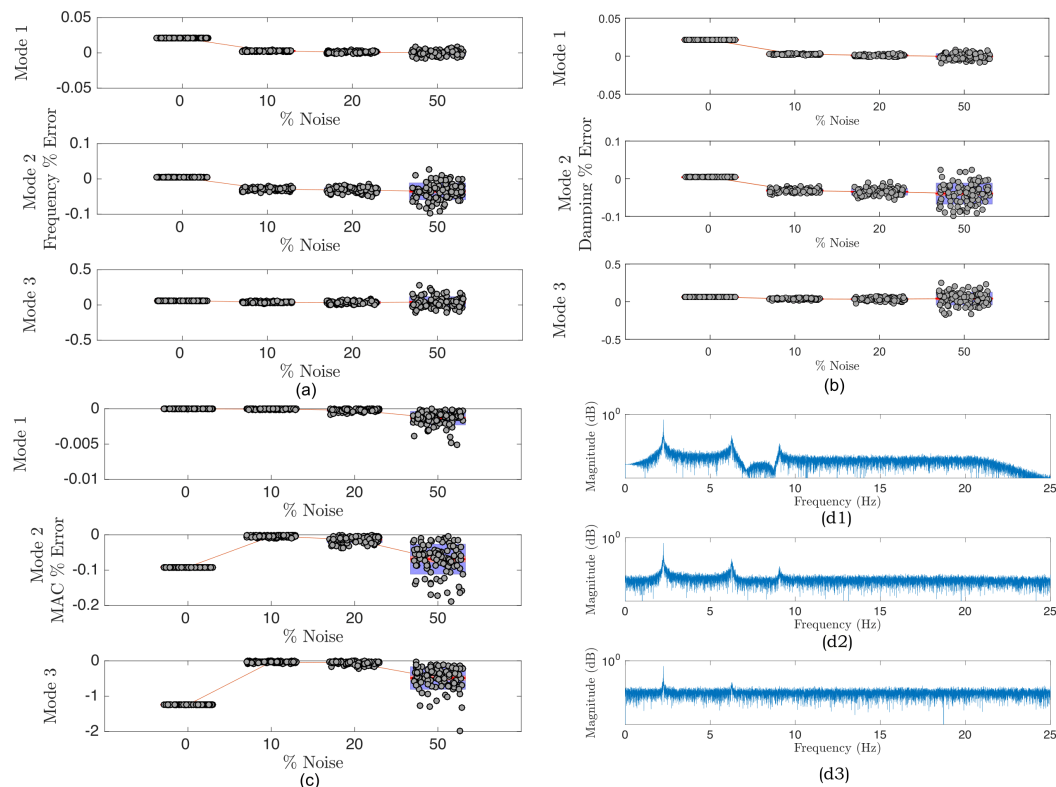


Figure 4.6: (a-c) Box and whisker plots of errors as a result of different noise levels. (d) FFT of signal with (d1) 0 % noise (d2) 10 % noise and (d3) 80 % noise

## 4.6 Reference Channels

Reference channels refer to a subset of channels (data subset) which can be used to reduce the computational cost on large data sets, as well as to improve estimates when certain sensors have lower S/N ratios or are measuring predominantly local mode behaviour. The increased computational efficiency when using a reference subset is clear and will not be investigated here - the relationship between speed and accuracy is suggested for future work regarding real time system implementation. The use of reference channels to improve the identification when certain sensors contain more noise, or measure predominantly local modes has not been described in detail in literature and remains an important question regarding the optimal use of SSI.

The idea is that when a large number of response DOFs are measured simultaneously, the parametric model fit may suffer from the presence of many noise modes in comparison to physical modes. Therefore by specifying a set of user defined reference channels, the amount of redundant information is decreased resulting in more accurate estimations. Reference channel selection can be guided by calculating the correlation coefficients and identifying channels which represent highly correlated channel clusters. Furthermore it has been found in practice that including sensors which are located on local structures such as aircraft engines or wing stores for example, reduce the accuracy of the identified global modes. This phenomenon is investigated using a tuned 5 DOF example as illustrated in Figure 4.7a. DOF's 4 and 5 are tuned, by reducing the mass and stiffness to act as local modes. The simulated FRF of the system to a step impulse is shown in Figure 4.7b with two local modes at 22 Hz and 57 Hz. The result of using all channels as references in SSI-Data is shown with  $+$  and using channels [1 2 3] as reference with  $\square$  in Figure 4.8. In Figure 4.8 (a) it is seen that using reference channels provides more accurate results at lower model orders. From the zoomed view in Figure 4.8 (b) the effect of using reference channels shows a marginal improvement in the identification of mode 1, but in general there is no clear trend or advantage to using reference channels at higher model orders to estimate the global modes.

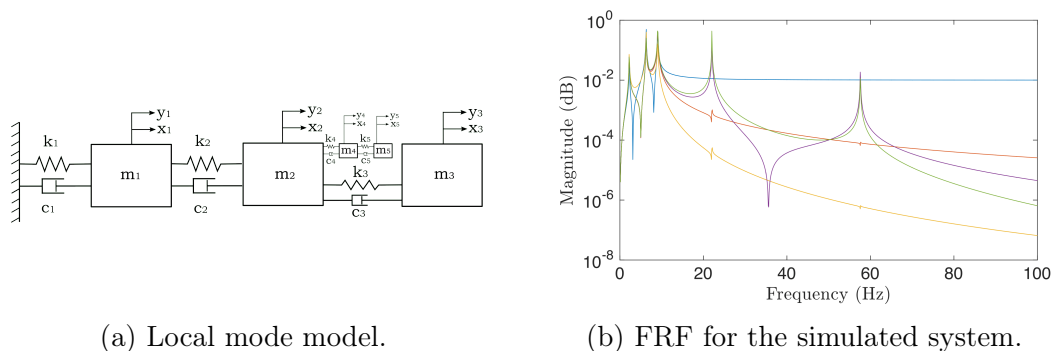


Figure 4.7: Reference channel investigation.

Peeters and De Roeck (1999) investigated the effect of reference channels on an antenna and found that the global modes agreed well when using all the data or a reference subset. Changes in the identification results are however observed and with no analytical solution it is impossible to tell which estimate is more accurate. Peeters and De Roeck (1999) also used the Total Prediction Error (TPE) to investigate reference channels and found that at best the channels which are chosen as reference will have the same TPE as when using all channels, and that channels which are not chosen as reference will always result in worse TPE. The TPE is however an indication of the ability to reconstruct the time signal. This means that SSI could identify global modes accurately but out of band, local or noise modes poorly resulting in a poor TPE. Further

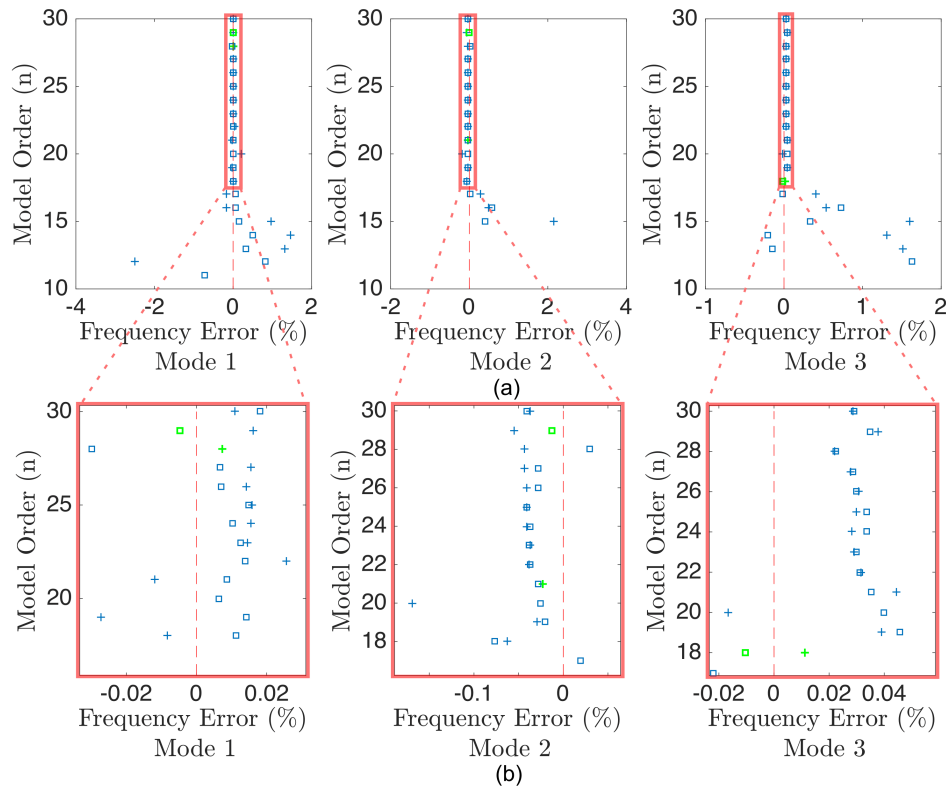


Figure 4.8: Frequency, errors for SSI-Data with all channels as references  $+$  and  $[1\ 2\ 3]$  as reference  $\square$  with block size  $[i\ 10]$ .

investigation of the TPE will be presented, and future investigations on a laboratory structure designed to have distinct local and global mode behaviour is recommended.

## 4.7 Damping

Energy dissipation through damping remains the greatest challenge for all the current system identification methods to identify accurately. The effect of damping on the SSI-Data modal parameter estimates for the 3 DOF system is shown in Figure 4.9. Damping levels of  $\zeta = 0.1\%$   $+$ ,  $\zeta = 1\%$   $\square$ ,  $\zeta = 5\%$   $\triangle$  were investigated. It can be seen that higher damping results in less accurate frequency and mode shape estimates. SSI is however able to identify the higher system damping levels more accurately than lower damping levels. It can also be seen that once the model order exceeds  $n = 30$  that the estimates become more chaotic, which is most notable for the damping estimates.

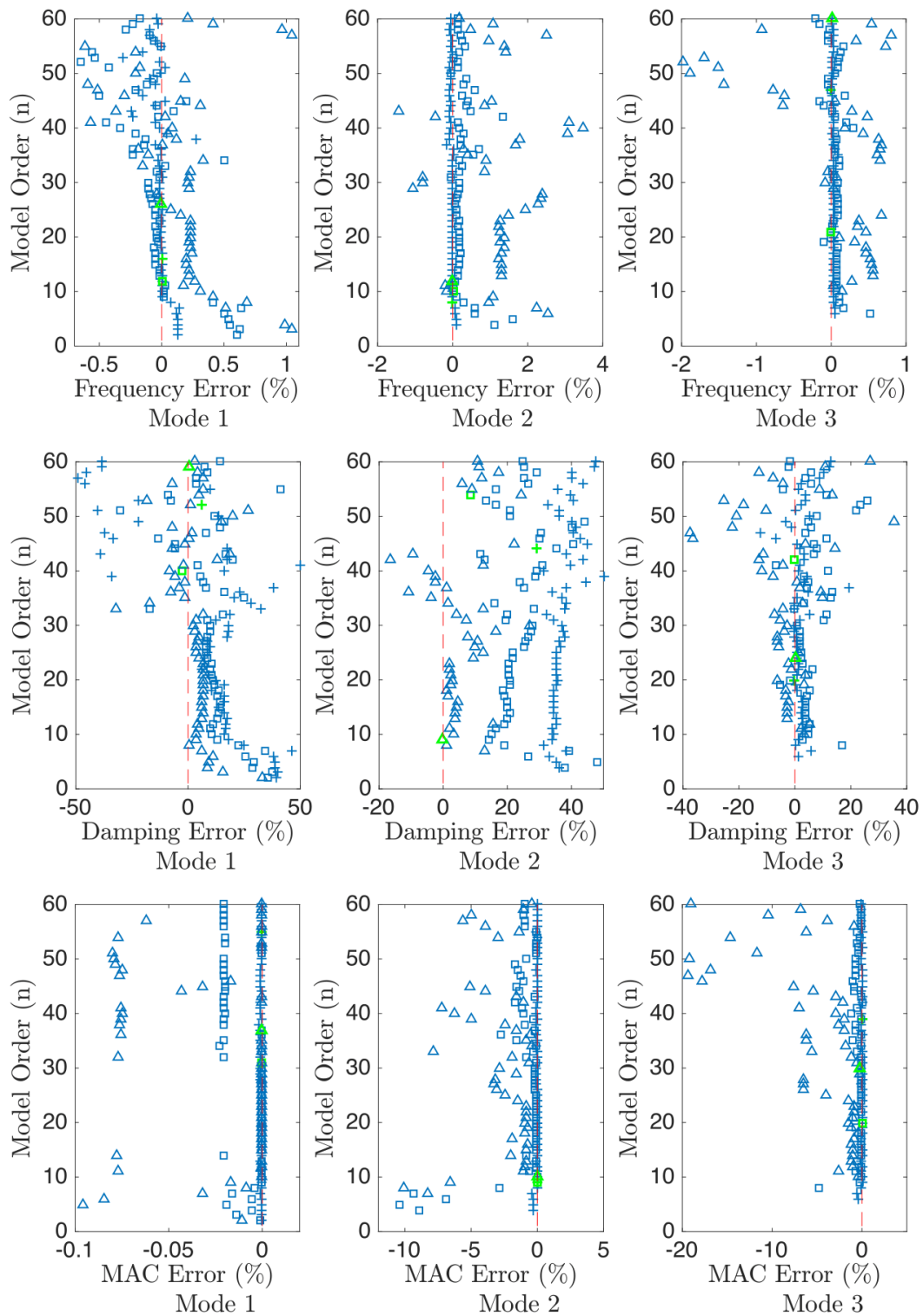


Figure 4.9: Frequency, damping and MAC errors for SSI-Data with  $\sim 0.1\%$  damping  $+$ ,  $1\%$  damping  $\square$  and  $5\%$  damping  $\triangle$  with block size  $[i = 30]$ .

## 4.8 Harmonics

A harmonic is a periodic wave that is an integer multiple of a base sinusoidal frequency, and occur when rotational machinery is present. Harmonics violate the assumption in SSI of Gaussian white noise excitation and can therefore be identified as physical poles or bias closely spaced physical poles. There are two classes of methods for dealing with harmonics in system identification: Method (1) includes the harmonics in the identification and subsequently removes them in post processing, see Brincker *et al.* (2000); Mohanty and Rixen (2004); Peeters *et al.* (2007). The drawbacks of these methods are that the harmonics may bias the results in a way which cannot be reversed. Method (2) removes the harmonic from the raw time or frequency data before performing the system identification, see Bienert *et al.* (2015); Brandt and Linderholt (2012); Vold *et al.* (2017). The drawbacks of these methods are that the harmonics must either be known a priori or measured using a tachometer.

In this section the effect of harmonic bias on the modal parameter estimates is investigated for harmonic frequencies of 1.001 and 1.01 times the natural frequency of the third mode. Figure 4.10 shows the frequency, damping and MAC errors for mode 3 using SSI-Data with no harmonic  $+$ , harmonic  $1.001 f_n$   $\square$  and harmonic  $1.01 f_n$   $\triangle$  for increasing model order with a fixed block size ( $i = 10$ ). It can be seen that the harmonics bias the estimate at low model orders, which is most notable in the damping and MAC errors. However when using higher model orders the algorithm is able to accurately identify the modal parameters without bias even from an harmonic at  $1.001 f_n$ . It should however be noted that with higher model orders SSI identifies the physical pole as well as the harmonic, and in cases where the harmonics are not known, or are changing they may be mistakenly identified as physical poles.

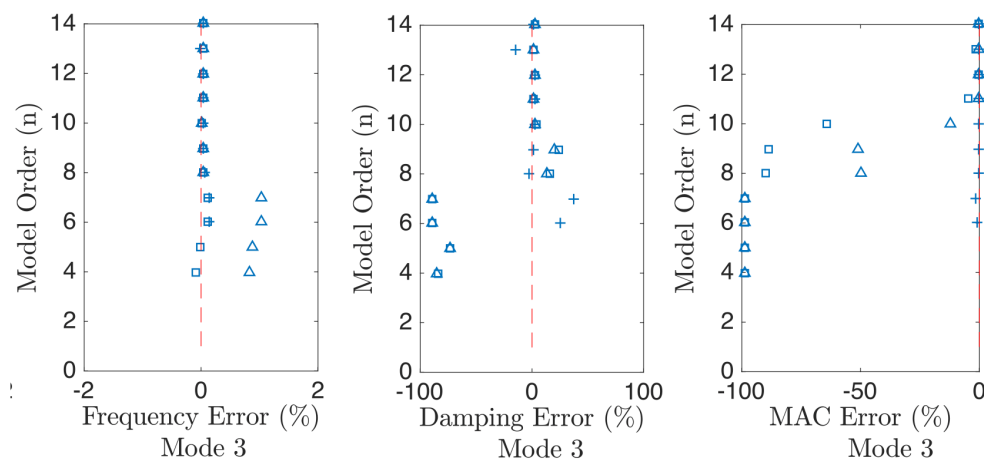


Figure 4.10: Frequency, damping and MAC errors for SSI-Data with no harmonic  $+$ , harmonic  $1.001 f_n$   $\square$  and harmonic  $1.01 f_n$   $\triangle$  for increasing model order with a fixed block size ( $i = 10$ ).

## 4.9 Linear Time Invariance

A system is said to be linear if the combined response consists of a summation of the individual system inputs, as well as when the system parameters are independent of the scaling of the input. In terms of a physical system this means that the resulting structural response can be decomposed into a linear combination of the fundamental system modes. It also means that the amplitude of the input excitation should not change the system properties. A system is said to be time invariant if its response to a given input is independent of absolute time. In a structural system this means that the mass  $M$ , damping  $D$  and stiffness  $K$  parameters are stationary. This is the basis of system modelling, and though it may seem an oversimplification, it is found in practice to produce useful results. Since no real structures are strictly linear time invariant, the question is what is the result in the presence of non-linear or time invariant systems?

In this section the result of a time varying system is investigated. A time varying 3 DOF system was simulated as shown in the spectrogram in Figure 4.11a. The system was composed of 3 sections, Section 1: stationary, symmetric mass matrix 100 kg resulting in a time vector (10000 x 3), Section 2: the mass matrix was increased linearly in 48 iterations of time vector length 200 from 100 kg - 148 kg, Section 3: stationary, symmetric mass matrix 148 kg resulting in a time vector (10000 x 3). The total time data length was therefore (29600 x 3). Time data blocks of length 1000 with 75 % overlap were used as inputs to SSI-Data with a block size  $i = 10$  and a model order  $n = 6$ . The resulting frequency identification is shown by the dashed lines on top of the spectrogram in Figure 4.11a and are seen to track the time varying changes accurately. The damping however shows large variations during the time varying part in Figure 4.11b with largest variation for mode 1. Further investigations are recommended into the effects of the magnitude of the time variance on the system identification results.

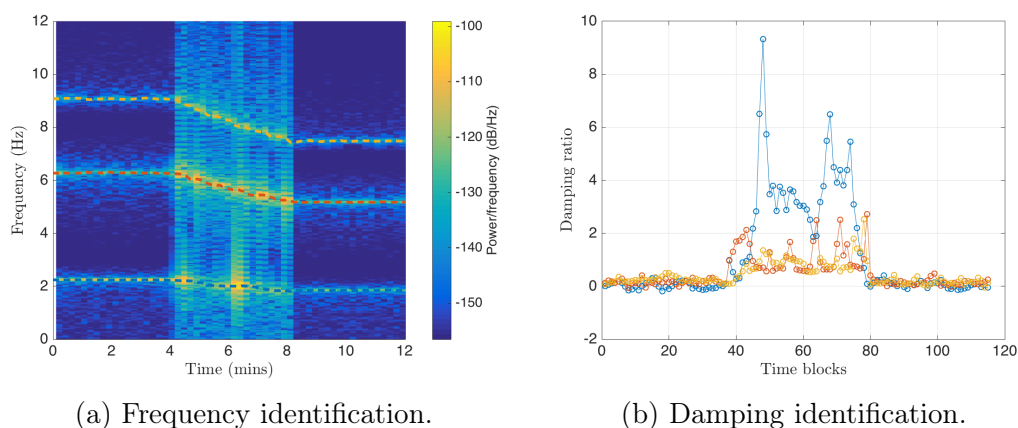


Figure 4.11: SSI identification of a time varying system.

## 4.10 Total Prediction Error (TPE)

The difference between the one step ahead prediction  $\hat{y}_k$  and the measured response  $y_k$  is the Total Prediction Error  $\epsilon_c$

$$\epsilon_c = \sqrt{\frac{\sum_{k=1}^N (y_k - \hat{y}_k)^2}{\sum_{k=1}^N (y_k)^2}} \quad (4.10.1)$$

This is an indication of how well the system identification is able to reconstruct the time signal, and can therefore be used as a quality metric. The 5 DOF system was used to investigate the effect of model order, block size and input force magnitude on the TPE. Figure 4.12 shows the Power Spectral Density (PSD) where it can be seen that channels 1 and 2 have largest input excitation while channels 3 and 5 have the lowest. The TPE results for increasing model order are presented in Figure 4.13a. Firstly it can be seen that the TPE initially improves with increasing model order, but then suddenly becomes very poor around model order 30. This indicates that there is an optimal TPE bandwidth. Secondly it can be seen that the lower the input force the worse the TPE. Figure 4.13b shows the TPE for increasing block size where it can be seen that the error becomes slightly worse for channels 1 and 2, and much worse for channels 3 and 5 but then stabilize around  $i = 8$ . Since the goal of modal analysis is to estimate the natural frequency, damping and mode shape, and not necessarily reconstruct the time signal it is important to make a note of this connection to the TPE. From Figure 4.2 and 4.3 it was seen that increasing the model order or the block size did not result in divergence or worse estimates. The TPE should therefore be used with caution as it includes the ability of the system identification to model noise and spurious modes which is not a true indication of the usefulness of the identification.

## 4.11 Conclusion

A parametric simulation study was conducted to investigate the performance of the SSI algorithms. Key findings include the effect of increasing model orders  $n$  showing no trend in determining an optimal order selection. Increasing the block size  $i$  showed convergence for both SSI-Data and SSI-Covariance even at extremely large block sizes, and the smallest % errors were seen in the region of high block size with low model order. Neither SSI-Data nor SSI-Covariance showed a conclusive trend of superior performance in terms of identification results. SSI-Covariance showed improved frequency estimates in some cases and SSI-Data showed improved damping and MAC estimates in other cases but this depended on the system, mode and input excitation. The ability to combine different system identification techniques according to their respective strengths rather than sticking to one method is proposed for future research.

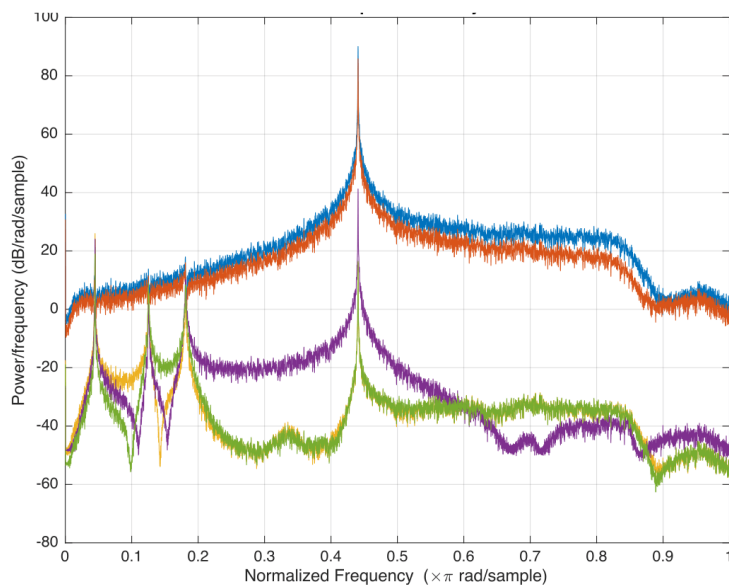
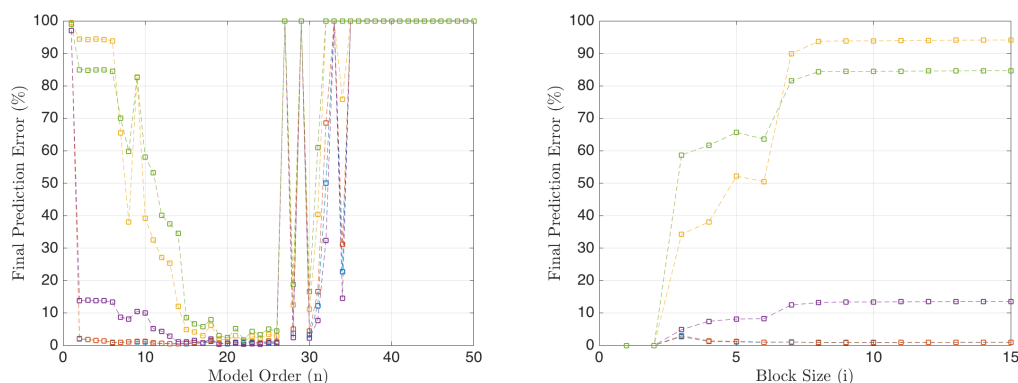


Figure 4.12: Power spectral density (PSD) of the 5 DOF system with different input force levels. Channel 1 ●, Channel 2 ●, Channel 3 ●, Channel 4 ●, Channel 5 ●



(a) Total prediction error (%) versus model order ( $n$ ). (b) Total prediction error (%) versus block size ( $i$ ).

Figure 4.13: Total prediction error (%) versus model order ( $n$ ) and block size ( $i$ ). Channel 1 □, Channel 2 □, Channel 3 □, Channel 4 □, Channel 5 □

In terms of physical phenomena, adding noise to the signal had the effect of improving the mean error in certain cases due to the Gaussian white noise assumption, but with high noise levels also increased the variance on the estimates. Reference channels provided more accurate results at lower model orders but did not make a significant improvement at higher model orders. Increased damping resulted in less accurate frequency and mode shape estimates but more accurate damping estimates at low model orders. At high model orders the results became more scattered. Harmonics were found to bias the

estimates at low model orders, most notably in the damping and MAC errors, but higher model orders were able to identify unbiased modal estimates. SSI was found to track the frequency changes very accurately of a linear time varying system, but showed large variations in the damping estimates. Total Prediction Error TPE was seen to initially improve with increasing model order, but then suddenly diverge at high model orders. It was also found that the lower the input force the worse the TPE. The TPE stabilised for increasing block sizes, but should be used with caution as a quality indicator since it includes the ability of the system identification to model noise and spurious modes which is not a true indication of the usefulness of the physical eigenvalues and eigenvectors.

## Chapter 5

# Polar Research Vessel, Arctic Expedition and Open Data

### 5.1 Description of the Vessel

The FS Polarstern, shown in Figure 5.1, is a German research icebreaker operated by the Alfred Wegener Institute for Polar and Marine Research (AWI) in Bremerhaven. The vessel was built in Germany and commissioned in 1982. It contains nine research laboratories for biological, geological, geophysical, glaciological, chemical, oceanographic and meteorological research. The Polarstern operates around 310 days a year in harsh polar and ocean environments as shown in Figure 5.2 and 5.3. The vessel has a design speed of 15.5 knots, can break through 1.5 m of ice at 5 knots and up to 3 m of ice by ramming.



Figure 5.1: Polar research vessel Polarstern. (AWI/W von Appen)

The Polarstern is 118 m in length with a 25 m beam, 11 m draft and

a displacement of 17 300 tonnes. Four diesel engines provide 14 000 kW of power through two shaft lines with variable pitch propellers. The vessel also has a bow and stern thruster for dynamic positioning. The Polarstern has a double hull design for ice breaking, resulting in a stiff hull structure. The main cargo hold is located in the bow, with additional cargo storage in the stern. The superstructure is positioned slightly towards the fore of the vessel, in the classic icebreaker layout. This allows the vessel to use the weight to break ice in bending rather than compression. For dynamic stability, the vessel has retractable stabilizing fins which are deployed during open water transits as well as a stabilizing water pump system.



Figure 5.2: Polarstern in an Arctic ice field.



Figure 5.3: Polarstern during a storm in open water. (AWI/F Mehrtens)

## 5.2 Measurement Setup and Equipment

The Polarstern was instrumented with 23 accelerometers as shown in Figure 5.4. Measurements were conducted in the hull on deck F and the bridge on deck A. Accelerometers were orientated in the vertical direction along the ship length to measure normal bending and were placed on both port and

starboard to measure torsion. Horizontal measurements were conducted to measure lateral bending and triaxial sensors were placed in the stern and bridge respectively.

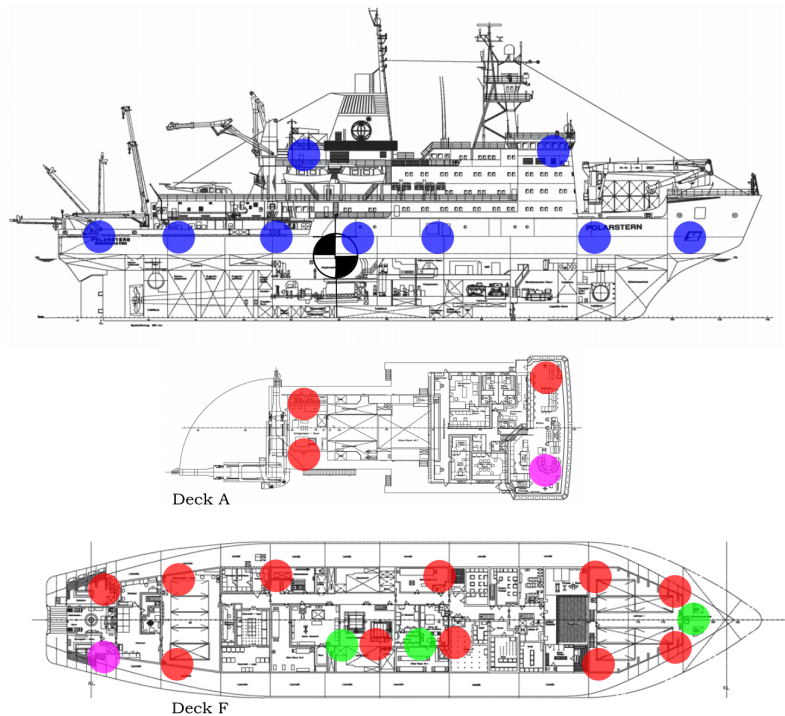
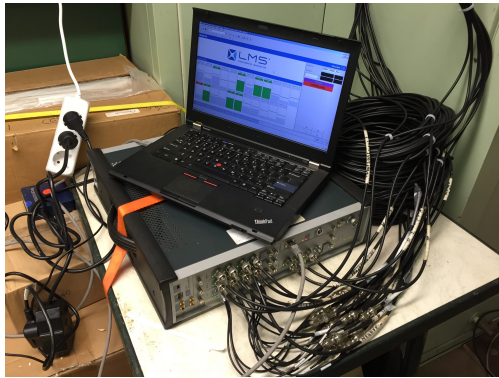


Figure 5.4: Measurement setup on the Polarstern: ● Accelerometer locations, ● Vertical (+Z) measurements, ● Transverse (+Y) measurements, ● Triaxial (+X, +Y, +Z) measurements

LMS Test.Lab Turbine Testing software and an LMS SCADAS III, see Figure 5.5a, were used to make synchronous and continuous vibration measurements saved in 5 minute files at sample frequency 2048 Hz. Over 2 km of coaxial BnC cable was routed from sensor locations to the SCADAS III in the centre of deck F. Cables were securely routed through cable trays, pipe ducts and water tight points and were kept away from sources of magnetic interference as far as possible. Before crimping the end connectors, all cables were shorted and their resistances were measured to identify possible manufacturing faults or installation damage.

Eight 100 mV/g PCB ICP accelerometers, see Figure 5.5c, capable of measurements to 0.5 Hz and fifteen 200 mV/g PCB DC accelerometers, see Figure 5.5d, with high low frequency accuracy were used. Accelerometers were mounted to main structural beams or plates to investigate global responses. HBM X60 two component glue was used to secure the sensors during the long voyage. Signal processing, system identification and modal tracking were performed in Matlab using in house algorithms developed by the Sound and Vibration Research Group at Stellenbosch University (South Africa) and the

Institut für Aeroelastik at the Deutsches Zentrum für Luft und Raumfahrt (Germany). Environmental conditions were logged to a data inventory system called Dship, see Figure 5.5b, which could be accessed via the local ship network.



(a) LMS SCADAS III and laptop.



(b) Dship measurement station.



(c) ICP accelerometer.



(d) DC accelerometer.

Figure 5.5: Measurement equipment.

### 5.3 Field Measurements in the Arctic

Full scale measurements were conducted during the PS100 research expedition to the Arctic in 2016. The cruise track of PS100 is shown in Figure 5.6. The expedition started in Tromsø, Norway, on the 18th July heading north west into the Greenland sea. The dots on the cruise track indicate scientific stations. A port call was made in Longyearbyen, Svalbard, followed by oceanographic research on a westerly transect in Fram strait. Near the meridian the vessel headed north into the Arctic sea ice reaching nearly  $81^\circ$  north, before moving west towards Greenland. Further oceanographic research was conducted in Fram strait before sailing to the  $79^\circ$  north glacier on the East Greenland coastline to conduct various research surveys. Finally the vessel headed back to Fram strait, returning to Tromsø on 6th September after 51 days at sea.

A wide variety of operational and environmental conditions were encountered during the voyage. Operational conditions included different cruising speeds, draft, trim and engine configurations. Different environmental conditions included swell heights, swell directions, swell periods, ice types, ice thickness's, air and water temperature variations and wind speeds and directions.

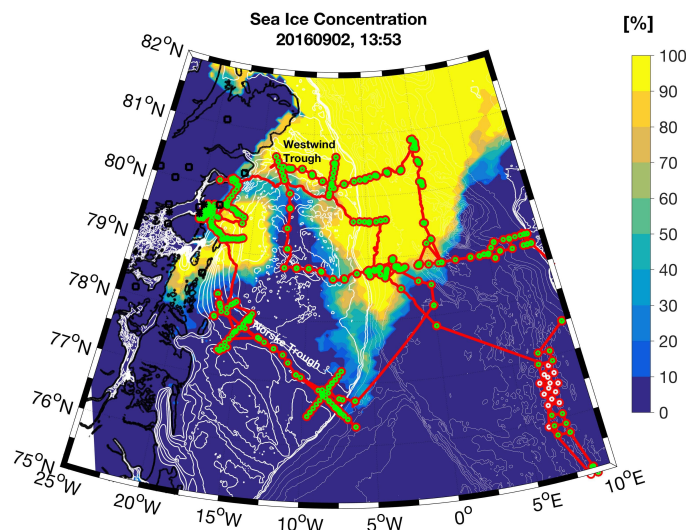


Figure 5.6: Cruise track of the PS100 expedition. (AWI/J Schaffer)

## 5.4 Open Data

The full scale data set from the PS100 expedition on the Polarstern to the Arctic is openly available at PANGAEA Data Archiving under publication number PDI-15785. The data set contains raw acceleration time data in *.mat* file format from 23 accelerometers. Environmental data from the data inventory system called Dship are also available. A metadata file contains information regarding measurement parameters and sensor locations. There are three main goals of making the data open source:

1. The results in this thesis can be tested, recreated and validated.
2. Opening the data to other researchers has the potential to be a force multiplier, bringing a diversity of ideas and optimal solutions and providing additional human capital to drive innovation.
3. A variety of open source data sets will allow open and transparent benchmarking of state of the art algorithms which can bring further innovation in the field of system identification in structural dynamics.

# Chapter 6

## Modal Tracking

### 6.1 Introduction

Modal parameter tracking deals with following the trail or movements of system modes. Modal parameters are directly related to the system parameters mass  $M$ , damping  $D$  and stiffness  $K$ . Changes in system parameters due to changing mass during cargo loading, or vessel modification effecting stiffness therefore change the modal parameters. Environmental conditions also effect these parameters through changes in temperature effecting Youngs modulus and thus stiffness. Operational changes such as increased vessel speed increase the draft and bow wave which add mass to the structure. The system identification and tracking algorithms need to be sensitive to detect these changes.

Since modal parameters may be closely spaced and shift around, they are able to cross one another. Modes may also be unidentified in certain conditions and reappear during later measurements. A modal tracking algorithm therefore needs to create a library of modes which it stores and references when new modes are identified. More information than a scalar frequency value is required to identify modal clusters or families and keep track of these when modes cross or disappear. This is achieved by using the eigenvalue and eigenvector properties of modal parameters.

Literature regarding full scale measurements on ships is rare. Significant research contributions were made by Rosenow *et al.* (2007), Rocca *et al.* (2009), Orlowitz and Brandt (2014) and Soal *et al.* (2015). This work was focused on the potential of obtaining modal parameters from OMA. The ability to characterise an operational profile for SHM however requires further research.

In this chapter system identification and modal tracking are performed on the full scale data from the Polarstern. System identification is performed using SSI and Least Squares Complex Frequency (LSCF). Investigations into modal tracking using a pole weighted Modal Assurance Criterion (MACXP) are conducted for different cases. Tracked modes are correlated with system inputs to investigate and identify inter variable relationships. The theory and implementation of SSI were presented in Chapter 3. The theory of the LSCF

method will be briefly explained below.

## 6.2 Least-Square Complex Frequency (LSCF)

The LSCF algorithm identifies the system parameters in the frequency domain from the spectra of the measured signals. It computes very quickly due to the efficiency of the Fast Fourier Transform (FFT) and can estimate the eigenvalues and corresponding mode shapes in desired frequency bands using a least-squares approach. A detailed description of LSCF can be found in Pintelon and Schoukens (2001) and Jelcic *et al.* (2015). For a Linear Time Invariant (LTI) system the Power Spectral Density (PSD) of the system outputs  $S_{yy}$  is a function of its input power spectral densities  $S_{xx}$  and frequency response function  $H_{xy}$

$$S_{yy}(i\omega) = H_{xy}(i\omega)S_{xx}(i\omega)H_{xy}(i\omega)^H \quad (6.2.1)$$

Assuming a constant broadband input spectrum  $S_{xx}(i\omega) = S_{xx}$ , the power spectral density can be decomposed as a function of system poles  $\lambda_i$ , residues  $\Phi_i$  and references  $L_i$

$$S_{yy}(i\omega) = \sum_{r=1}^m \frac{\Phi_r L_r^T}{i\omega - \lambda_r} + \frac{\Phi_r^* L_r^H}{i\omega - \lambda_r^*} + \frac{\Phi_r L_r^T}{-i\omega - \lambda_r} + \frac{\Phi_r^* L_r^H}{-i\omega - \lambda_r^*} \quad (6.2.2)$$

The measured spectra are described by rational polynomials in the discrete z-domain as follows

$$S_{yy}(i\omega) = \sum_{r=1}^m [\beta_r] z^r \left( \sum_{r=1}^m [\alpha_r] z^r \right)^{-1} \quad (6.2.3)$$

where  $\beta_r$  is the matrix of numerator polynomial coefficients,  $\alpha_r$  is the denominator polynomial coefficients and  $m$  is the highest coefficient exponent also called the model order. Both matrix coefficients are unknown and are obtained using a least-squares approach. The eigenvalues of the system are then determined from the roots of the denominator polynomial

$$\sum_{r=1}^m [\alpha_r] e^{-i\omega \Delta t r} = 0, \quad \rightarrow \lambda, \lambda^* \quad i = 1, 2, \dots, m \quad (6.2.4)$$

## 6.3 Mode Tracking

Polar vessels have a large operational profile. This includes different open water conditions, wave heights, swell periods and cruising speeds. A variety of ice types, thickness's and breaking and ramming manoeuvres. Different air and water temperatures and wind speeds. As well as different cargo, ballast, fuel

and trim configurations. The variation of these inputs cause shifts in the modal parameters. The objective of modal tracking is to identify a reference cluster or library of physical modes. Each new identification will then be compared to this reference library. The library will then be updated by adding positive identifications as well as storing unknown modes which may be identified in future measurements.

Tracking the movements of scalar values such as the natural frequencies is however not possible. This is due to modes which may be unidentified in certain data blocks and reappear later. As well as modes which may come close to or cross one another. This problem can be dealt with by using the eigenvector associated with each natural frequency. The original Modal Assurance Criterion (MAC), see equation 6.3.1, is the normalized inner dot product of the eigenvector at each common node point. This can also be thought of as the square of the correlation between two modal vectors  $\phi_i$  and  $\phi_j$ . If a linear relationship exists between the vectors the MAC value will be one. If the vectors are orthogonal the MAC value will be zero.

$$MAC(\phi_i, \phi_j) = \frac{|\phi_i^T \phi_j|^2}{\left(\phi_i^T \phi_i\right) \left(\phi_j^T \phi_j\right)} \quad (6.3.1)$$

The MAC value is limited by a low number of measurement degrees of freedom, low response amplitudes and complex mode shape patterns which may not result in clear modal identification. The MAC from full scale data on the FS Polarstern is shown in Figure 6.1b. Here it can be seen that an indistinguishable mode family exists between modes 1, 2, 3 and 5.

The MACXP proposed by Vacher (2010) expands this criteria by a pole weighting, see equation 6.3.2. Both the real and imaginary parts of the poles are included as additional weighting on the correlation of two mode shapes. The MACXP can also be interpreted as the correlation function between the real decay responses of the associated modes. Figure 6.1a shows the MACXP of the same FS Polarstern dataset which provides a clear correlation and is able to differentiate between modes 1, 2, 3 and 5. This makes the MACXP a sensible choice in a tracking algorithm.

$$MACXP(\phi_i, \phi_j) = \frac{\left(\frac{|\phi_i^* \phi_j|}{|\lambda_i + \lambda_j|} + \frac{|\phi_i^T \phi_j|}{|\lambda_i + \lambda_j|}\right)^2}{\left(\frac{\phi_i^* \phi_i}{|Re\lambda_i|} + \frac{|\phi_i^T \phi_i|}{2|\lambda_i|}\right) \left(\frac{\phi_j^* \phi_j}{|Re\lambda_j|} + \frac{|\phi_j^T \phi_j|}{2|\lambda_j|}\right)} \quad (6.3.2)$$

The mode tracking algorithm developed in the current work proceeds in two steps. First a MACXP matrix is computed from the eigenvalues and eigenvectors  $\lambda_1, \phi_1$  and  $\lambda_2, \phi_2$  of the first two time data blocks. The indices

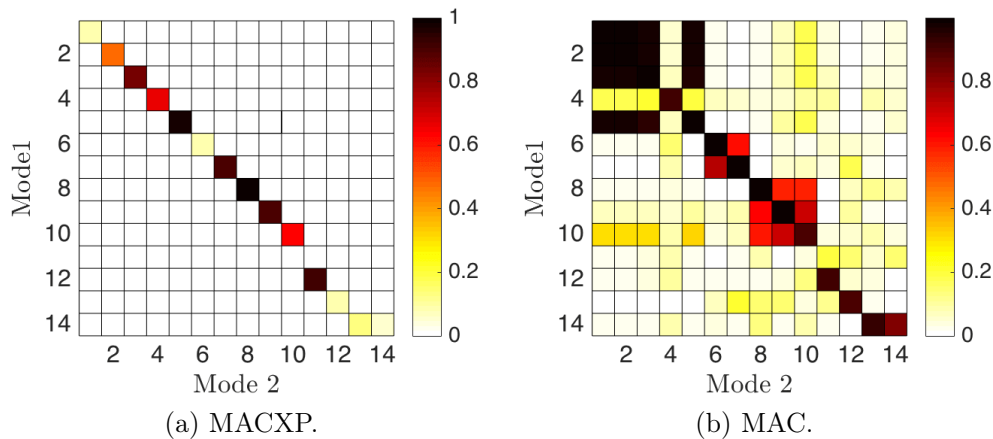


Figure 6.1: Modal assurance criterion.

of the MACXP values exceeding a user defined threshold  $mcpair$ , are then used to build a reference library  $\lambda_{rl}, \phi_{rl}$ . The parameters below the  $mcpair$  threshold are then concatenated to the reference library resulting in  $\lambda_c, \phi_c$ . In the second step the MAXCP between  $\lambda_c, \phi_c$  and  $\lambda_3, \phi_3$  is computed. The indices of the values exceeding the  $mcpair$  are then used to build the time dependant dimension of the mode library at time step  $t = 2$ . If new correlations are found outside the reference library, these are added to  $\lambda_{rl}, \phi_{rl}$  as new members. The updated reference library  $\lambda_{rl}, \phi_{rl}$  is then concatenated with the remaining values from  $\lambda_3, \phi_3$  before continuing to  $\lambda_4, \phi_4$  at time step 3. The algorithm then proceeds through all available time blocks  $t = 1, 2, 3, \dots, n$ . It should also be noted that the algorithm updates the available eigenvectors at each time data block in order to correlate new data to the most recent mode shapes.

## 6.4 Results

Five cases were selected from the broad spectrum of operational and environmental conditions for this study as presented in Table 6.1. Cases were chosen to provide insight into key characteristics of a polar vessel's operational profile. A limited number of cases allow greater analysis depth and insight as compared to investigating two months of data in one analysis. The time data for all sensors from the five cases are shown in Figure 6.2.

### 6.4.1 Signal Processing

Time data was first detrended to remove linear DC offsets and then decimated to  $fs = 64$  Hz using a lowpass Chebyshev Type I filter. The time histories show unique signatures for each case in Figure 6.2. The vibration amplitude is observed to increase with speed which is most visible in case 3 and 5. Case 1 and 4 show relatively stationary time data. Case 2 shows impulsive vessel

Table 6.1: Operational profile case study.

No.	Case	Date	Time
1	Stationary	31-07-2016	14h00 - 16h00
2	Ice Breaking	31-07-2016	16h30 - 18h30
3	Temperature Variation	02-09-2016	06h00 - 09h00
4	Constant Speed	22-07-2016	12h00 - 14h00
5	Alternating Speed	25-07-2016	04h30 - 09h00

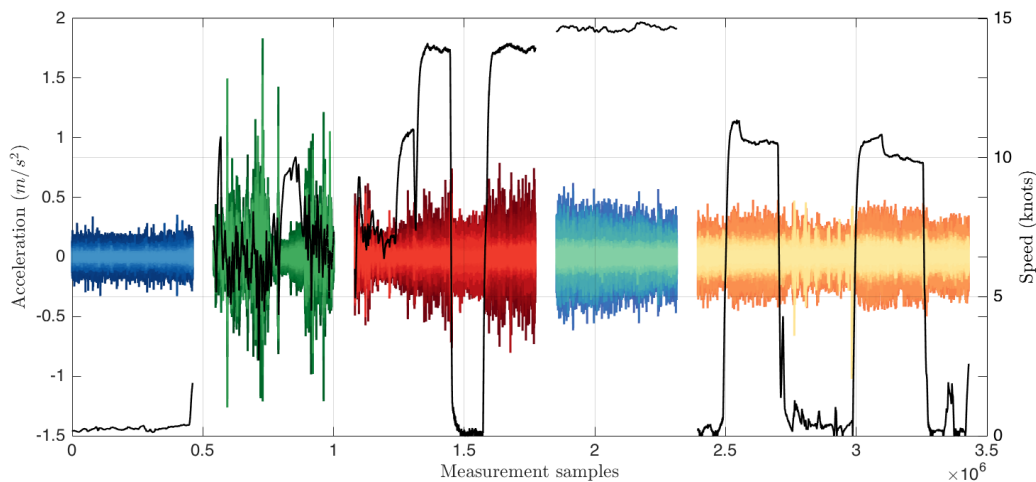


Figure 6.2: Time data of all accelerometers for five selected cases.

response due to ice loading. The largest vibration amplitudes occur during ice breaking in case 2 at  $1.5 \text{ m/s}^2$  followed by case 3 in open water when the vessel reaches 14 knots.

The measurement quality and data characteristics were investigated using the first four principal moments as presented in Figure 6.3. The statistical moments were calculated using a sliding window with 50 % overlap and a window size of 20 000 samples (5.7 minutes). Mean values around zero were observed with low variance  $< 0.08$ . The variance was seen to increase when the vessel was moving at higher speeds or breaking ice. Skewness provides a measure of how symmetric the distribution is around its mean value. All cases except case 2 show fairly symmetric distributions. Kurtosis provides a measure of the weight of the tails of the distribution. It is therefore well suited to detect impulses. This was used during signal pre-processing to identify and remove faulty signals, as well as during the voyage to detect and fix loose cable connections. The kurtosis is seen to be low for all cases except case 2 where the impulsive ice loading provides physically meaningful peaks in the vessel response.

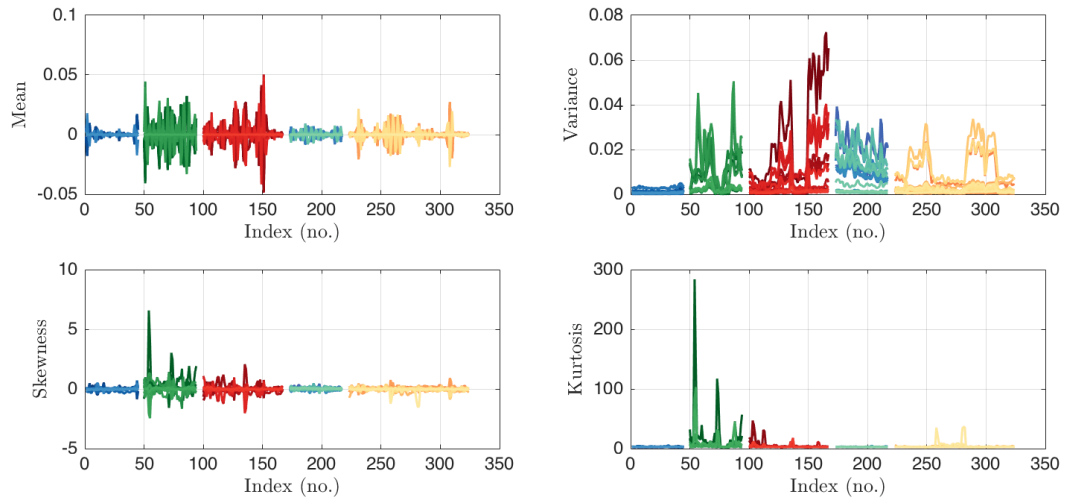


Figure 6.3: Statistical moments.

## 6.4.2 Frequency Spectra

The Auto Power Spectral Densities (APSD) of the vertical accelerometer on the starboard side of the bow for the five cases are shown in Figure 6.4. The PSD's are averaged using a Hanning window over a full data block from each case with a block length of 8192 FFT points resulting in a frequency resolution of 0.0078 Hz.

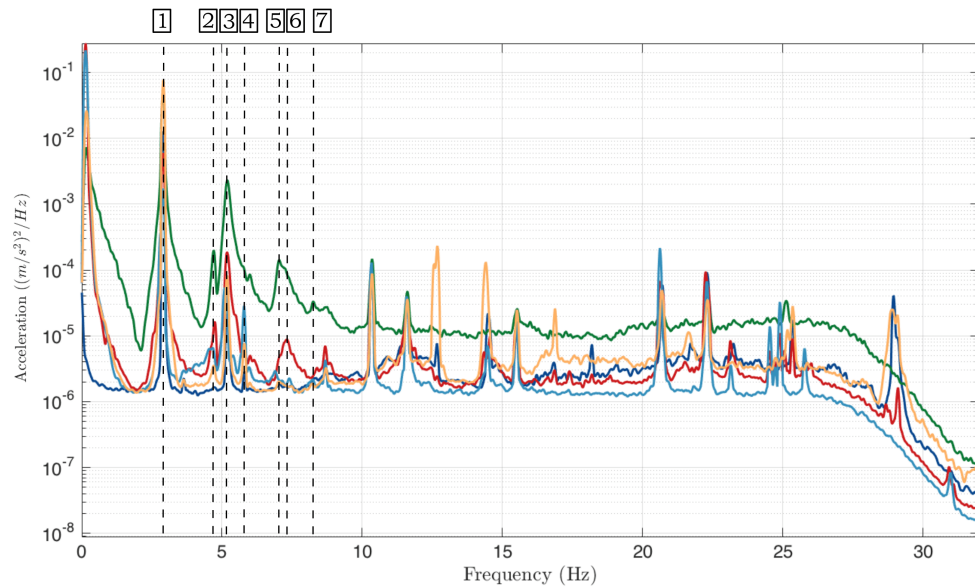


Figure 6.4: Auto power spectral densities (APSD) ● Case 1 ● Case 2 ● Case 3 ● Case 4 ● Case 5.

Firstly the spectra show higher broadband response during case 2, in green, due to the impulsive nature of ice loading. The peak around 2.9 Hz, later

identified as the first elastic mode, is however an exception, showing largest amplitude during case 5 in yellow. The rigid body motion can be identified by peaks below 0.5 Hz which is lowest in case 1 when the vessel is stationary. Distinct peaks are observed throughout all spectra, with peaks under 10 Hz being broader and having higher amplitudes. This is an indication of physical modes as opposed to the harmonics which can be seen as the narrow peaks in the higher frequency range. Harmonic excitation from the rotational speed of the shaft line at 174 rpm can be seen at 2.9 Hz. The rotational speed of the engine at 650 rpm can be identified at 10.8 Hz, and the first blade pass frequency at 11.6 Hz. Seven peaks can be counted in the range 2 - 10 Hz indicating the density of global modes in this bandwidth. The peaks across cases 1 - 5 are not exactly coincident and do not have the same amplitudes or steepness. This indicates that modes are excited differently and modal parameters should therefore be identified differently. Changes in frequency (location of the peaks) and damping (steepness of the peaks) are expected to change depending on the boundary conditions and vessel parameters (draft, fuel, ballast etc.). It is also observed that certain operating conditions will be more conducive to the excitation of certain modes. The fourth peak around 5.4 Hz is for example more excited during case 4 and 5 relative to the other peaks than case 2 where it is barely visible. Rigid body modes below 0.5 Hz can be seen to contain more energy than elastic modes and will be an important consideration for inverse force estimation in future research.

The auto and cross power spectral densities of all accelerometers with the vertical accelerometer on the starboard side of the bow for case 1 and 2 are shown in Figure 6.5.

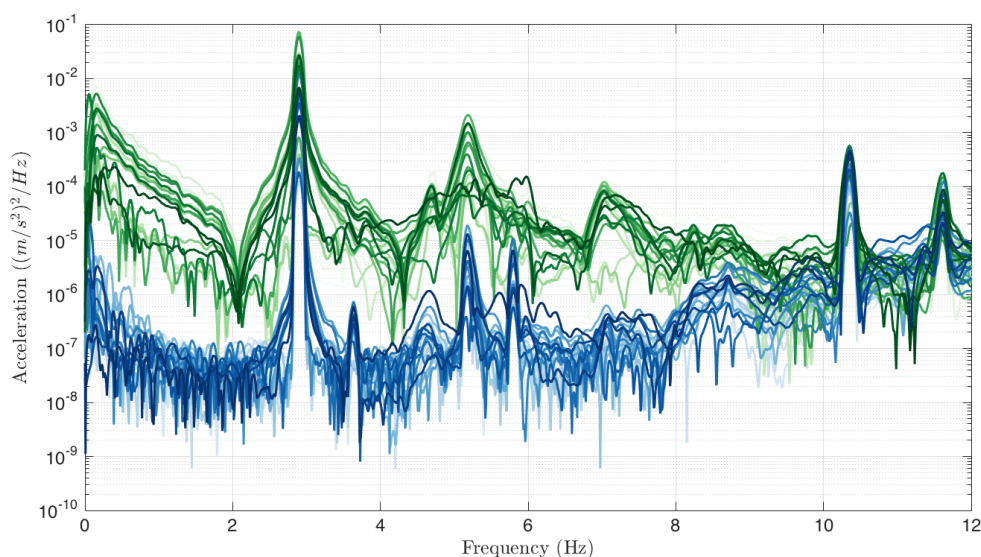


Figure 6.5: Auto and cross power spectral densities of all accelerometers with the vertical accelerometer on the starboard side of the bow ● Case 1 ● Case 2.

The shape of the spectra are seen to differ distinctly under 10 Hz. Larger excitation results in higher amplitudes, and the peaks are observed to be broader, indicating higher damping. Increased damping during ice breaking is thought to be due to the dissipation of vibrational energy into the ice in the breaking process. The first harmonic of the shaft line rotation is dominant in case 1 at 2.9 Hz. During case 2 the first normal bending mode which is coincident with the first harmonic can be accurately identified. Investigations into harmonic removal using the Gauss-Newton time domain method Bienert *et al.* (2015), and Periodogram smoothing frequency domain method Brandt and Linderholt (2012) were conducted. It was found that the Gauss-Newton method was extremely slow to converge, which would make processing large data sets impractical. The Periodogram smoothing did not significantly change the result, and could not be used to recover a time domain signal for use in SSI. Since the harmonics in the current data are stationary and only affect the first bending mode, and since SSI has proven robust in the presence of harmonics, further investigations into harmonic removal were not conducted in the context of the current thesis aim.

Three peaks between 4.7 Hz and 5.4 Hz show distinct physical character in case 2 unlike in case 1. Higher peaks between 7.1 Hz and 8.3 Hz also become visible in case 2. A peak around 3.7 Hz in case 1 is however observed to completely disappear in case 2. Since the mode shape could not be interpreted physically this mode was not considered in the current analyses.

The spectrograms for case 1 and 2 are shown in Figure 6.6. A characteristic pattern can be observed. The first harmonic and coincident first elastic mode remain dominant in both cases at 2.9 Hz. Higher modes (horizontal yellow lines) are more pronounced in case 2, where they are also seen to shift around more than the stationary case 1. The most notable difference is the broadband response due to the impulsive ice loads seen as vertical yellow lines in case 2.

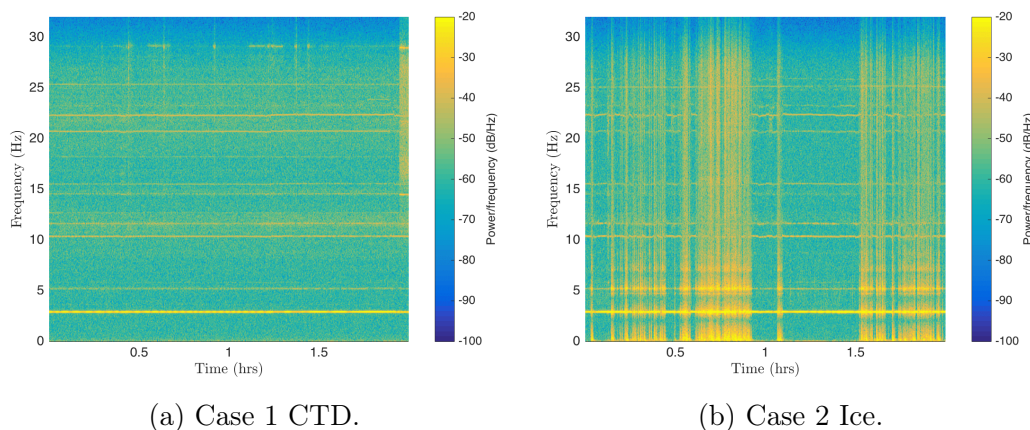


Figure 6.6: Spectrograms of case 1 and 2.

### 6.4.3 System Identification

System identification provides estimates of the eigenvalues and eigenvectors of the system. A plot of the identified eigenvalues versus model order, called a stabilisation diagram, can be used to identify and separate physical and spurious modes. Time data blocks of 20 minutes with 75 % overlap are used for the identification - i.e. each 20 minute block is shifted 5 minutes after each identification.

An automatic modal analysis algorithm was developed as described in Schwochow and Jelacic (2015). This allows the removal of manual user interaction which is impractical for large data sets and also standardizes the modal parameter selection method. The SSI-Data algorithm uses a user defined block size and maximum model order to identify a base library of modes using the MACXP criterion. The base library is composed of modes existing in five consecutive model orders below the user defined maximum. The algorithm then proceeds to identify modes at decreasing model orders until one of the base library is no longer identified. The automatic modal selection is then made at the model order prior to the lost modal library member. Since SSI is band sensitive it is important to first bandpass filter the data. In the current work a lowpass filter with cutoff at 15 Hz is used. Figure 6.7 shows the SSI stabilisation diagram for a 20 minute time data block during ice navigation in case 2. Stable poles can be clearly identified and the diagram has been cleaned using the MACXP criterion. The model order selection is made at  $n = 194$  and the mode indicator function in red confirms that poles have been identified near peaks in the spectra.

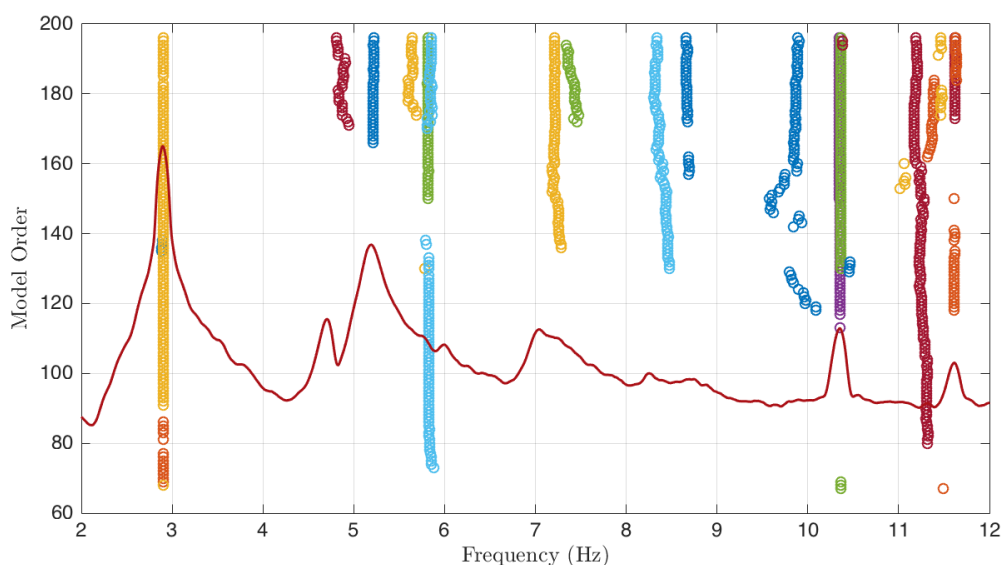


Figure 6.7: SSI stabilisation diagram.

The LSCF algorithm uses Cross Power Spectral Densities (CPSD) from user defined references. References were chosen which contained the desired spectral information, were normally distributed, stationary and had similar variance to provide improved estimates. The LSCF stabilisation diagram in Figure 6.8 contains 3 bands from 1 - 10 Hz with model order 5 up to 30. Since every system pole requires four model orders up to 6 modes can be identified per band. In Figure 6.8 the red line is the measured spectrum, the blue line is the reconstructed spectrum using the identified modal parameters, the vertical grey lines show the identified poles with the associated damping value in black and Mode Indicator Function (MIF) in blue. LSCF makes an automatic modal parameter selection at the user defined maximum model order. The blue reconstructed spectrum is seen to fit well to the measured spectrum in red.

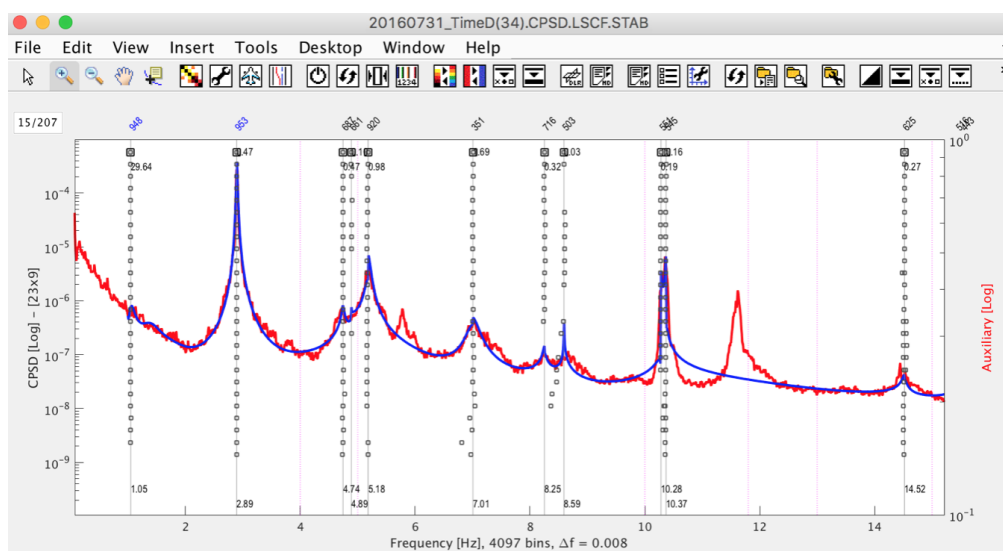


Figure 6.8: LSCF stabilisation diagram.

The reference library of eigenvectors from SSI and LSCF is shown in Figure 6.9. Seven modes are identified in the bandwidth 2 - 10 Hz. These include the first (2.9 Hz), second (5.2 Hz) and third (7.1 Hz) vertical bending modes, the first (4.7 Hz) and second (7.6 Hz) lateral bending modes and first (5.4 Hz) and second (8.3 Hz) torsional modes.

#### 6.4.4 Mode Tracking

The results of the modal tracking algorithm on the automatic SSI system identification results are shown in Figure 6.10. The tracked frequencies show considerable scatter and the migration of the modal families is not immediately clear. The damping estimates show larger scatter with no clear trends. The modal library identified in Figure 6.9 was then flagged and plotted in Figure

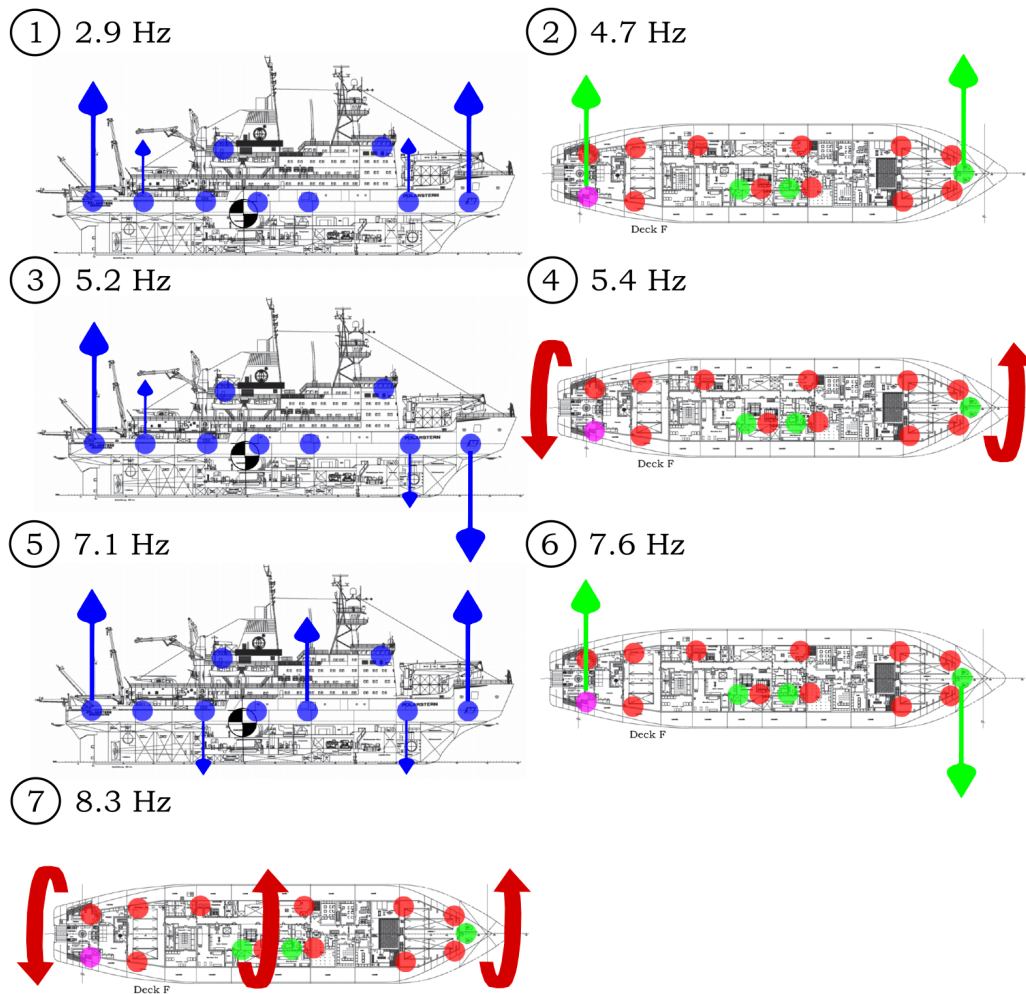


Figure 6.9: Polarstern mode shapes.

6.11. The modal trails are then more visible, and much of the chaos is removed from the damping estimates.

From Figure 6.11 it can be seen that not all eigenvalues are identified or tracked at all time instants. Mode 1 is for example not identified at all during case 1. This occurs when a mode is not excited sufficiently, or when stochastic effects or noise distort the signal and violate the system identification assumptions. An interesting phenomenon can be seen when modal clusters or families change colour, see the first and second modes for case 5 in Figure 6.11. Despite updating the eigenvectors at each new identification these parameters are placed in new clusters despite very similar eigenvalues and eigenvectors. This is an important observation regarding the ability to train a model to make future predictions. This phenomenon will be further discussed in the section on correlation.

The results of the modal tracking from the LSCF modal parameters are presented in Figure 6.12. LSCF is found to identify fewer modes than SSI and

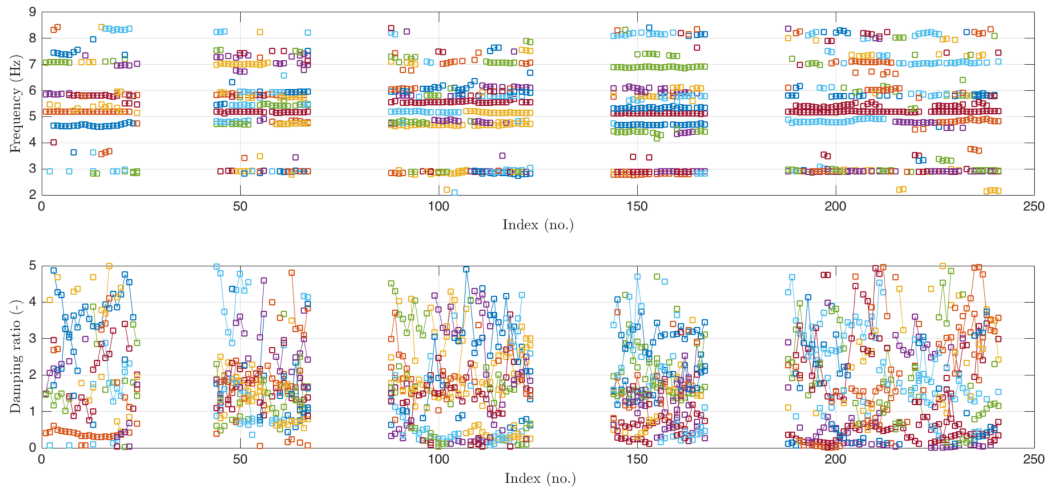


Figure 6.10: SSI mode tracking during the five selected cases.

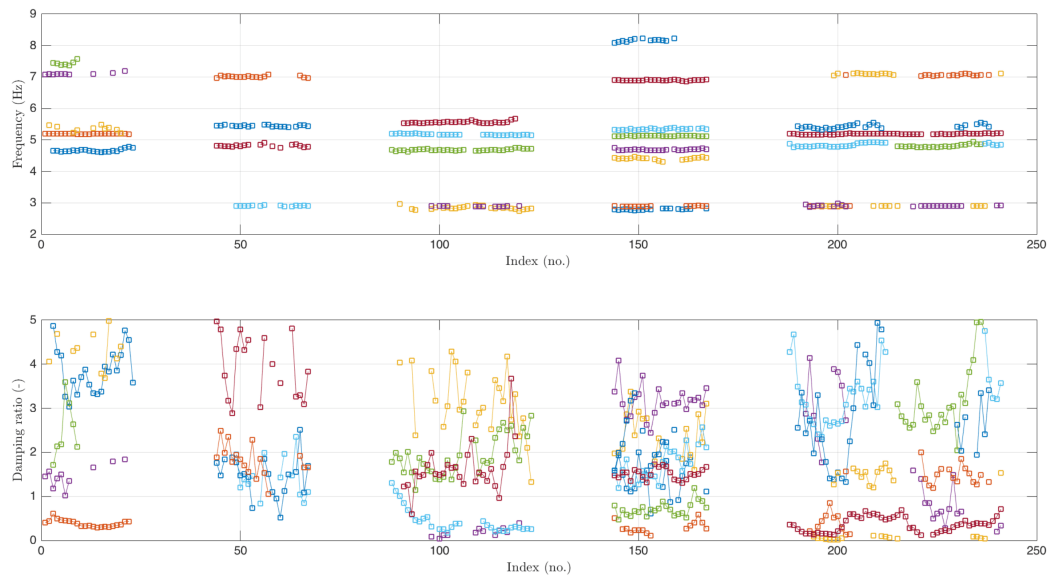


Figure 6.11: SSI modal clusters.

provides lower damping estimates, mostly below 0.5 %. Figure 6.13 shows the result of combining the SSI modal clusters across the five cases. Here it is observed that the green squares of the second vertical bending mode at 5.2 Hz have consistently the lowest damping values of below 0.5 % together with the few identifications in orange of the first vertical bending mode at 2.9 Hz. The first lateral bending mode at 4.7 Hz and the first torsion mode at 5.4 Hz have the highest damping values reaching a maximum of 5 %.

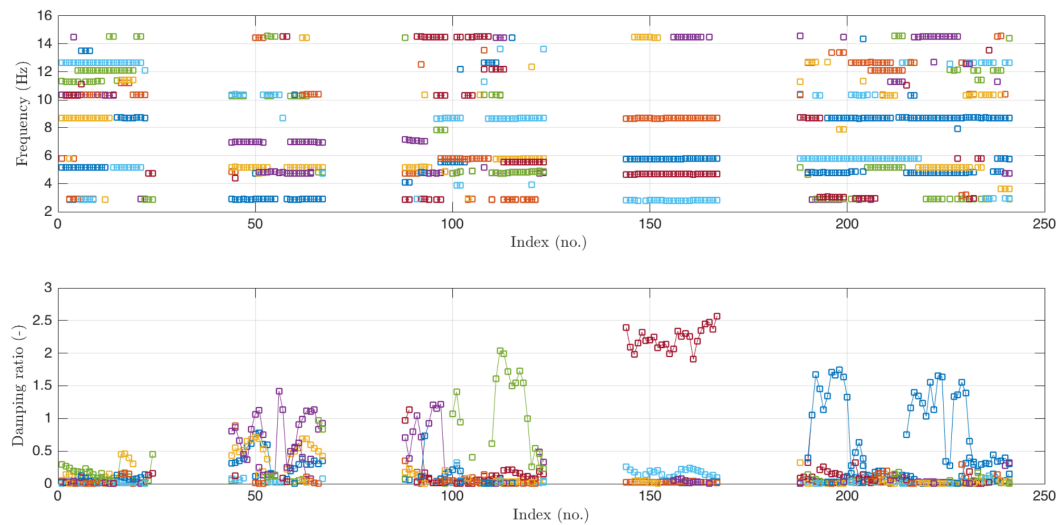


Figure 6.12: LSCF mode tracking during the five cases.

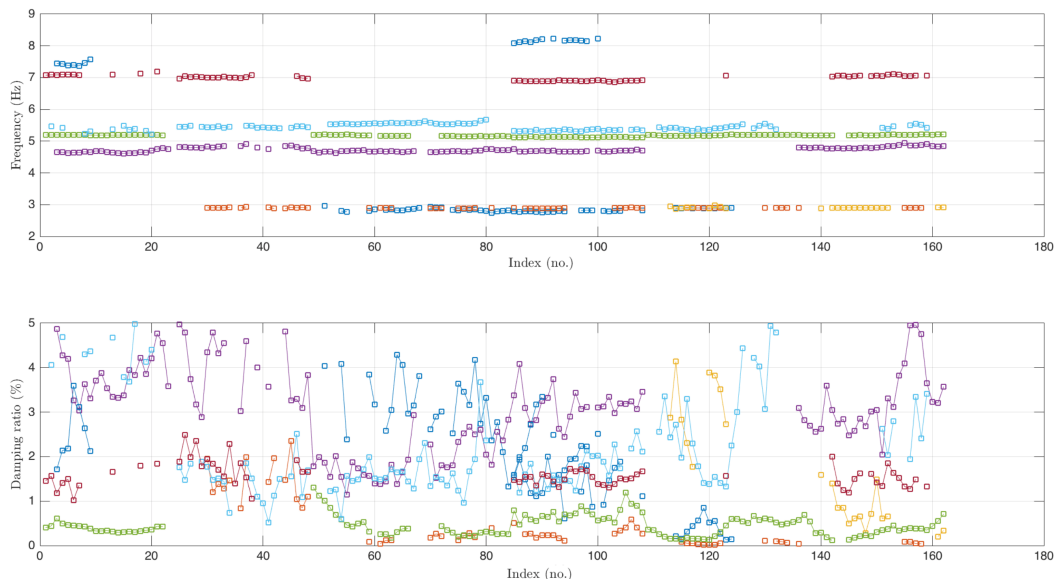


Figure 6.13: Modal clusters frequency and damping.

### 6.4.5 Modal Correlation

Correlation plots for cases 3, 4 and 5 are shown in Figure 6.14, Figure 6.15 and Figure 6.16. The tracked modes are correlated against ship speed (Speed), water temperature (Wtemp), air temperature (Atemp), wind velocity (Wvel) and wind direction (Wdir). Environmental parameters are averaged over 20 minutes for correlation with the system identification results.

Considering the complexity of the measured physical phenomena together with the data processing techniques, useful correlation coefficients are expected to occur in the range of 0.5 - 0.7. Correlation coefficients are plotted in each

block and red values indicate a  $p$  value  $< 0.05$  indicating the result is statistically significant. Statistically significant correlations are observed among various modes and input parameters. The first vertical bending mode indicated by *var2* in Figure 6.14 for example, shows significant correlation with *speed*, *wind velocity* and *wind direction*. This suggests that these input variables would be good predictors of *var2*. The maximum correlation coefficient of 0.94 is between the first vertical bending mode at 2.9 Hz and water temperature during case 5. Since the aim of the correlation investigation is to determine whether trends can be used to make future predictions, correlation coefficients above 0.5 which are also significant ( $p < 0.05$ ) are considered useful.

Investigations were then conducted to determine if there are variables which always trend together e.g. first bending and speed for example. It was however found that despite strong inter variable relationships, that no constant relationship emerged across the five cases. Figure 6.17 shows the total correlation after stitching together the data from all five cases. Here it can be seen that the correlations decrease in general and that there are no obvious trends. This is an important observation which confirms the complexity of the system. It also indicates that useful modelling and prediction will rely on a detailed understanding and classification of operating and environmental parameters into suitable cases. Models describing different cases can then be built and trained on real data in order to make optimal future predictions.

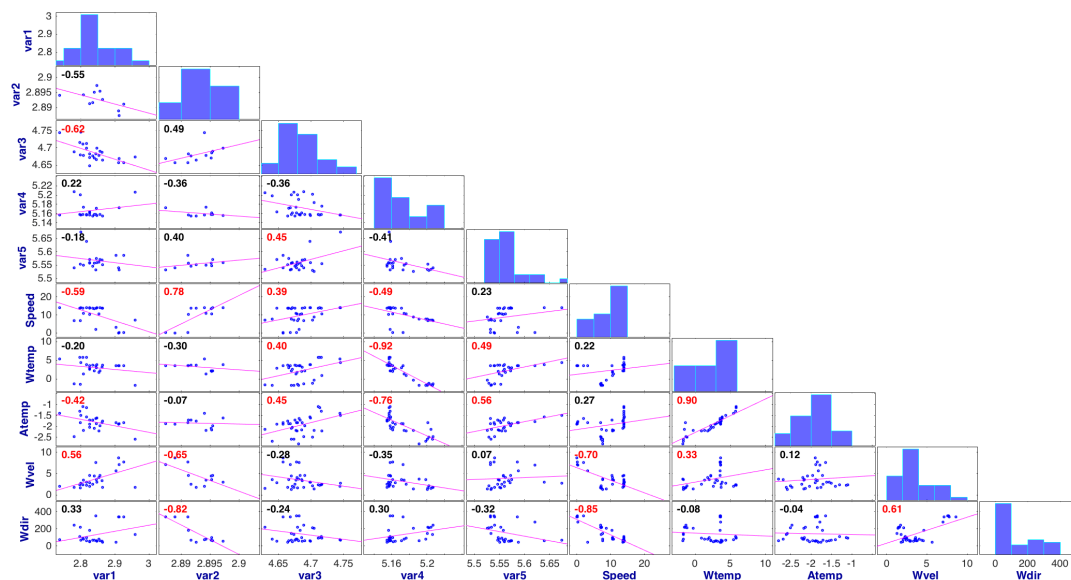


Figure 6.14: Case 3 correlation.

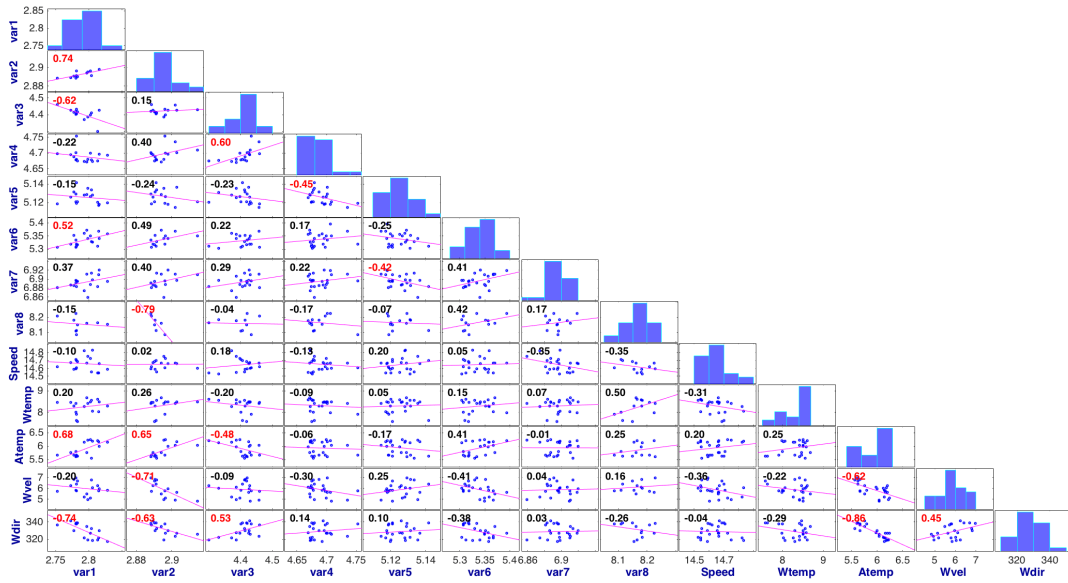


Figure 6.15: Case 4 correlation.

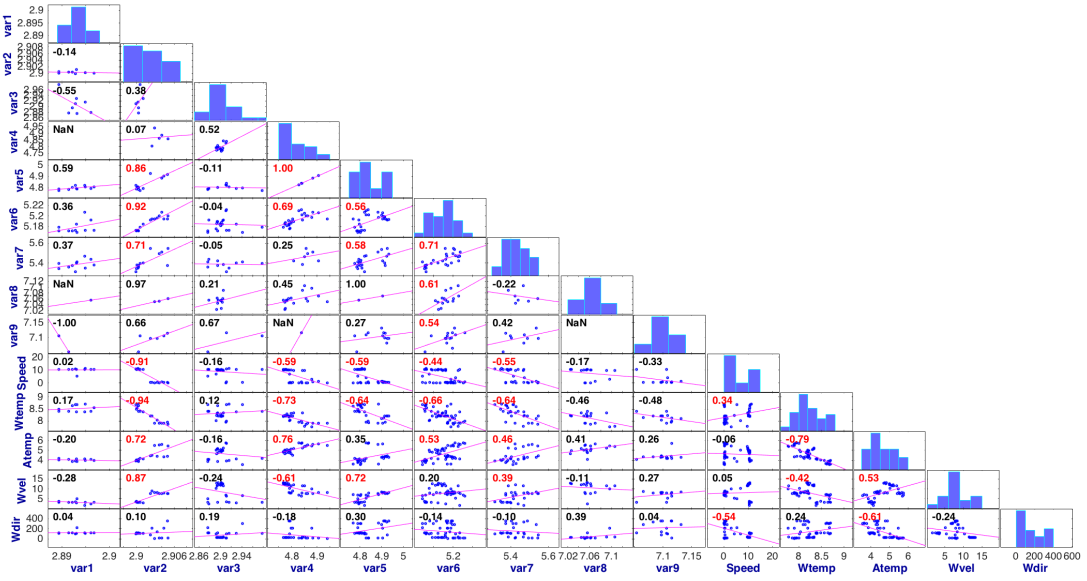


Figure 6.16: Case 5 correlation.

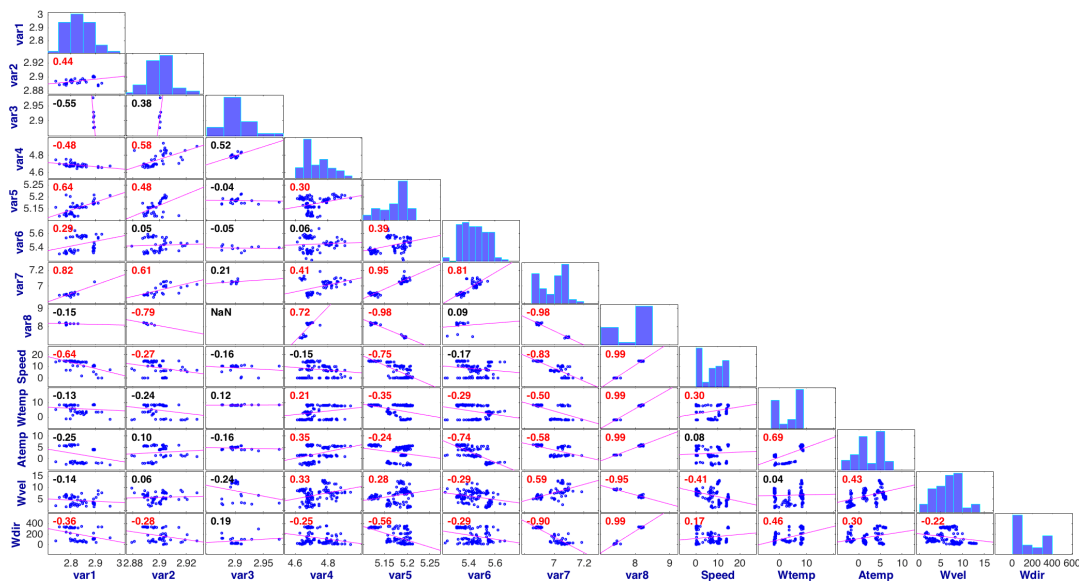


Figure 6.17: Total correlation.

## 6.5 Conclusion

System identification and modal parameter tracking was conducted on full scale data from the polar research vessel Polarstern. Similarities between two different identification techniques working in time and frequency domain provided confirmation that physical modes were identified. Differences in the estimates of the two methods were also observed, most notably in damping. Future research into combined modal models using each methods respective strengths is proposed.

A library of seven global modes was identified in the bandwidth 2 - 10 Hz. These included the first (2.9 Hz), second (5.2 Hz) and third (7.1 Hz) vertical bending modes, the first (4.7 Hz) and second (7.6 Hz) lateral bending modes and first (5.4 Hz) and second (8.3 Hz) torsional modes. A mode tracking algorithm using the MACXP was able to track modes across different operating cases. Statistically significant correlations were observed among various modes and input parameters. This confirmed the hypothesis that inter variable relationships exist and can be used for model training and prediction. Furthermore the identified relationships were found to be complex and did not trend together across different operating cases. Useful modelling and prediction will therefore rely on a detailed understanding and classification of operating and environmental parameters into suitable cases. Models can then be built and trained within their operating classifications in order to make optimal future predictions for applications in structural health monitoring, automatic modal parameter selection or inverse force estimation.

# Chapter 7

## Models for Modal Prediction using System Inputs

### 7.1 Introduction

In order to perform Inverse Force Estimation (IFE) and Structural Health Monitoring (SHM) modal parameters must be accurately identified and sensitively tracked. This is not a trivial task when dealing with real structures with complex inputs, low excitation forces and noise. As discussed in Chapter 3 OMA can be used to identify modal parameters without knowledge of the input forces. This is achieved by making assumptions about the unmeasured forces which are modelled as stochastic white noise quantities. The drawback is that long time records are often needed to fulfil these assumptions. This can result in a smearing of modal estimates across changing input parameters, which can mask modal shifts due to structural damage and provide insufficient resolution during force reconstruction.

The sensitivity of modal estimates to changing system inputs is therefore of primary importance. A key observation is that changes in physical parameters will cause detectable changes in the vibration properties (Liu and DeWolf, 2007). These physical changes are propagated through the system properties (mass, damping and stiffness) as follows:

1. Environmental conditions - such as temperature, change the Youngs modulus and consequently the system stiffness.
2. System configuration - through discrete mass changes due to cargo or vehicle traffic for example.
3. Boundary conditions - such as ice compared to open water which effects damping and added mass differently.

This chapter presents an idea to improve the sensitivity of system identification and tracking using a statistical model and a Kalman filter. A key

objective was to make observed data maximally informative. This led to the development of a sliding predictive model using an optimized linear regression method to use system inputs which are not included in the standard system identification. Since both the model prediction and the system identification estimates contain different uncertainties the Kalman filter is proposed as a method to combine both estimates in an optimal way.

## 7.2 Background

By considering a structure such as a bridge, ship or aircraft as a ‘system’ it is possible to use the system identification framework to build a model relating the inputs to the outputs. This is illustrated in the context of a ship in Figure 7.1. System identification techniques such as Stochastic Subspace Identification (SSI) (Peeters and De Roeck, 1999) estimate the system parameters from output acceleration measurements with certain assumptions about the input forces. There are however other system inputs such as environmental and operational parameters. If the variation of these inputs are slower than system identification estimation lengths then this does not present a problem. However, if the input parameters change significantly during the system identification estimation, there will be a smearing of the modal estimates. Therefore a thorough understanding of the sensitivity of the input parameters on the system properties is essential (Zhou and Yi, 2014).

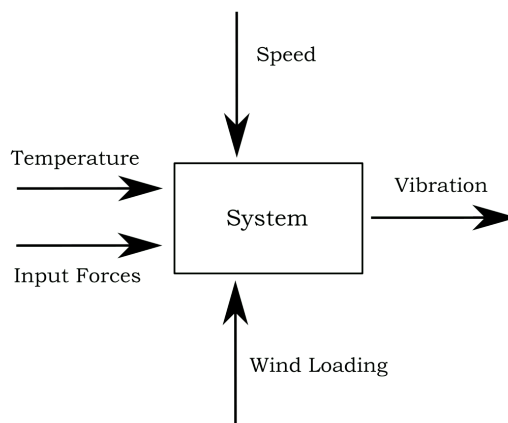


Figure 7.1: Ship system.

Research in this field has been conducted mainly into understanding the effects of temperature on the vibration properties of long-span bridges. Investigations were conducted into theoretical methods using equations relating Young's modulus to natural frequencies of beam elements by Xia *et al.* (2006). The complexity of long-span bridges however limited the effectiveness of these

closed form solutions. Trend analyses were conducted by various researchers with notable contributions by Cornwell *et al.* (1999); Wahab and De Roeck (1997); Peeters and De Roeck (2001); Gonzales *et al.* (2013). Significant correlations were observed with modal frequencies decreasing with increasing temperatures in general. It was also observed that different trends occurred with increasing temperatures as compared to decreasing temperatures. The development of quantitative models was investigated using linear models by Sohn *et al.* (1999), nonlinear models by Ding and Li (2011) and learning models using support vector machines by Ni *et al.* (2005). These models provided valuable insight and predictive power into the relationships between temperature and modal parameters. The use of quantitative models was established as a powerful tool in system modelling.

Output only system identification was developed from deterministic input-output system identification. Despite the usefulness of the assumptions made about the unknown input forces, it is known from control theory, see Ljung (1987); Franklin *et al.* (1990), that including any additional system inputs can improve the identification. Reynders and De Roeck (2008) developed a combined deterministic-stochastic subspace identification technique called OMAX. OMAX included known input forces from shakers, resulting in improved modal estimates as well as the ability to scale the mode shapes. The use of hybrid techniques are emerging as robust and accurate identification techniques.

Finally, the automation of system identification is required to process large amounts of data without expert user interaction. Automation is also important to maintain consistency in the estimates. Especially when investigating trends in data as a result of physical input parameters which could be masked by variations of mathematical parameters within the system identification algorithm. A large variety of state of the art automation techniques exist. Since the method proposed in this chapter can also be implemented as an automatic technique, a review of key automatic modal parameter selection methods is provided in the following section.

### 7.3 Automated Modal Parameter Selection

An overview of relevant automatic modal parameter selection methods is presented in Table 7.1 and will be summarized in the following section. Non-parametric techniques such as Frequency Domain Decomposition (FDD) are based on simple peak picking. These methods have been automated using the modal coherence around each identified peak in the singular value plot according to predefined limits by Brincker *et al.* (2007) and Rainieri and Fabbrocino (2010). Magalhães *et al.* (2008) found these methods to be sensitive to noise in the spectra, user defined frequency resolution, signal periodicity and spatial resolution affecting the Modal Assurance Criterion (MAC). FDD does not provide estimates for damping and extensions such as Enhanced Fre-

quency Domain Decomposition (EFFD) methods are known to underestimate damping due to windowing in the FFT averaging.

Improved estimates using parametric methods have been reported in studies by Peeters (2000); Magalhães *et al.* (2008); Reynders (2009). Consequently the automation of these techniques have attracted the most research interest. The usefulness of the stabilisation diagram as a tool for all parametric methods was used to develop the first automatic selection techniques. Scionti *et al.* (2003) developed a methodology and algorithm to mimic the decisions of an experienced modal analyst during examination of a stabilization diagram. This rule-based intelligence approach was based on observations that an engineer first selects a vertical column of poles which are then assessed based on the variance of frequency and damping ratio. This translated into a column selection using histogram bins and Euclidean norm distance weightings. These weightings were then used together with the frequency and damping variance to make an automatic pole selection. The consistent mode indicator method developed by Pappa *et al.* (1998) used a similar rule-based methodology to condense multiple estimates from the eigensystem realization algorithm (ERA) for the tail rudder of the NASA space shuttle. Govers (2012) and Mohanty *et al.* (2007) built on the observation of vertical pole selection to develop a Fully Automatic Modal Parameter Selection (FAMPS) technique. FAMPS used overlapping bands to classify consistent modal families. Damping variance and MAC values were then used to make the final pole selection.

Deraemaeker *et al.* (2008) and Reynders and De Roeck (2008) used a metric called the modal transfer norm which was based on the modal decomposition of the positive output PSD. This provided a measure of the error made when the  $i^{th}$  mode was removed from the model. The modal transfer norm was plotted in a stabilisation diagram as a rule-based criterion for automatic pole selection. Schwochow and Jelcic (2015) used the MACXP to track mode clusters at consecutive model orders starting from a user defined maximum. The MACXP was found to produce clear stabilisation diagrams with accurate model order tracking.

The grouping of modal clusters at different model orders lead naturally to the use of clustering techniques which are capable of grouping objects based on certain characteristics. Magalhães *et al.* (2009) used hierarchical clustering based on the Euclidian norms to group poles. A user defined “tree cut level” then determined the number of clusters from which to make the parameter selection. Verboven *et al.* (2002) expanded this technique using fuzzy clustering which allowed poles to belong to multiple clusters simultaneously. Statistical criteria were used together with modal phase collinearity and mode complexity to make the final mode selection. Andersen *et al.* (2007) developed a graph theory approach using poles (vertices) to build edge connections. A user defined minimum length of alignment was specified and used together with frequency, damping and MAC differences to automatically select poles in the stabilisation diagram. Neu *et al.* (2017) developed a multi stage clustering approach to deal

specifically with the issue of removing all user defined parameters. This was achieved using feature vectors and statistically profound threshold values from the measured Probability Density Functions (PDFs).

All the methods presented thus far deal with the automatic modal parameter selection from one set of data. A different approach to this problem involves using current knowledge of the system to improve future identifications. This can be especially beneficial when conducting continuous monitoring to ensure optimal predictions using as much information as is available. Carden and Brownjohn (2008) investigated the use of fuzzy C means clustering as a data condensation technique to track changes in the system state from environmental inputs. The idea was that if the system changes with environmental inputs the modes will shift. This would cause the centres of the fuzzy clusters to shift also. The tracking of these cluster centres was therefore used as an indicator of the dynamic characteristics based on an initial model. Goethals *et al.* (2004) proposed a supervised learning approach for automatic interpretation of stabilization diagrams. The algorithm was based on the theory of Least Squares Support Vector Machines (LSSVM). The self learning method automatically tuned thresholds and parameters based on a training data set. Since LSSVM is a binary classifier it defined poles as belonging to a physical or spurious group.

Table 7.1: Automatic modal parameter selection methods. (Stab = Stabilisation)

No.	Method	Lead Author	Operation
1	Modal Coherence	Brinker	FDD
2	LEONIDA	Rainieri	FDD
3	Rule-based Intelligence	Scionti	Stab
4	Consistent Mode Indicator	Pappa	Stab
5	FAMPS	Govers	Stab
6	Modal Transform Norm	Deraemaeker	SSI (Stab)
7	MACXP	Schwochow	SSI (Stab)
8	Hierarchical Clustering	Magelhaes	SSI Con (Stab)
9	Fuzzy Clustering	Verboven	LSCF (Stab)
10	Graph Theory	Andersen	SSI (Stab)
11	Multi Stage Clustering	Neu	Stab
12	Fuzzy C-Means clustering	Carden	Tracking
13	Self Learning	Goethals	Tracking

The conceptual idea of using a statistical model and a Kalman filter to improve system identification and tracking will now be developed, beginning with the Kalman filter which plays a central role.

## 7.4 Kalman Filter

The Kalman filter, Kalman (1960), is a predictor-corrector estimator that tries to obtain an optimal estimate of desired quantities from uncertain and noisy observations. It is based on a state space model of a system and real noisy measurements. The discrete time, deterministic stochastic state space model is presented in Equation 7.4.1.

$$\begin{aligned}x_{k+1} &= Ax_k + w_k \\ y_k &= Hx_k + v_k\end{aligned}\tag{7.4.1}$$

where  $x_k$  is the discrete time state vector and  $A$  is the discrete state matrix. The measurement equation contains the measured outputs  $y_k$  and the observation matrix  $H$ . Stochastic noise components are included as  $w_k$  process noise due to disturbances and modelling inaccuracies and  $v_k$  measurement noise from the sensors and cables.

The filter progresses iteratively with (1) a forward prediction of the system state in time (time update) followed by (2) a correction based on the predicted and measured system output (measurement update). The filter is optimal in the sense that if the noise is Gaussian, it minimizes the mean square error (error covariance) of the estimated parameters. The process is illustrated in Figure 7.2.

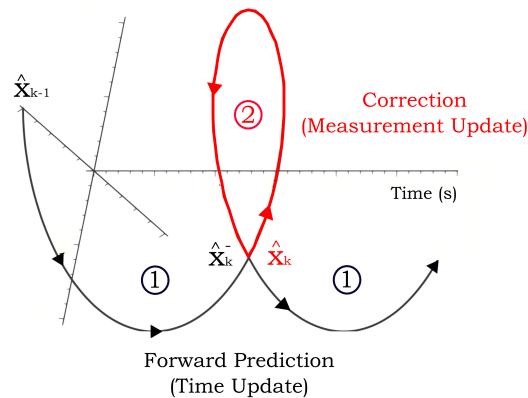


Figure 7.2: Kalman filter.

The Kalman filter is initiated with user defined parameters  $Q$ ,  $R$ ,  $P_{k-1}$  and  $\hat{x}_{k-1}$ .  $Q$  and  $R$  are the time invariant process and measurement noise covariances. The noise covariances are used to tune the model to rely more on (trust) either the model or the measurements. The error covariance  $P_{k-1} = E[e_{k-1}^- e_{k-1}^{-T}]$  is used as a minimization function by the Kalman gain  $K$  and can be initiated as any non zero value. The initial state estimate  $\hat{x}_{k-1}$  can also be chosen arbitrarily and updated if faster convergence is required.

The iterative filter begins with a forward prediction of the state from  $\hat{x}_{k-1}$  to  $\hat{x}_k^-$  based on the model as shown in Equation 7.4.2. This is known as the

priori or ‘reason’ estimate. The error covariance is also projected forward through the model to  $P_k^-$  in Equation 7.4.3. The measurement update then estimates the Kalman gain matrix  $K$  in Equation 7.4.4. The Kalman gain is then used to blend the priori estimate with the residual ( $y_k - H\hat{x}_k^-$ ) to determine the posteriori or ‘experience’ state estimate  $\hat{x}_k$  in Equation 7.4.5. The error covariance is then also updated based on the new Kalman gain in Equation 7.4.6. The filter then proceeds iteratively with forward predictions followed by measurement updates with optimal error covariance updates.

### (1) Time update equations

$$\hat{x}_k^- = A\hat{x}_{k-1} \quad (7.4.2)$$

$$P_k^- = AP_{k-1}A^T + Q \quad (7.4.3)$$

### (2) Measurement update equations

$$K_k = P_k^- H^T (HP_k^- H^T + R)^{-1} \quad (7.4.4)$$

$$\hat{x}_k = \hat{x}_k^- + K(y_k - H\hat{x}_k^-) \quad (7.4.5)$$

$$P_k = (I - K_k H)P_k^- \quad (7.4.6)$$

## 7.5 Idea

The idea is to reduce the uncertainty of system identification and tracking using a statistical model and a Kalman filter. The model will be trained using environmental inputs and system identification outputs. In the current work on the polar research vessel Polarstern, the environmental inputs include water and air temperature - which effect the Youngs modulus and thus the stiffness, ship speed - which effects the draft and bow wave, which add mass, and wind velocity and wind direction. These will be used to build the state matrix  $A$  in Equations 7.4.1 and 7.4.2. The predictive model will be used by the Kalman filter to make forward predictions based on new environmental inputs and then combined in an optimal way with the system identification estimate at the future time step. The method can be implemented in two ways, as shown in Figure 7.3.

The fundamental principle involves combining the forward prediction in red, with a measured value in blue to produce a Kalman estimate in green. Option A Kalman filters the regression model prediction from block  $b_1$  to block  $b_2$ , shown by the red arrow, with the automatic system identification estimate indicated by the blue circle, resulting in the green diamond. Option B Kalman filters the regression model prediction with the system identification estimate nearest the future prediction in the stabilisation diagram, indicated by the blue plus symbol. Option A therefore relies on a previous automatic pole selection, while option B also functions as an automatic modal parameter selection technique.

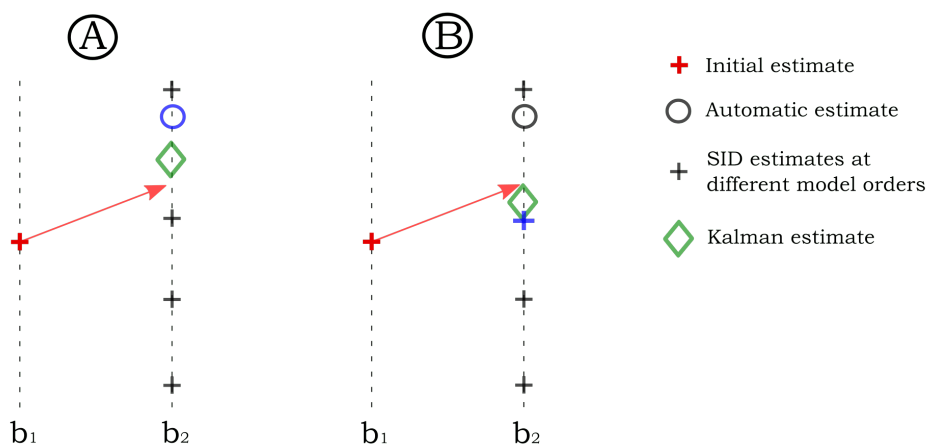


Figure 7.3: Kalman filter options.

## 7.6 Numerical Simulation

The method is first demonstrated numerically using a five Degree Of Freedom (DOF) system. A data set of 20 observations of each frequency is created and a normally distributed random error is added to each observation. A sinusoidal temperature variation is simulated through an approximate relationship between temperature, Young's modulus and natural frequency. The measurement noise covariance  $R$  is calculated from the simulated data and the model noise covariance  $Q$  is tuned to trust the model slightly more than the measurements. The error covariance matrix  $P$  is updated in a loop in order to begin filtering with an optimal error covariance. The results of the simulation are presented for mode 3 and mode 4 in Figure 7.4a and 7.4b. The Kalman filter estimates are seen to be closer to the true values in general, and also show the sinusoidal trend in the temperature variation. The cumulative error is improved by 85 % for mode 3 and 89 % for mode 4.

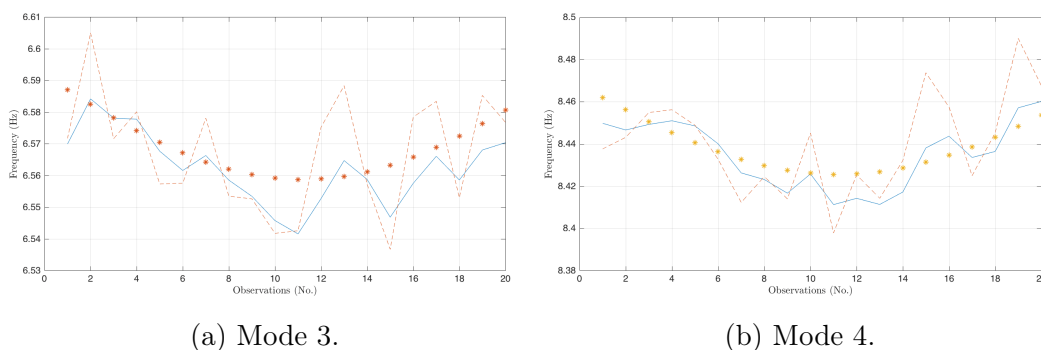


Figure 7.4: Numerical simulation. \* True value  $--\rightarrow$  True value + noise + temperature variation  $\rightarrow$  Kalman filter estimate.

## 7.7 Results

### 7.7.1 Signal Processing

The signal processing applied to the raw data is illustrated in Figure 7.5. The response variables were detrended and decimated from 2048 Hz to 64 Hz. The signal was then band pass filtered between 2 Hz and 12 Hz. Stochastic Subspace Identification (SSI) was used to estimate the system's eigenvalues and eigenvectors. SSI was performed on 20 minute data blocks with 75 % overlap. The 20 minute block was chosen to be long enough to include sufficient spectral information and over 3000 cycles of the lowest frequency, without over smearing the slower variations in environmental parameters. Modal tracking was then performed using a pole weighted Modal Assurance Criterion called the MACXP (Vacher, 2010). This enabled the identification and tracking of modes belonging to the same cluster.

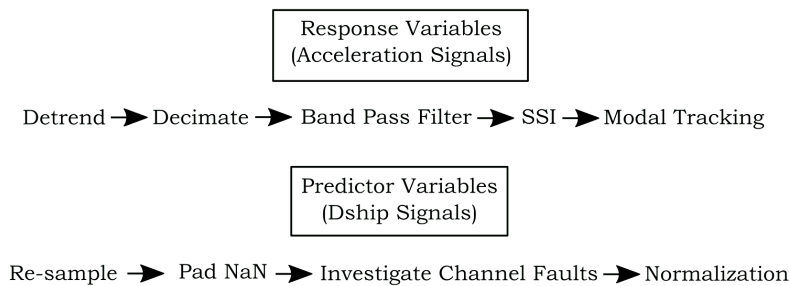


Figure 7.5: Signal processing of response and predictor variables.

The predictor variables were recorded by an on board system called Dship. Each variable has a different sensor, measurement unit and sample frequency. The signals were first re-sampled to 20 minute averages with 75 % overlap in agreement with the SSI estimates. Missing data was padded with NaN for indexing purposes. Investigations of faulty channels through the statistical Kurtosis value revealed spurious measurements due to loose connectors, bad grounding or other interference. Predictor variables were then normalized to account for non-uniform measurement units and amplitudes which cause bias in predictive models.

Correlations between measured predictor variables in Figure 7.6 were used to define a parsimonious predictor subset. Trends can be seen between water temperature and air temperature and wind velocity and wind velocity relative. Since two trend lines are observed between water and air temperature, and since temperature is expected to be an important predictor of modal parameters, both variables are retained for model training. Only absolute wind velocity is used since wind velocity relative includes ship speed which is already accounted for in the predictor set. The relative wind direction is used for modelling since there is no information about the ship heading. Uncorrelated

predictor variables are a good indication that each variable adds new (independent) information. Histograms on the matrix diagonal are not normally distributed, since certain conditions occur more often than others. The normal distribution of measured predictor variables is however not a requirement for statistical modelling, but rather the normal distribution of the residuals or error terms.

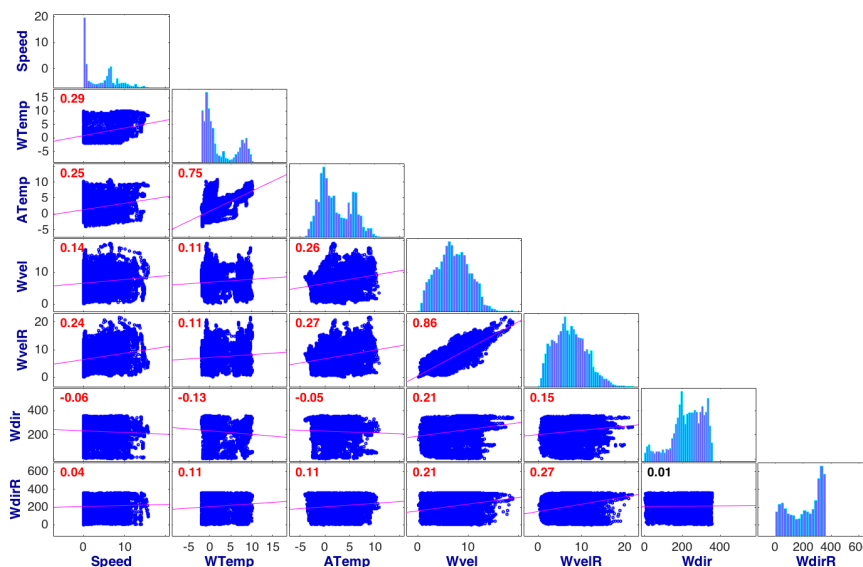


Figure 7.6: Correlation of measured predictor variables.

Figure 7.7 shows the vibration response channels which contained NaN values during the voyage. It can be seen that channels 5, 6, 13 and 22 contained most NaN values. This was due to a faulty cable on channel 5, poor grounding on channel 6, a loose end connector on channel 13 and unknown electrical interference on channel 22. These problems were detected and fixed during the voyage. However due to matrix multiplication using the dot product in SSI and mode tracking resulting in fully populated NaN matrices, it was decided that these four channels would be removed from the data completely. These are associated challenges of real data on large structures over long durations.

## 7.7.2 Model Training

The first predictive model investigations were aimed at identifying case specific models. This was based on research by Gonzales *et al.* (2013) who found that data driven bridge models showed clearer trends when split between increasing and decreasing temperature. Constant vessel speeds between 5 - 8 knots for over 100 minutes was defined as a test case. An algorithm was written which allowed a user to navigate through the data and interactively

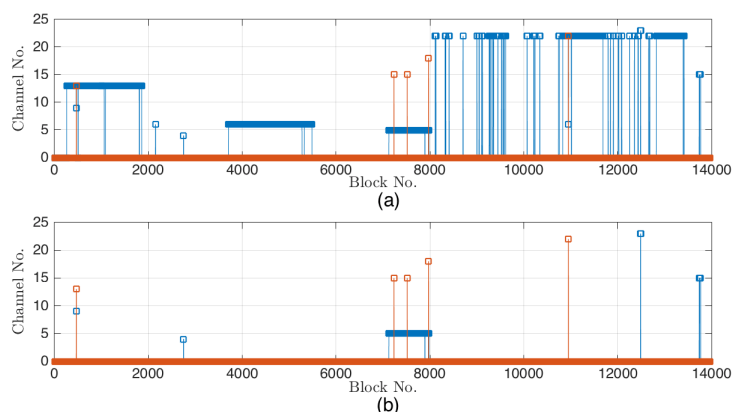


Figure 7.7: Vibration channels containing NaN's during the voyage (a) before (b) after channel removal.

train the predictive model. The predictor variables of the current data cluster were plotted by purple circles together with the corresponding modal tracking and correlation results. The user could then select which modes to predict as well as whether to accept the current cluster, which would then turn green, or reject the current cluster, turning red. The results of the predictor variables with 20 green clusters are shown in Figure 7.8.

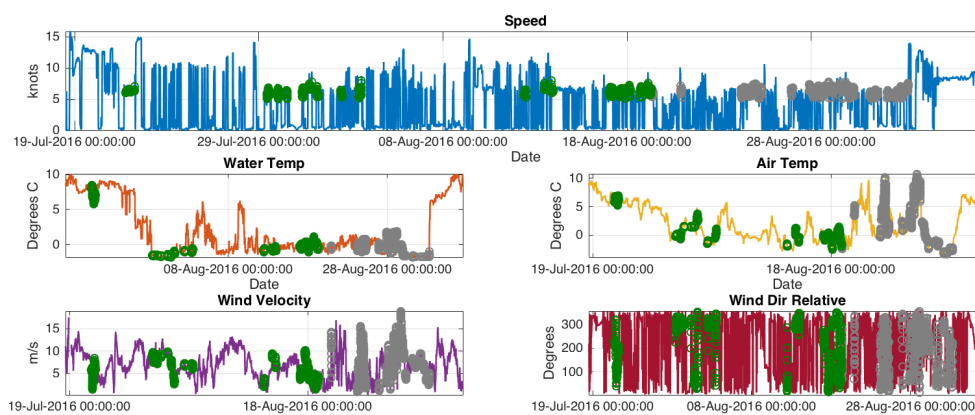


Figure 7.8: Constant speed model training.

The corresponding modal tracking is presented in Figure 7.9. The global modes can be identified by dominant lines at 2.9 Hz, 4.7 Hz, 5.2 Hz, 5.4 Hz, 7.1 Hz and 7.6 Hz. From the associated eigenvectors shown in Figure 7.10 these modes are seen to consist of the first 2.9 Hz, second 5.2 Hz and third 7.1 Hz vertical bending modes, the first 4.7 Hz and second 7.6 Hz lateral bending modes and first 5.4 Hz torsional mode.

During the model training it was observed that modes were not tracked in the same clusters or modal families throughout the data set, despite updating the eigenvalues and eigenvectors at each identification. This can be seen by

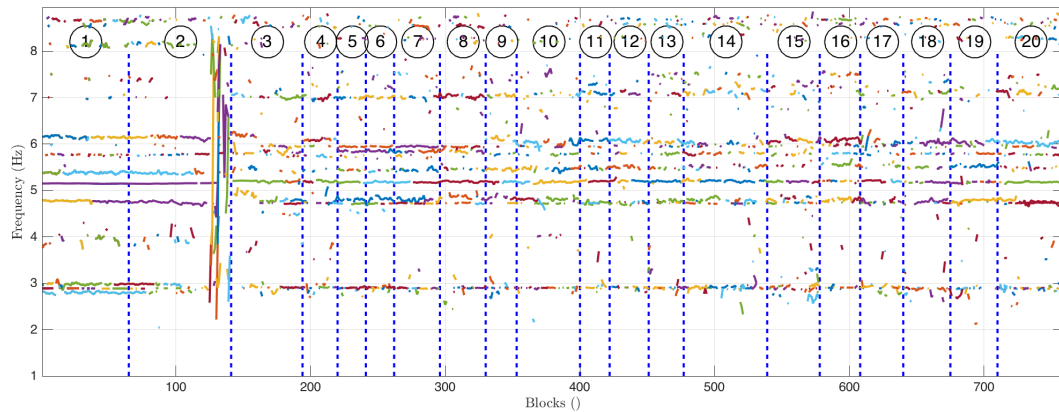


Figure 7.9: Constant speed modal parameter tracking.

the colour variations in the dominant lines in Figure 7.9. It was also observed that other predictor variables could change considerably during constant speed cases. No intuitive case equivalent to bridge temperature was observed. It was also noted that significant structural changes took place during the voyage due to burning approximately 2000 tons of diesel as well as changing ballast at discrete intervals.

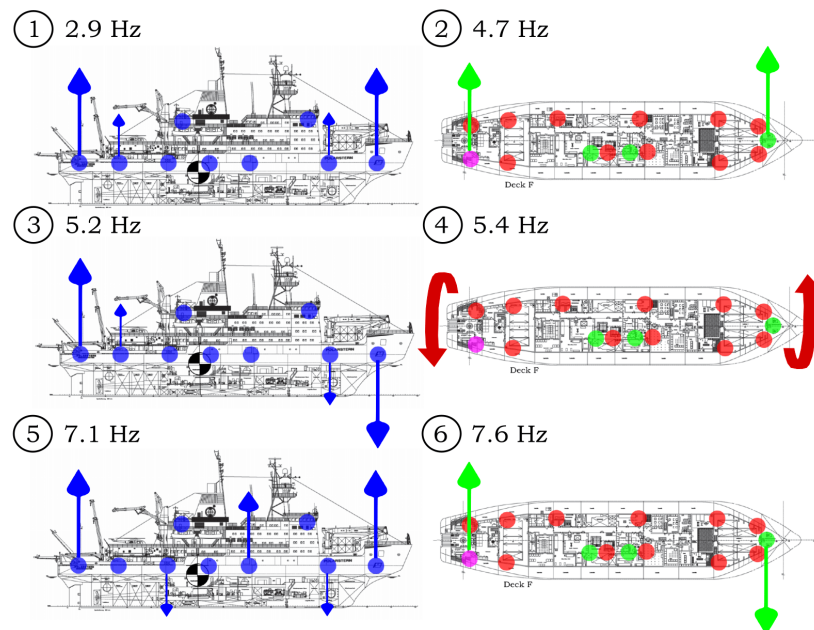


Figure 7.10: Polarstern mode shapes.

From these observations it was decided that the most logical model would need to update or slide with the vessel - so called predictive sliding model. This would account for modal cluster or family changes by making predictions based on the most recent modes. The sliding model would also only use recent

predictors which are appropriate for the current system parameters. Since the vessel properties such as mass vary more slowly than the predictors this would allow for accurate predictions in the vessels current configuration. The length of the window used to train the forward prediction model could also be adjusted by lengthening to account for operations with slowly varying parameters such as open water navigation or reducing to account for more rapidly changing conditions such as during ice navigation.

### 7.7.3 Predictive Sliding Model

The predictive sliding model was investigated on the two cases shown in Figure 7.11. Case 1 was a constant speed case containing 25 data blocks. Case 2 was an alternating speed case between 0 and 10 knots containing 65 data blocks.

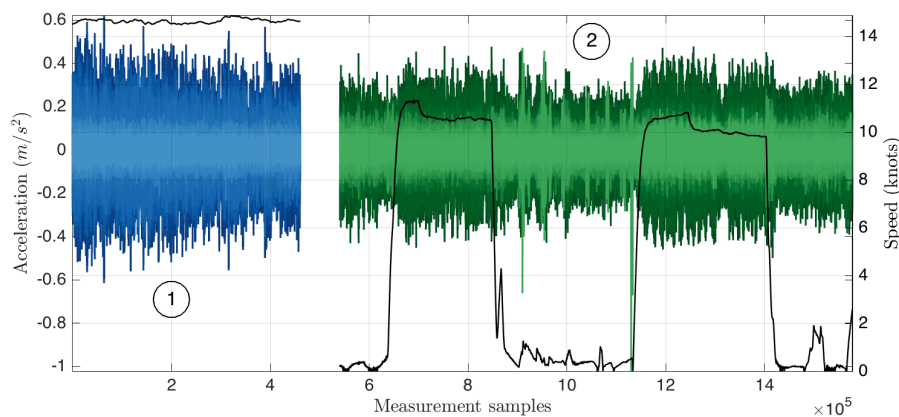
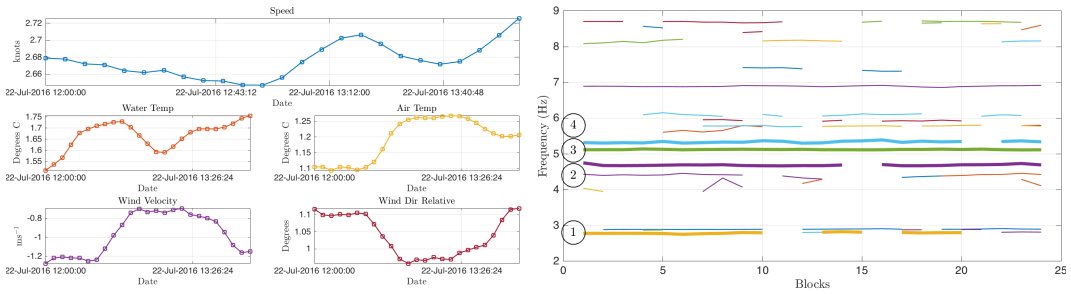


Figure 7.11: Acceleration time histories and ship speed for case 1 and 2.

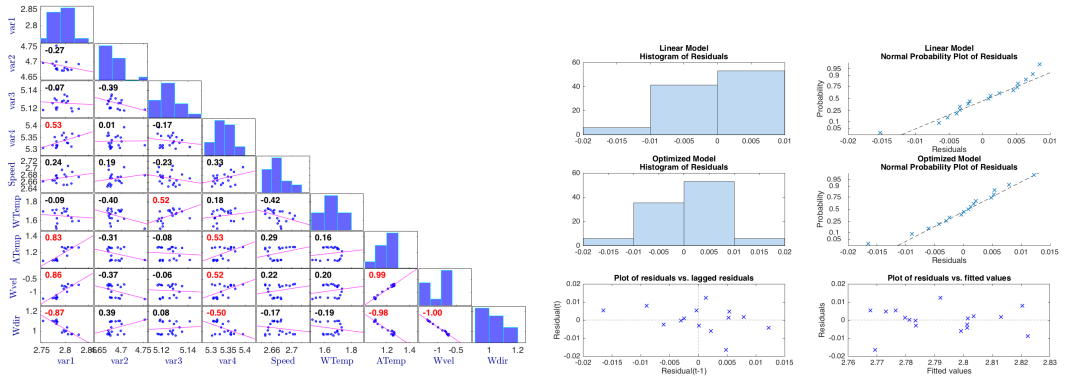
Figure 7.12 presents the predictive model work flow for case 1. The normalized predictor variables are shown in Figure 7.12a and are seen to be non-stationary. The results of the modal tracking algorithm on the SSI estimates is shown in Figure 7.12b. The first four modes are identified and flagged for prediction. The correlation plot in Figure 7.12c indicates where linear trends among variables exist. The predictor and response variables are then used to fit a linear regression model in Matlab using *fitlm.m*. The model is then optimized using the Matlab *step.m* function which chooses the most significant terms to add or remove. The histogram and normal probability of residuals for the linear model and optimized linear model are shown in Figure 7.12d. Plots of the residuals versus lagged residuals and residuals versus fitted values are also shown to determine whether there was predictive power in the residuals as indicated by trends. The residuals are seen to become more normally distributed after the step optimization and no trends in the residuals were observed.

CHAPTER 7. MODELS FOR MODAL PREDICTION USING SYSTEM INPUTS



(a) Predictor variables.

(b) Modal tracking.



(c) Correlation.

(d) Residuals.

Figure 7.12: Predictive model work flow for case 1.

The statistical prediction model of each natural frequency  $f_n$  was then written in terms of the predictor variables and regression coefficients from the optimized model as follows:

$$f_n = C_n + \alpha_n * Speed + \beta_n * Wtemp + \gamma_n * Atemp + \delta_n * Wvel + \mu_n * Wdir + \varphi_n * Speed * Wtemp \tag{7.7.1}$$

The optimal predictive model parameters for each mode are shown in Table 7.2. In order to use this model in the Kalman filter the system matrix  $A$  and state estimate  $\hat{x}_{k-1}$  are written as shown in Equation 7.7.2.

Table 7.2: Predictive model parameters for case 1.

No.	$C$ Intercept	$\alpha$ Speed	$\beta$ Wtemp	$\gamma$ ATemp	$\delta$ Wvel	$\mu$ Wdir	$\varphi$ SpeedWtemp
1	4.0944	-0.3875	-0.1115	0	0.0836	0	0
2	-64.1856	25.2316	40.6531	1.0438	-0.3476	0	15.2423
3	5.0390	0	0.0527	0	0	0	0
4	-80.5023	31.9889	50.7084	0.1459	0	0	-18.9363

$$A = \begin{bmatrix} 0 & 0 & 0 & 0 & C_1 & \alpha_1 & \beta_1 & \gamma_1 & \delta_1 & \mu_1 & \varphi_1 \\ 0 & 0 & 0 & 0 & C_2 & \alpha_2 & \beta_2 & \gamma_2 & \delta_2 & \mu_2 & \varphi_2 \\ 0 & 0 & 0 & 0 & C_3 & \alpha_3 & \beta_3 & \gamma_3 & \delta_3 & \mu_3 & \varphi_3 \\ 0 & 0 & 0 & 0 & C_4 & \alpha_4 & \beta_4 & \gamma_4 & \delta_4 & \mu_4 & \varphi_4 \\ 0 & 0 & 0 & 0 & 1 & 0 & 0 & 0 & 0 & 0 & 0 \\ 0 & 0 & 0 & 0 & 0 & 1 & 0 & 0 & 0 & 0 & 0 \\ 0 & 0 & 0 & 0 & 0 & 0 & 1 & 0 & 0 & 0 & 0 \\ 0 & 0 & 0 & 0 & 0 & 0 & 0 & 1 & 0 & 0 & 0 \\ 0 & 0 & 0 & 0 & 0 & 0 & 0 & 0 & 1 & 0 & 0 \\ 0 & 0 & 0 & 0 & 0 & 0 & 0 & 0 & 0 & 1 & 0 \\ 0 & 0 & 0 & 0 & 0 & 0 & 0 & 0 & 0 & 0 & 1 \end{bmatrix}, \hat{x}_{k-1} = \begin{Bmatrix} f_1 \\ f_2 \\ f_3 \\ f_4 \\ C \\ Speed \\ Wtemp \\ Atemp \\ Wvel \\ Wdir \\ SpeedWtemp \end{Bmatrix} \quad (7.7.2)$$

The results of the prediction model and Kalman filter for case 1 are shown in Figure 7.13. The first 20 blocks are used to train the predictive model. The blue circles are the SSI estimates, the red crosses show the model prediction of the training data and the dotted line shows the 95 % confidence bound. The model is seen to recreate the training data very accurately with a tight confidence bound.

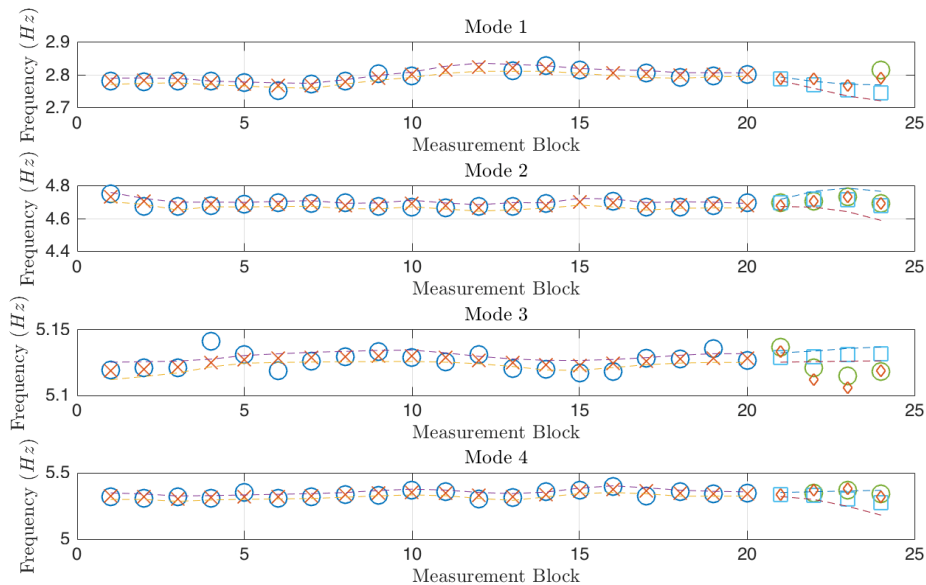


Figure 7.13: Kalman prediction for case 1.  $\circ$  SSI training set  $\times$  Training set prediction  $\square$  Statistical model prediction  $\circ$  SSI estimates  $\diamond$  Kalman estimates

The forward prediction of the model is shown by blue squares at blocks 21 - 24, and SSI estimates are shown by green circles (were available). The result of the Kalman filter is shown by the red diamonds. The model and measurement noise covariance matrices  $Q$  and  $R$  were set to trust the SSI estimates slightly more at roughly 65 %. The error covariance matrix  $P$  was

optimized in a loop in order to initialize the final Kalman filter result with an optimal  $P$  due to the short prediction sequence. The predictive model and SSI estimates show good agreement and follow similar trends. The Kalman filter shows promising results as an optimal blending technique between the model and the data which both contain uncertainties and noise.

Case 2 contains a longer data sequence with significant changes in all predictor variables. The normalized predictor variables in Figure 7.14a show the alternating vessel speed, decreasing water temperature, increasing air temperature and varying wind conditions. The modes were not identified as clearly and it was decided to track the first lateral, second bending and first torsional modes as indicated in Figure 7.14b. The correlation plot in Figure 7.14c show more dominant inter variable relationships. It should be noted that  $R^2$  values around 0.5 - 0.6 with p-value  $< 0.05$  are considered significant due to the nature of complex real data. The residual plots in Figure 7.14d show only a slight improvement in the step optimization. A weak trend is visible in the lagged residuals which is expected to have a negative influence on the results.

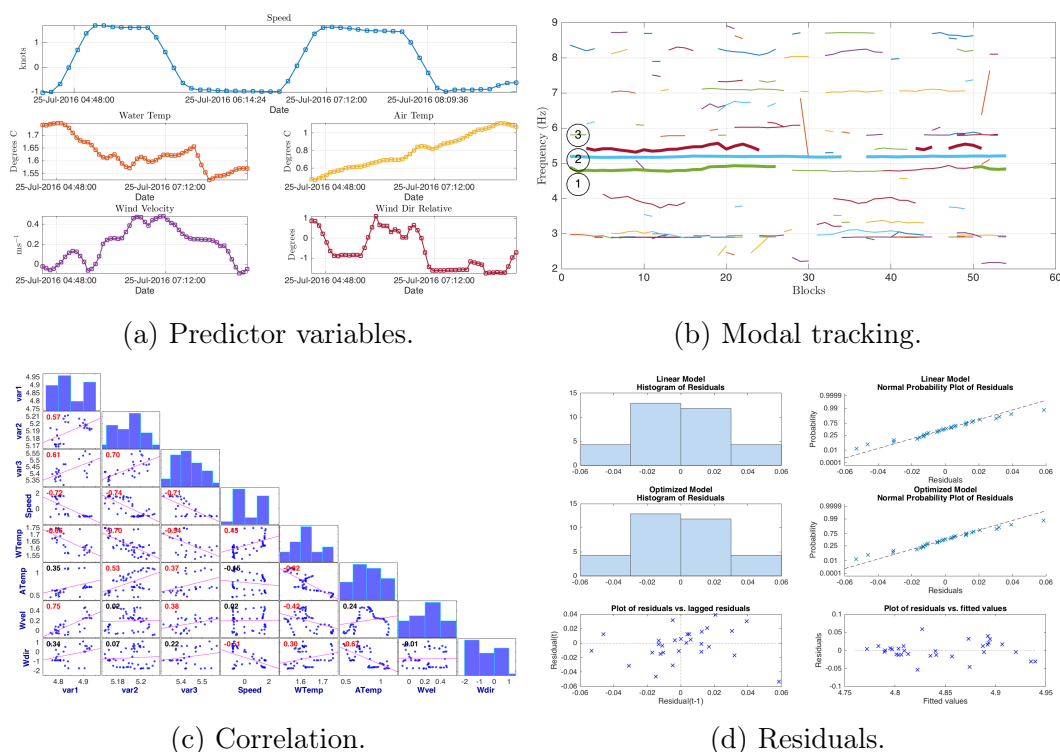
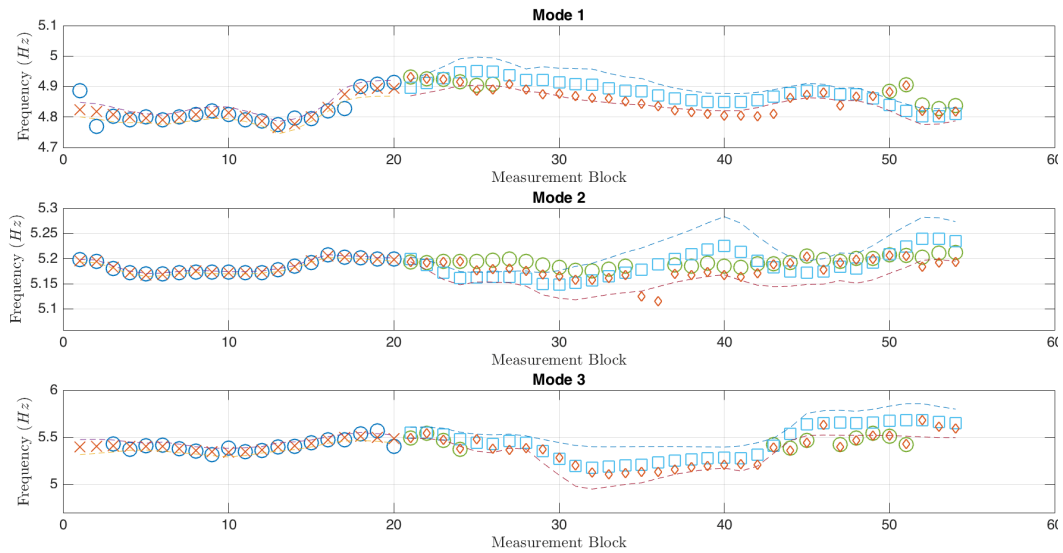


Figure 7.14: Predictive model work flow for case 2.

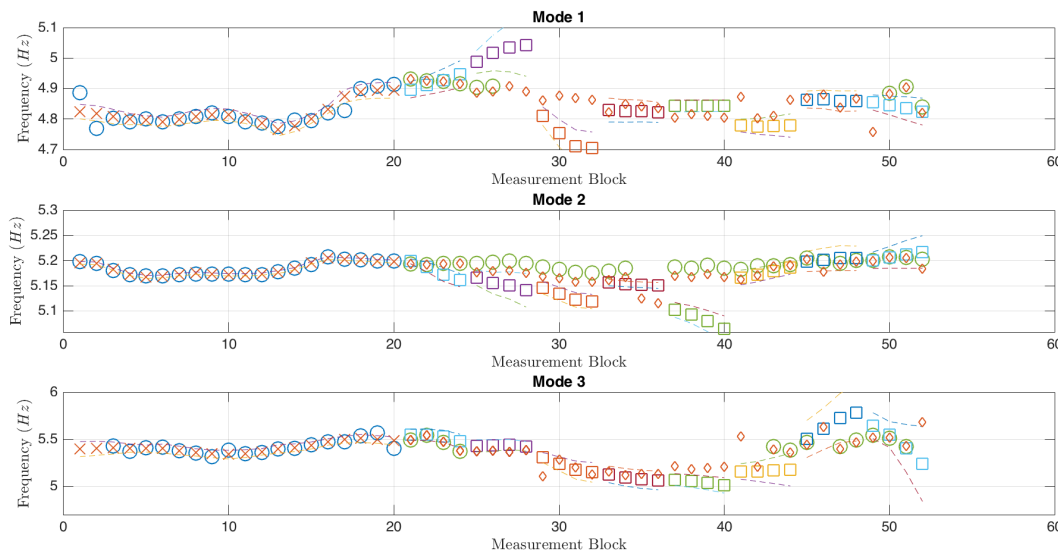
The optimal predictive model parameters for each mode are shown in Table 7.3. The results of the prediction model and Kalman filter for case 2 are shown in Figure 7.15. The first 20 blocks are again used to train the model, with SSI estimates indicated by blue circles and model predictions indicated by red crosses. The model is therefore seen to accurately re-construct the training

CHAPTER 7. MODELS FOR MODAL PREDICTION USING SYSTEM INPUTS

set (blocks 1 - 20). Two different methods were then investigated as shown in Figure 7.15a and 7.15b.



(a) 34 block forward prediction.  $\circ$  SSI training set  $\times$  Training set prediction  $\square$  Statistical model prediction  $\circ$  SSI estimates  $\diamond$  Kalman estimates



(b) 4 block forward prediction.  $\circ$  SSI training set  $\times$  Training set prediction  $\square$   $\square$   $\square$  Statistical model prediction  $\circ$  SSI estimates  $\diamond$  Kalman estimates

Figure 7.15: Kalman prediction for case 2.

Figure 7.15a shows the result of using the prediction model to make a 34 block forward prediction (from block 21 - 54) as shown by the light blue squares, with dotted lines showing the 95 % confidence bound. Available SSI estimates are indicated by green circles. The Kalman filter is iterated through

Table 7.3: Predictive model parameters for case 2.

No.	$C$ Intercept	$\alpha$ Speed	$\beta$ Wtemp	$\gamma$ Atemp	$\delta$ Wvel	$\mu$ Wdir	$\varphi$ Speed- Wtemp	$\kappa$ Speed- Atemp	$\vartheta$ Wtemp- Wvel
1	4.8109	-0.0181	0	0	0.2566	0	0	0	0
2	5.6715	-0.4563	-0.2884	0.0166	-3.0647	0	0.2168	0.1267	1.8115
3	6.9366	-1.4661	-0.8861	0	-0.3652	0	0.8472	0	0

the 34 forward prediction blocks, and the Kalman estimate is shown by the red diamonds. It can be observed that the Kalman estimates show a balanced combination of the model predictions and SSI estimates. The Kalman estimates are not overly or consistently biased by the SSI estimates. It is also observed that in the absence of SSI data (blocks with no green circles) the Kalman estimates do not show chaotic or unexpected variations and form a smooth transition back to blocks where SSI estimates are once again available.

Figure 7.15b shows the results of using the 20 block predictive model to make a 4 block forward prediction. The 4 blocks are then Kalman filtered and the 20 block training model window is slid forward by 4 blocks to now include the latest Kalman estimates. Each cluster of 4 block forward predictions is indicated by a different colour grouping of squares. These forward predictions show greater variability and lack continuity. Discontinuities are visible, most notably where there are no SSI estimates such as blocks 28 - 29 in mode 1. Very interestingly, the Kalman estimates show balance and continuity and do not seem to be highly effected where large model discontinuities exist. This is expected to be as a result of the Kalman filter optimization of the error covariance  $P$  for each 4 block cluster in a loop. In fact when the Kalman estimates are plotted on the same axes, as shown in Figure 7.16 they match almost exactly. The exception is only the first estimate of each 4 block cluster and furthermore only when there is no SSI estimate in the 4 block cluster transition.

## 7.8 Conclusions

A new method to improve the uncertainties in system identification and tracking using a statistical model and a Kalman filter was presented. The idea developed from the objective to make large data sets maximally informative. This was achieved by using measured system inputs to build an optimized regression model. The model was used in a Kalman filter together with SSI estimates to make optimal predictions. The idea was demonstrated on a simulated data set where it was found that the Kalman estimates improved system identification predictions, and also contained underlying data trends.

The method was then investigated on full scale data from the polar research vessel Polarstern. Initial model training led to the development of a predictive sliding model, which was tested on two different cases. The statis-

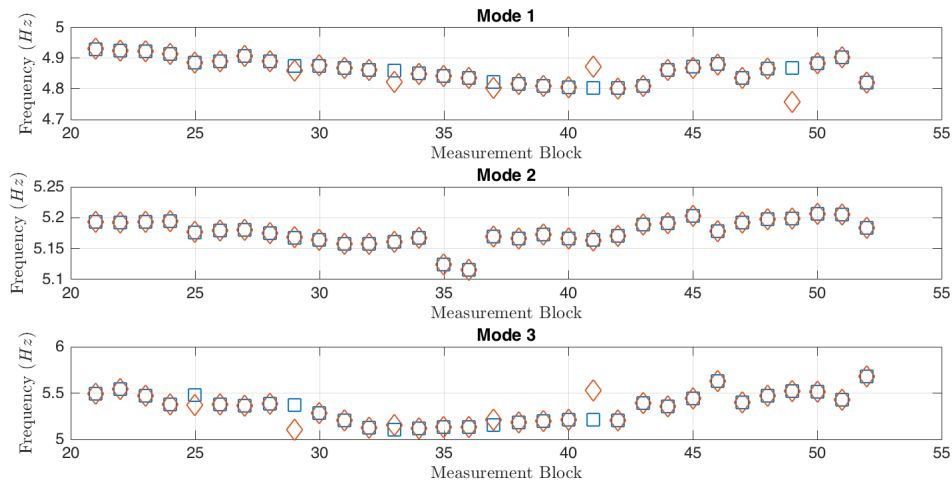


Figure 7.16: Kalman filter estimates for method 1  $\square$  and method 2  $\diamond$ .

tical model was trained on 20 data blocks and showed accurate reconstruction of the training data. Forward predictions were demonstrated using a 34 and 4 block variation. The statistical model was found to make more consistent future predictions for 34 blocks. The Kalman estimates were however not overly or consistently biased by the SSI estimates or the model predictions. It was also observed that in the absence of SSI data the Kalman estimates did not show chaotic or unexpected variation and formed a smooth transition back to blocks where SSI estimates were once again available. Comparison of Kalman estimates showed very high agreement across both implementations. In general the Kalman estimates show balanced and consistent results which based on numerical testing provide improved system identification estimations. Further research into understanding the effect of model training lengths and forward prediction lengths for different operating conditions is suggested.

# Chapter 8

## Conclusions and Future Research

### 8.1 Conclusions

This thesis investigated the use of system identification and modal tracking on polar vessels towards the development of a decision aiding system. Current SSI methods were found to be available only as commercial closed software. This limited understanding of the data flow through the mathematical algorithms. Open source software and development has proven to drive innovation, result in more robust code and be a force multiplier (Balter, 2015). The need for an open source toolbox which could be used both as a learning and research tool was identified. This led to the development of openSID, an open source toolbox for system identification using SSI. The toolbox is available on github, and interest from young researchers led to improvements and new ideas. It is also envisioned to use this platform to demystify SSI and help researchers find new applications of these powerful techniques in different fields. A parametric simulation study was conducted to investigate fundamental properties and provide insight from simple systems which can aid in understanding more complex results from real structures.

Full scale measurements were conducted on the research vessel Polarstern during a voyage to the Arctic. This is the first comprehensive data set including vibration responses and environmental parameters to span the entire operational profile of a research voyage to the Arctic. The vessel was instrumented with over 2 km of cable in Bremerhaven, Germany. The final instrumentation of accelerometers and the Data Acquisition System (DAQ) was performed in Tromsø, Norway. The expedition from 18 July 2016 to 6 September 2016 generated a valuable data set containing a broad spectrum of operational and environmental conditions. These include different cruising speeds, swell heights, swell directions and swell periods, ice types and ice breaking manoeuvres, water and air temperature variations as well as different vessel parameters such as draft, trim and engine configurations. Furthermore, this data set has been made openly available at PANGAEA data archiving under publication number PDI-15785. The main goals for making the data

open access are (1) so that results in this thesis can be tested, recreated and validated (2) opening the data to other researchers has the potential to bring a diversity of ideas and optimal solutions and provide additional human capital to drive innovation (3) a variety of open source data sets will allow open and transparent benchmarking of state of the art algorithms.

System identification was investigated on full scale data where it was found to identify seven global modes in the bandwidth 2 - 10 Hz. Not all modes were identified at all time instances due to the different excitation forces and magnitudes. Comparisons between SSI and LSCF were used to cross check modal clusters based on the eigenvectors. A modal tracking algorithm using a pole weighted Modal Assurance Criterion (MACXP) was developed and successfully used to track modal clusters across different operational profiles.

A novel method to improve the uncertainty and sensitivity of system identification and tracking was presented based on a data driven statistical model and a Kalman filter. A key objective was to make experimental data maximally informative by using additional system inputs. The idea was demonstrated on a simulated data set where it was found that the Kalman estimates improved system identification results. Model training on full scale data led to the development of a sliding predictive model using an optimized linear regression method. The model was found to accurately re-create the training data set and was used to make predictions based on future system inputs. Since both the model prediction and the system identification estimates contain different uncertainties the Kalman filter was used to combine both estimates in an optimal way. The Kalman filter estimates were observed to produce balanced and consistent results. The Kalman estimates were also not overly or consistently biased by the SSI estimates or the model predictions.

## 8.2 Future Research

Based on the current research findings and with the vision of a decision support system in mind, the following key points are proposed for future research.

### **Automation algorithms**

Automatic algorithms are required to process large amounts of data without expert user interaction. Automatic algorithms also allow for consistency across results. In this thesis an automatic SSI technique using the MACXP was explained. It was also shown how the novel Kalman filter method could be used as an automatic modal parameter selection method. Further investigations into the stability of these algorithms as well as their performance in real time is suggested.

## Big data

Measurements lasting several months and years generates huge amounts of data. The efficient storage and indexing of big data will facilitate optimal post processing. Condensing large sets of results into key indicators would allow these to be streamed to stations on land where alarms could alert researchers to interesting phenomena.

## Semi-real time performance

In order for the system to function as a useable tool semi-real time performance is required. Since system identification estimates require a certain data set length a sliding window could be used to provide estimates of a chosen block length i.e 5 or 20 minutes. This block length could be made shorter during ice breaking when conditions are changing more rapidly, aided by large excitation amplitudes and a typical white noise spectrum, and made longer during operations in calm open water when excitation is lower and longer data blocks are required for accurate modal estimations. A software architecture needs to be developed which automatically streams data in the desired format to a computer performing signal processing, system identification and modal tracking and then displays the result in a GUI over the local area network connection on the bridge.

## Permanent measurement technology

Full scale measurements on vessels operating in the ocean and polar regions face challenges of corrosion, large temperature variations, moisture and impact events. In order to make accurate measurements over many years the sensor attachment methods, housings, cable and cable end connections, data acquisition system (DAQ) and DAQ mounting need to be as robust as possible.

## Combined system identification algorithms

As explained in Chapter 6 different system identification algorithms have different strengths and weaknesses. It is therefore proposed for future research to investigate the potential of building modal models from combined system estimates so that each system identification technique can be used according to it's respective strong points.

## Operational and environmental profiling

In Chapter 6 it was observed that statistical relationships were complex and did not trend together across different operating cases. It was proposed that useful modelling and prediction would rely on a detailed understanding and classification of operating and environmental parameters into suitable cases.

In Chapter 7 this lead to the development of the predictive sliding model. Further investigations into operational and environmental profiling could reveal important patterns in the data and also allow for improved system identification estimates and model predictions.

### **Harmonics**

Although the Gauss-Newton and Periodogram smoothing harmonic removal techniques were not found to significantly improve system identification estimates on the current data set. Further investigations into the affects of the shaft line harmonic on the first vertical bending mode are suggested.

### **Eigenvector scaling**

The scaling of the identified eigenvalues is important for the reconstruction of the mass, damping and stiffness matrices. Changes in vessel draft, ballast and fuel were made during the voyage specifically to investigate the potential of using sensitivity based scaling methods. This will be an interesting topic for further investigation.

# List of References

- Andersen, P., Brincker, R., Goursat, M. and Mevel, L. (2007). Automated Modal Parameter Estimation for Operational Modal Analysis of Large Systems. In: *International Operational Modal Analysis Conference (IOMAC)*. Copenhagen, Denmark.
- AWI (2017). Alfred-Wegener-Institut Research Focus Areas. Available at: [www.awi.de](http://www.awi.de)
- Balter, B. (2015). 6 Motivations for Consuming or Publishing Open Source Software. Available at: [www.opensource.com](http://www.opensource.com)
- Bienert, J., Andersen, P. and Aguirre, R. (2015). A Harmonic Peak Reduction Technique for Operational Modal Analysis of Rotating Machinery. In: *International Operational Modal Analysis Conference (IOMAC)*. Gijon, Spain.
- Bjerkås, M., Skiple, A. and Iver Røe, O. (2007). Applications of Continuous Wavelet Transforms on Ice Load Signals. *Engineering Structures*, vol. 29, no. 7, pp. 1450–1456.
- Brandt, A. (2011). *Noise and Vibration Analysis Signal Analysis and Experimental Procedures*. John Wiley and Sons.
- Brandt, A. (2013). The ABRAVIBE Toolbox for Teaching Vibration Analysis and Structural Dynamics. *Conference Proceedings of the Society for Experimental Mechanics Series*, vol. 6, no. 203, pp. 131–141.
- Brandt, A. (2015). Comparison and Assessment of Methods to Treat Harmonics in Operational Modal Analysis. In: *International conference on structural engineering dynamics (ICEDyn)*. Lagos, Portugal.
- Brandt, a. and Linderholt, A. (2012). A Periodogram-Based Method for Removing Harmonics in Operational Modal Analysis. In: *Proceedings of the International Conference on Noise and Vibration Engineering (ISMA)*. Leuven, Belgium.
- Brincker, R. and Andersen, P. (2003). A Way of Getting Scaled Mode Shapes in Output Only Modal Testing. In: *International Modal Analysis Conference (IMAC)*. Kissimmee (FL), USA.

- Brincker, R., Andersen, P. and Jacobsen, N. (2007). Automated Frequency Domain Decomposition for Operational Modal Analysis. In: *International Modal Analysis Conference (IMAC)*. Orlando, Florida.
- Brincker, R., Andersen, P. and Moller, N. (2000). An Indicator for Separation of Structural and Harmonic Modes in Output Only Modal Testing. In: *International Modal Analysis Conference (IMAC)*, pp. 1649–1654. San Antonio, Texas.
- Brincker, R. and Ventura, C. (2015). *Introduction to Operational Modal Analysis*. Wiley.
- Broman, M. and Nordqvist, P. (2013). Global Response of Ship Hull During Ramming of Heavy Ice Features. Tech. Rep., Chalmers University of Technology.
- Carden, E. and Brownjohn, M. (2008). Fuzzy Clustering of Stability Diagrams for Structural Health Monitoring. *Computer-Aided Civil and Infrastructure Engineering*.
- Chen, Y.-K., Tunik, A. and Chen, A. (1990). Global Ice Forces and Ship Response to Ice - Analysis of Ice Ramming Forces. Tech. Rep., Ship Structure Committee, Washington.
- Coppotelli, G., Dessi, D. and Rimondi, R.M.M. (2008). Output-Only Analysis for Modal Parameter Estimation of an Elastically Scaled Ship. *Ship Research*, vol. 52, pp. 45–56.
- Cornwell, P., Farrar, C., Doebling, S. and Sohn, H. (1999). Environmental Variability of Modal Properties. *Experimental Techniques*, vol. 23, no. 6, pp. 45–48.
- Deraemaeker, A., Reynders, E., De Roeck, G. and Kullaa, J. (2008). Vibration-based Structural Health Monitoring using Output-only Measurements under Changing Environment. *Mechanical Systems and Signal Processing*, vol. 22, no. 1, pp. 34–56.
- Ding, Y.L. and Li, A.Q. (2011). Temperature-Induced Variations of Measured Modal Frequencies of Steel Box Girder for a Long-Span Suspension Bridge. *International Journal of Steel Structures*, vol. 11, no. 2, pp. 145–155.
- Edwards, R.Y., Lewis, J.W., Wheaton, J.W. and Coburn, J. (1972). Full-Scale and Model Tests of a Great Lakes Icebreaker. *Transactions of the Society of Naval Architects and Marine Engineers*, vol. 80.
- Ettema, R., Stern, F. and Lazaro, J. (1987). Dynamics of Continuous-Mode Icebreaking by a Polar Class Icebreaker Hull. Tech. Rep., Iowa Institute of Hydraulic Research, Iowa.

- Ewins, D.J. (2000). *Modal Testing: Theory and Practice*. 2nd edn. Research Studies Press LTD., Letchworth, Hertfordshire, England.
- Foltête, E. (2008). Multiple Operational Mode Shapes Normalisation from Mass Changes. In: *International Conference on Noise and Vibration Engineering (ISMA)*. Leuven, Belgium.
- Franklin, G., Powell, J. and Workman, M. (1990). *Digital Control of Dynamic Systems*. 3rd edn. Pearson, Boston, MA, USA.
- Goethals, I., Vanluyten, B. and De Moor, B. (2004). Reliable Spurious Mode Rejection using Self Learning Algorithms. In: *International Conference on Noise and Vibration Engineering (ISMA)*. Leuven, Belgium.
- Gonzales, I., Ülker-Kaustell, M. and Karoumi, R. (2013). Seasonal Effects on the Stiffness Properties of a Ballasted Railway Bridge. *Engineering Structures*, vol. 57, pp. 63–72.
- Goursat, M., Dohler, M., Mevel, L. and Andersen, P. (2010). Crystal Clear SSI for Operational Modal Analysis of Aerospace Vehicles. In: *International Modal Analysis Conference (MAC-XXVIII)*. Springer, Jacksonville, Florida USA.
- Govers, Y. (2012). *Parameter Identification of Structural Dynamic Models by Inverse Statistical Analysis*. Ph.D. thesis, Deutsches Zentrum für Luft- und Raumfahrt (DLR).
- Heylen, W., Lammens, S. and Sas, P. (1997). *Modal Analysis Theory and Testing*. Leuven: KUL Press.
- Heyn, H.-M. and Skjetne, R. (2015). Estimation of Forces caused by Ship-Ice Interaction using on-board Sensor Measurements. In: *Port and Ocean Engineering under Arctic Conditions (POAC)*. Trondheim, Norway.
- Jacobsen, N., Andersen, P. and Brincker, R. (2007). Eliminating the Influence of Harmonic Components in Operational Modal Analysis. In: *25th International Modal Analysis Conference (IMAC-XXV)*. Orlando, Florida.
- Jelicic, G., Schwochow, J., Govers, Y., Hebler, A. and Böswald, M. (2015). Fast Online Monitoring and System Identification for the Application in the Field of Aeroelasticity. In: *International Conference on Engineering Vibration*. Ljubljana, Slovenia.
- John, J.S. and Minnick, P. (1995). Ice Load Impact Study on NSF R/V National B. Palmer. *Ship Structure Committee*.
- Johnston, M., Timco, G., Frederking, R. and Miles, M. (2001). Whole-Ship Motions of USCGC Healy as Applied to Global Ice Impact. In: *Port and Ocean Engineering under Arctic Conditions (POAC)*. Ottawa, Ontario, Canada.

- Johnston, M., Timco, G.W., Frederking, R. and Miles, M. (2008). Measuring Global Impact Forces on the CCGS Terry Fox with an Inertial Measurement System called MOTAN. *Cold Regions Science and Technology*, vol. 52, no. 1, pp. 67–82.
- Kalman, R.E. (1960). A New Approach to Linear Filtering and Prediction Problems. *Journal of Basic Engineering*, vol. 82, no. 1.
- Kärnä, T. and Jochmann, P. (2003). Field Observations on Ice Failure Modes. In: *Port and Ocean Engineering under Arctic Conditions (POAC)*. Trondheim, Norway.
- Liu, C. and DeWolf, J.T. (2007). Effect of Temperature on Modal Variability of a Curved Concrete Bridge under Ambient Loads. *Journal of Structural Engineering*, vol. 133, no. 12, pp. 1742–1751.
- Ljung, L. (1987). *System Identification Theory for the User*. Prentice Hall, Englewood Cliffs, NJ, USA.
- Magalhães, F., Cunha, A. and Caetano, E. (2009). Online Automatic Identification of the Modal Parameters of a Long Span Arch Bridge. *Mechanical Systems and Signal Processing*, vol. 23, no. 2, pp. 316–329.
- Magalhães, F., Cunha, S. and Caetano, E. (2008). Permanent Monitoring of Infante D. Henrique Bridge Based on FDD and SSI-COV Methods. In: *International Conference on Noise and Vibration Engineering (ISMA)*. Leuven, Belgium.
- Maia, N., Silva, J., He, J., Lieven, N., Lin, R., Skingle, G., To, W.-M. and Urgueira, A. (1997). *Theoretical and Experimental Modal Analysis*. Research Studies Press LTD., Hertfordshire, England.
- Matusiak, J. (1982). Dynamic Loads and Response of Icebreaker SISU during Continuous Icebreaking. Tech. Rep., Aalto University, Helsinki, Finland.
- Matusiak, J. (2013). *Dynamics of a Rigid Ship*. Aalto University, Helsinki, Finland.
- Minnick, P. and John, J.S. (1990). Global Ice Forces and Ship Response to Ice. A Second Season. *Ship Structure Committee*.
- Mohanty, P., Reynolds, P. and Pavic, A. (2007). Automated Interpretation of Stability Plots for Analysis of a Non-Stationary Structure. *Conference Proceedings of the Society for Experimental Mechanics Series*.
- Mohanty, P. and Rixen, D.J. (2004). A Modified Ibrahim Time Domain Algorithm for Operational Modal Analysis Including Harmonic Excitation. *Journal of Sound and Vibration*, pp. 375–390.

- Mueller, A. and Ettema, R. (1984). Dynamic Response of an Ice-Breaker Hull to Ice Breaking. Tech. Rep., Iowa Institute of Hydraulic Research, Iowa.
- Neu, E., Janser, F., Khatibi, A.A. and Orifici, A.C. (2017). Fully Automated Operational Modal Analysis using multi-stage clustering. *Mechanical Systems and Signal Processing*, vol. 84, pp. 308–323.
- Ni, Y.Q., Hua, X.G., Fan, K.Q. and Ko, J.M. (2005). Correlating Modal Properties with Temperature using Long-Term Monitoring Data and Support Vector Machine Technique. *Engineering Structures*, vol. 27, no. 12 SPEC. ISS., pp. 1762–1773.
- Nyseth, H., Frederking, R. and Sand, B. (2013). Evaluation of Global Ice Load Impacts Based on Real-Time Monitoring of Ship Motions. In: *22nd International Conference on Port and Ocean Engineering Under Arctic Conditions (POAC'13)*. Espoo, Finland.
- Orlowitz, E. and Brandt, A. (2014). Modal Test Results of a Ship under Operational Conditions. In: *IMAC XXXIII Conference and Exposition on Structural Dynamics*. Orlando, Florida.
- Pappa, R.S., James, G.H. and Zimmerman, D.C. (1998). Autonomous Modal Identification of the Space Shuttle Tail Rudder. *Journal of Spacecraft and Rockets*, vol. 35, no. 2, pp. 163–169.
- Parloo, E., Verboven, P., Guillaume, P. and Van Overmeire, M. (2002). Sensitivity-Based Operational Mode Shape Normalisation. *Mechanical Systems and Signal Processing*.
- Peeters, B. (2000). *System Identification and Damage Detection in Civil Engineering*. Ph.D. thesis, Katholieke Universiteit Leuven.
- Peeters, B., Cornelis, B., Janssens, K. and Auweraer, H.V.D. (2007). Removing Disturbing Harmonics in Operational Modal Analysis. In: *International Operational Modal Analysis Conference (IOMAC)*. Copenhagen, Denmark.
- Peeters, B. and De Roeck, G. (1999). Reference-Based Stochastic Subspace Identification for Output-Only Modal Analysis. *Mechanical Systems and Signal Processing*, vol. 13, no. 6, pp. 855–878.
- Peeters, B. and De Roeck, G. (2001). One-year monitoring of the Z 24-Bridge: environmental effects versus damage events. *Earthquake engineering & structural dynamics*, vol. 30, no. January 2000, pp. 149–171.
- Peeters, B., Vanhollebeke, F. and Van Der Auweraer, H. (2005). Operational PolyMAX for Estimating the Dynamic Properties of a Stadium Structure during a Football Game. *IMAC-XXIII: Conference & Exposition on Structural Dynamics - Structural Health Monitoring*.

- Penzl, T. (1998). Numerical Solution of Generalized Lyapunov Equations. *Advances in Computational Mathematics*, vol. 8, pp. 33–48.
- Pintelon, R. and Schoukens, J. (2001). *System Identification: A Frequency Domain Approach*. Institute of Electrical and Electronic Engineers (IEEE).
- Rainieri, C. and Fabbrocino, G. (2010). Automated Output-Only Dynamic Identification of Civil Engineering Structures. *Mechanical Systems and Signal Processing*, vol. 24, no. 3, pp. 678–695.
- Reynders, E. (2009). *System Identification and Modal Analysis in Structural Mechanics*. Ph.D. thesis, KU Leuven.
- Reynders, E. and De Roeck, G. (2008). Reference-based Combined Deterministic-Stochastic Subspace Identification for Experimental and Operational Modal Analysis. *Mechanical Systems and Signal Processing*, vol. 22, no. 3, pp. 617–637.
- Rocca, G., Shuri, H., Peeters, B. and Ota, R. (2009). Experimental Ship Hull Dynamic Characterization using Operational Modal Analysis. In: *International Operational Modal Analysis Conference (IOMAC)*. Portonovo, Italy.
- Rosenow, S. (2007). *Identification of the Dynamic Behaviour of Marine Construction Structures*. Ph.D. thesis, Universität Rostock.
- Rosenow, S.-e., Uhlenbrock, S. and Schlottmann, G. (2007). Parameter Extraction of Ship Structures in Presence of Stochastic and harmonic Excitations. In: *International Operational Modal Analysis Conference (IOMAC)*. Copenhagen, Denmark.
- Schwochow, J. and Jelacic, G. (2015). Automatic Operational Modal Analysis For Aeroelastic Applications. In: *6th International Operational Modal Analysis Conference (IOMAC)*. Gijon, Spain.
- Scionti, M., Lanslots, J., Goethals, I., Vecchio, A., Van der Auweraer, H., Peeters, B. and De Moor, B. (2003). Tools to Improve Detection of Structural Changes from In-Flight Flutter Data. *the VIII Int. Conf. on Recent Advances in Structural Dynamics*.
- Soal, K. (2014). *Vibration Response of the Polar Supply and Research Vessel the S.A. Agulhas II in Antarctica and the Southern Ocean*. MEng thesis, Stellenbosch University.
- Soal, K., Bienert, J. and Bekker, A. (2015). Operational Modal Analysis on the Polar Supply and Research Vessel the S.A. Agulhas II. In: *International Operational Modal Analysis Conference (IOMAC)*. Gijon, Spain.

- Sohn, H., Dzwonczyk, M., Straser, E., Kiremidjian, A., Law, K. and Meng, T. (1999). An Experimental Study of Temperature Effect on Modal Parameters of the Alamosa Canyon Bridge. *Earthquake engineering & structural dynamics*.
- Suominen, M., Romanoff, J., Remes, H. and Kujala, P. (2015). The Determination of Ice-Induced Loads on the Ship Hull from Shear Strain Measurements. In: *International Conference on Marine Structures MARSTRUCT*. Southampton, England.
- Timco, G. and Weeks, W.F. (2010). A Review of the Engineering Properties of Sea Ice. *Cold Regions Science and Technology*, vol. 60, pp. 107–129.
- Vacher, P. (2010). Extensions of the MAC Criterion to Complex Modes. In: *International Conference on Noise and Vibration Engineering (ISMA)*. Leuven, Belgium.
- van Overschee, P. (2002). Subspace Identification for Linear Systems. Available at: <https://de.mathworks.com/matlabcentral/fileexchange/2290-subspace-identification-for-linear-systems>
- Van Overschee, P. and De Moor, B. (1996). Subspace Identification for Linear System: Theory - Implementation - Applications. *Conference Proceedings of the International Conference of IEEE Engineering in Medicine and Biology Society*, pp. 4427–30.
- Varsta, P. (1983). *On the Mechanics of Ice Load on Ships in Level Ice in the Baltic Sea*. Ph.D. thesis, Helsinki University of Technology.
- Verboven, P., Parloo, E., Guillaume, P. and Van Overmeire, M. (2002). Autonomous Structural Health Monitoring—Part I: Modal Parameter Estimation and Tracking. *Mechanical Systems and Signal Processing*, vol. 16, no. 4, pp. 637–657.
- Vold, H., Miller, B. and Reinbrecht, C. (2017). The Vold-Kalman Order Tracking Filter Implementation and Applications.
- Wahab, M. and De Roeck, G. (1997). Effect of Temperature on Dynamic System Parameters of a Highway Bridge. *Structural Engineering International*, pp. 266–270.
- Xia, Y., Hao, H., Zanardo, G. and Deeks, A. (2006). Long Term Vibration Monitoring of an RC Slab: Temperature and Humidity Effect. *Engineering Structures*, vol. 28, no. 3, pp. 441–452.
- Yue, Q., Guo, F. and Karna, T. (2009). Dynamic Ice Forces of Slender Vertical Structures due to Ice Crushing. *Cold Regions Science and Technology*, vol. 56, pp. 77–83.

- Zhang, Y., Häckell, M., Lynch, J.P. and Rolfes, R. (2015). Model Validation and Uncertainty Quantification, Volume 3. In: *Model Validation and Uncertainty Quantification*, vol. 3, pp. 161–170. Springer.
- Zhou, G.D. and Yi, T.H. (2014). A Summary Review of Correlations Between Temperatures and Vibration Properties of Long-Span Bridges. *Mathematical Problems in Engineering*.

## List of publications for PhD thesis titled System Identification and Modal Tracking of Ship Structures

22 January 2018

### Submitted

1. Soal, K., Bekker, A., Bienert, J., 2018, openSID: Open Source Stochastic Subspace Identification Toolbox for Structural Dynamics - Implementation, Analysis and GUI, *Journal of Mechanical Systems and Signal Processing* (at editor)
2. Soal, K., Govers, Y., Bienert, J., Bekker, A., 2018, Automatic Modal Parameter Selection using a Statistical Model and a Kalman Filter, *International Conference on Noise and Vibration Engineering (ISMA)*, (at editor)

### In Progress

1. Soal, K., Bekker, A., Bienert, J., 2018, Development of a Decision Support System for Ice Navigation using System Identification, *Journal of Cold Regions Science and Technology*, (submission pending)
2. Soal, K., Jelicic, G., Bekker, A., Bienert, J., 2018, Modal Parameter Tracking and Statistical Evaluation of a Polar Research Vessel with Open Data, *Journal of Ocean Engineering*, (written, feedback from co-authors received, soon to be submitted)
3. Soal, K., Govers, Y., Bienert, J., Bekker, A., 2018, System Identification and Tracking using a Statistical Model and a Kalman Filter, *Journal of Mechanical Systems and Signal Processing (MSSP)* (written, feedback from co-authors received, soon to be submitted)